CATIONIC ORGANOMAGNESIUM COMPLEXES AS HOMOGENEOUS CATALYSTS FOR THE RING–OPENING POLYMERIZATION OF LACTONES

BENJAMIN JOHN IRELAND
B. Sc., the University of Lethbridge, 2007

A Thesis
Submitted to the School of Graduate Studies
of the University of Lethbridge
in Partial Fulfillment of the
Requirements for the Degree

Master of Science

Department of Chemistry and Biochemistry
University of Lethbridge
LETHBRIDGE, ALBERTA, CANADA

For everyone who has taken the time to teach me something new

Abstract

Polylactones are biodegradable polymers which may be used as alternatives to conventional plastics and have shown promise in novel medical applications. Industrial production of polylactones requires the use of a catalyst. The work described herein is directed toward the development of novel cationic magnesium-based lactone-polymerization catalysts. These cationic species are produced by alkide abstraction from a neutral precursor; a strategy which has seen only preliminary exploration in the context of lactone polymerization.

The target catalyst system features a neutral phosphinimine-derivative ligand structure which was developed and produced specifically for the purpose of lactone polymerization catalysis. Target complexes were obtained by reaction of neutral alkylmagnesium precursors with protonated ligand derivatives. Syntheses and characterization of novel species are described herein.

These catalysts are very active in the polymerization of 6-caprolactone, generating high molecular weight polymers in mere minutes under mild conditions. A preliminary study of polymerization catalysis is also reported.

Acknowledgements

I would like to thank my supervisor, Dr. Paul Hayes for providing the opportunity to work and study as a member of his research group. His enthusiasm and insight have been invaluable to my development as a chemist. He has introduced me not only to the practice of synthetic chemistry, but to the community which surrounds it. I am particularly thankful of his support in sharing my research through national and international conferences as this has given me the exposure and opportunity to pursue my own career. Thank you.

Many thanks to the members of my thesis supervisory committee: Drs. René Boeré, Michael Gerken, Steven Patitsas, for their feedback and advice over the last two years. I am particularly indebted to Drs. Boeré and Gerken for their time in providing basic X-ray crystallography training. Additionally, I thank Dr. Eric Rivard of the University of Alberta for agreeing to serve as an external examiner for my thesis defense as well as Dr. Stacey Wetmore who has agreed to chair my examination committee. Dr. Andrew McWilliams of Ryerson University is acknowledged for GPC measurement of polymer samples and Dr. Adrien Côté of the Xerox Research Centre of Canada for expert assistance with X-ray crystallography. I also thank Drs. Andrew Hakin and Steven Mosimann for encouraging me to get involved in research as an undergraduate student.

Of the members of my research group, I would particularly like to thank Craig Wheaton for facing many of the same challenges that I have and for providing his insight. Mr. Wheaton is also acknowledged for a portion of the

crystallographic work presented herein, specifically the crystal structures of species **L_1**, **L_4** and **C_2**. Kevin Johnson, Dr. Delphine Julienne, Shayne Rybchinski, Breanne Kamenz, Kate Brockman, Alex Borisov, Jasmine Hango and Joline Utri are also thanked for their support and camaraderie over the past few years. Kristapher Fischer, Dr. Dinu Iuga, and Tony Montina are acknowledged for technical assistance and Susan Hill is acknowledged for administrative support.

The University of Lethbridge, the Natural Sciences and Engineering Research Council of Canada, Alberta Ingenuity, and the Alberta Heritage Foundation are acknowledged for their generous financial support in the form of student assistantships and scholarships.

Special thanks to my closest friends: Brent Koehler, Elizabeth Baker, and Xin (Karinna) Yu for helping me to keep things in perspective. Finally, I would like to thank my family - my sister, Rose, and my parents, John and Bonnie, who have shown me nothing but love and support my entire life.

Table of Contents

List of Tables

List of Figures

List of Schemes

List of Charts

List of Novel Compounds

Ligands

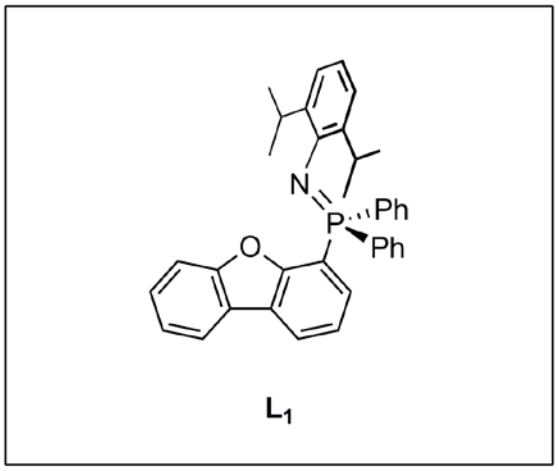

L_1

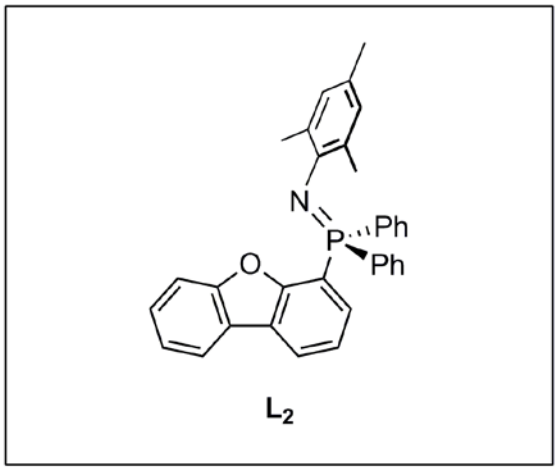

L_2

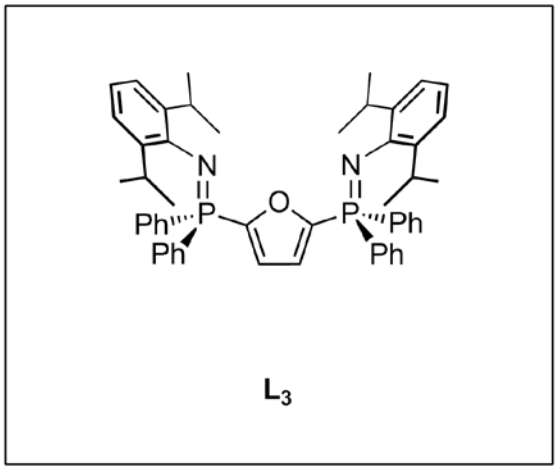

L_3

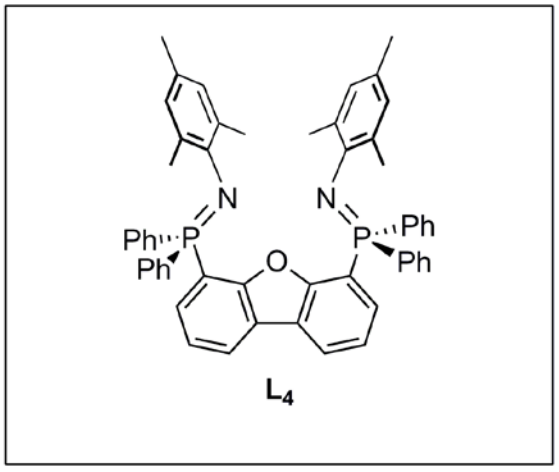

L_4

Activators

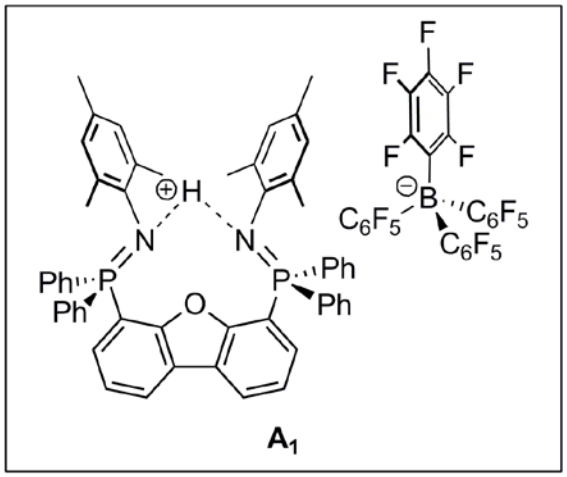

A1

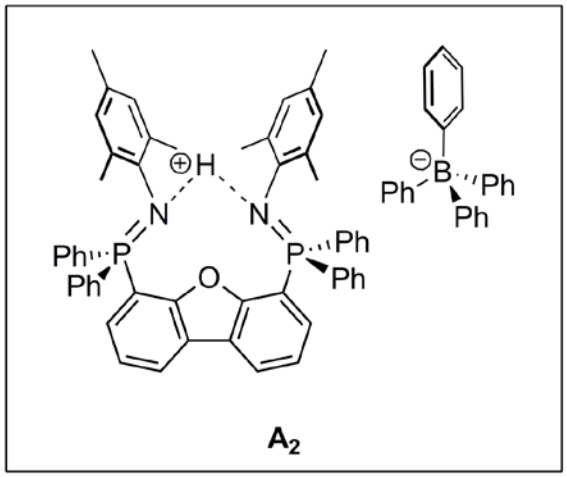

A2

Complexes

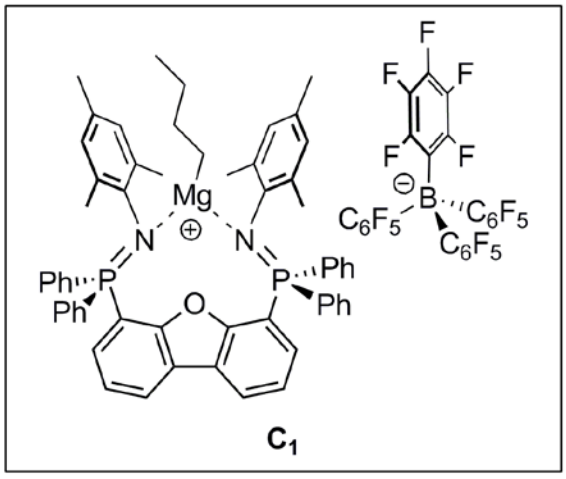

C1

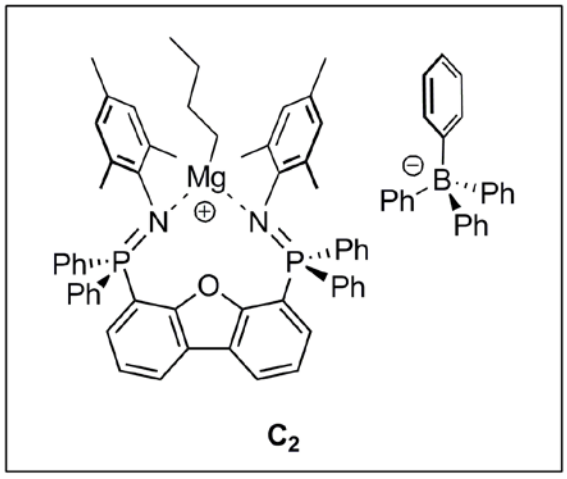

C2

List of Abbreviations (Alphabetical)

A_1	Protonated ligand activator $[\mathbf{L_4}H]^+[B(C_6F_5)_4]^-$ ($\mathbf{L_4}$ = 4,6-*bis*((2,4,6-trimethylphenyl)diphenylphosphinimino)dibenzofuran)
A_2	Protonated ligand activator $[\mathbf{L_4}H]^+[BPh_4]^-$ ($\mathbf{L_4}$ = 4,6-*bis*((2,4,6-trimethylphenyl)diphenylphosphinimino)dibenzofuran)
ACE	Activated chain end
AEM	Azacrown macrocycle
Ar	Any aryl group in the context of an abbreviated substructure within a molecular structure
BKA	β-ketoamino
^{n}Bu	*n*butyl
^{sec}Bu	*sec*butyl (1-methylpropyl)
^{t}Bu	*tert*buyl (1,1(dimethyl)ethyl)
C_1	Magnesium complex $[\mathbf{L_4}Mg^{n}Bu]^+[B(C_6F_5)_4]^-$ ($\mathbf{L_4}$ = 4,6-*bis*((2,4,6-trimethylphenyl)diphenylphosphinimino)dibenzofuran)
C_2	Magnesium complex $[\mathbf{L_4}Mg^{n}Bu]^+[BPh_4]^-$ ($\mathbf{L_4}$ = 4,6-*bis*((2,4,6-trimethylphenyl)diphenylphosphinimino)dibenzofuran)
CIN	Coordination-insertion
CL	6-caprolactone
COSY	Correlation spectroscopy
Cp	Cyclopentadienyl
(d)	doublet (in the context of tabulated NMR data)
DEPT	Distortionless enhancement by polarization transfer
DFT	Density functional theory
DNA	Deoxyribonucleic acid
Dbf	Dibenzofuran (used within structure or structure fragment names)

Dipp	2,6–Di*iso*propylphenyl
ESD	Estimated standard deviation
Et	Ethyl
FAB	Perfluoroarylborane
GPC	Gel-permeation chromatography
h	hours
HSC	Heteroscorpionate
HSQC	Heteronuclear single quantum coherence
IPQM	Iminophosphorano(8-quinolyl)methanide
IR	Infrared
L or L_n	An unspecified ligand
L_1	4-((2,6-di*iso*propylphenyl)diphenylphosphinimino)dibenzofuran
L_2	4-((2,4,6-trimethylphenyl)diphenylphosphinimino)dibenzofuran
L_3	2,5-*bis*((2,6-di*iso*propylphenyl)diphenylphosphinimino)furan
L_4	4,6-*bis*((2,4,6-trimethylphenyl)diphenylphosphinimino)dibenzofuran
M	Any metallic atom
m-	*meta*-
MALDI	Matrix-assisted laser desorption ionization
MAO	Methylaluminoxane
Me	methyl
Mes	2,4,6–trimethylphenyl aka “mesityl”
min	minutes
M_n	Number average molecular weight
M_w	Weight average molecular weight

MW	Molecular weight (used interchangeably with molecular mass)
NAC	“Nac-Nac” - possessing the substructure $(N–CR–CH–CR–N)^-$
NMR	Nuclear magnetic resonance
o-	*ortho*-
Oct	Octoate
p-	*para*-
PCL	Polycaprolactone
PDI	Polydispersity index
PGA	Polyglycolic acid (polyglycolide)
Ph	phenyl
PHB	Polyhydroxybutyrate
PHL	Phenolate
PLA	Polylactic acid (polylactide)
Ph	Phenyl
ppm	parts per million
^{i}Pr	*iso*propyl aka 2-propyl
PVC	Polyvinyl chloride
(q)	quartet (in the context of tabulated NMR data)
R	Any alkyl group
Ref.	Reference number (when used in a table)
RNA	Ribonucleic acid
ROP	Ring-opening polymerization
s	seconds
(s)	singlet (in the context of tabulated NMR data)

SEC	Size-exclusion chromatography
(sp)	septet (in the context of tabulated NMR data)
(t)	triplet (in the context of tabulated NMR data)
THF	Tetrahydrofuran
TMEDA	Tetramethylethylenediamine
TOF	time-of-flight
VTU	Variable-temperature unit
X	Any stable, naturally occurring halogen atom (F, Cl, Br, I)

Chapter 1

Introduction: Polymers, Catalysts and Catalysis

1-1: *Polylactones and Other Biodegradable Polymers*

Polymers can be broadly defined as linear macromolecular assemblies of repeating polyatomic structural units. Polymeric materials influence almost every aspect of modern life, from the commercial products we use regularly, to the tools of modern medicine, to the very infrastructure of our cities. The human body itself could not function without the aid of polymers of nucleic acids (DNA, RNA) and amino acids (proteins, structural materials such as collagen or keratin). The production of synthetic polymers for industrial, medical, and personal use includes a broad range of materials such as polyethylene, polypropylene, polyvinyl chloride (PVC), polystyrene, polyacrylonitrile, various polyesters, polyethers, polyamides (including nylons), and many, many more.[1,2] Biodegradable polymers present the opportunity to develop environmentally friendly alternatives to conventional plastics. These materials have shown promise in a variety of conventional applications (packaging materials, coatings, fibers, etc.) as well as novel biomedical uses (implantable materials, absorbable sutures, slow-release pharmaceutical matrices).[3]

With respect to polymers, “biodegradable” may refer to a number of different characteristics, all of which involve the decomposition of the material under environmental or physiological conditions.[3] Polymer “biodegradation” may, in the broadest sense, refer to “environmentally biodegradable,” meaning any

material which, under environmental conditions (with or without the aid of organisms), will deteriorate into smaller units. By this definition, all polymers are “biodegradable”; however, conventional hydrocarbon-based polymers deteriorate so slowly that they are not normally referred to in this sense. In polymer science, “degradation” refers strictly to depolymerization (division of a polymer to its constituent monomeric units) thus, biodegradation could refer to any process by which a polymer is split into monomeric units by a living organism. In the narrowest sense, “biodegradable polymer” may be considered synonymous with “metabolizable polymer” - a polymeric material which is not only broken down by living organisms, but absorbed into, or harnessed by, the organism in some way.[3] For example, while polyolefins could only classify as “environmentally biodegradable,” proteins would fit all three classifications as they may be metabolized and harnessed by organisms. For the purposes of discussion herein, the term “biodegradable” will refer to biologically-mediated depolymerization, while the term “metabolizable” will be reserved for materials which may be subsequently incorporated into living systems.

Biodegradable polymers include both natural and synthetic materials according to their occurrence or absence in nature. While the major classifications (Figure 1-1) include materials of commercial interest, discussion will largely be limited to polylactones, a biodegradable subset of polyesters. Polyhydroxyalkanoates (natural, biodegradable polyesters analogous to polylactones) will be discussed only briefly. Proteins, polysaccharides, vinylic, and other polymers (a category composed of dozens of primarily unrelated

materials) are well beyond the scope of the studies described herein.

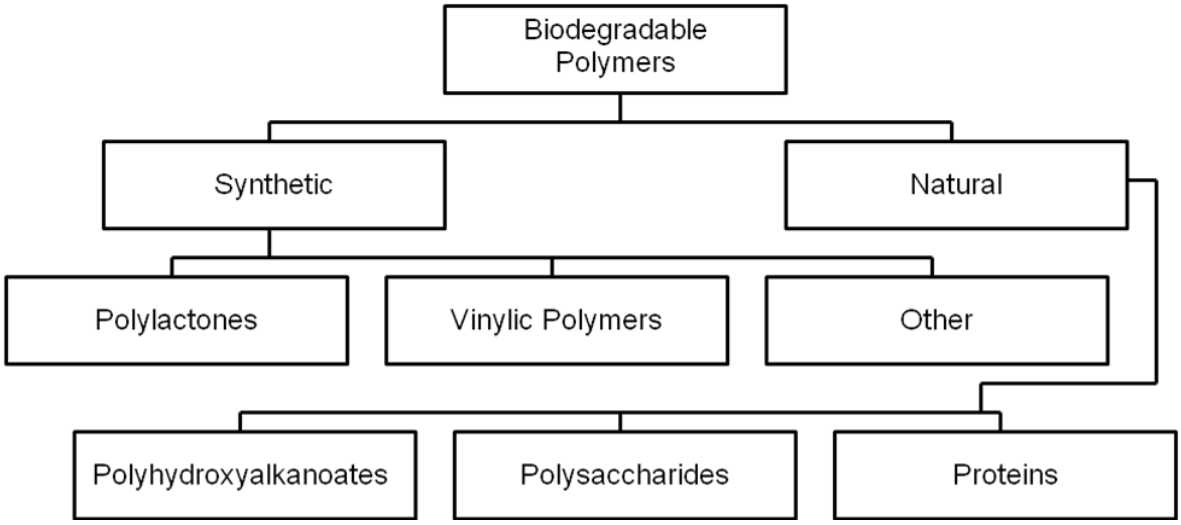

Figure 1-1: Simplified classification scheme for biodegradable polymers of commercial interest.[3]

Synthetic polylactones are generated in high molecular weight via ring-opening polymerization (ROP) of lactones (cyclic esters). Polylactones include an array of polyesters; however, only polymers of 6-caprolactone, lactide, and glycolide (Chart 1-1) constitute the subset of synthetic polylactones which have achieved commercial viability.[4] All of these polymers are biodegradable and may be absorbed into the human body, while polylactide and polyglycolide degrade to lactic acid and glycolic acid, respectively – both of which may be further metabolized via the Krebs cycle.[5]

Polyhydroxyalkanoates (including polyhydroxybutyrate and polyhydroxyvalerate) are structurally analogous to synthetic polylactones and may be generated via ROP of cyclic esters.[6] This route is not thoroughly explored as these materials occur in nature. Industrial processes for polyhydroxyalkonate production tend to focus on harvesting polymers produced by genetically

engineered organisms;[7] thus, these materials are not generally classified as "synthetic."

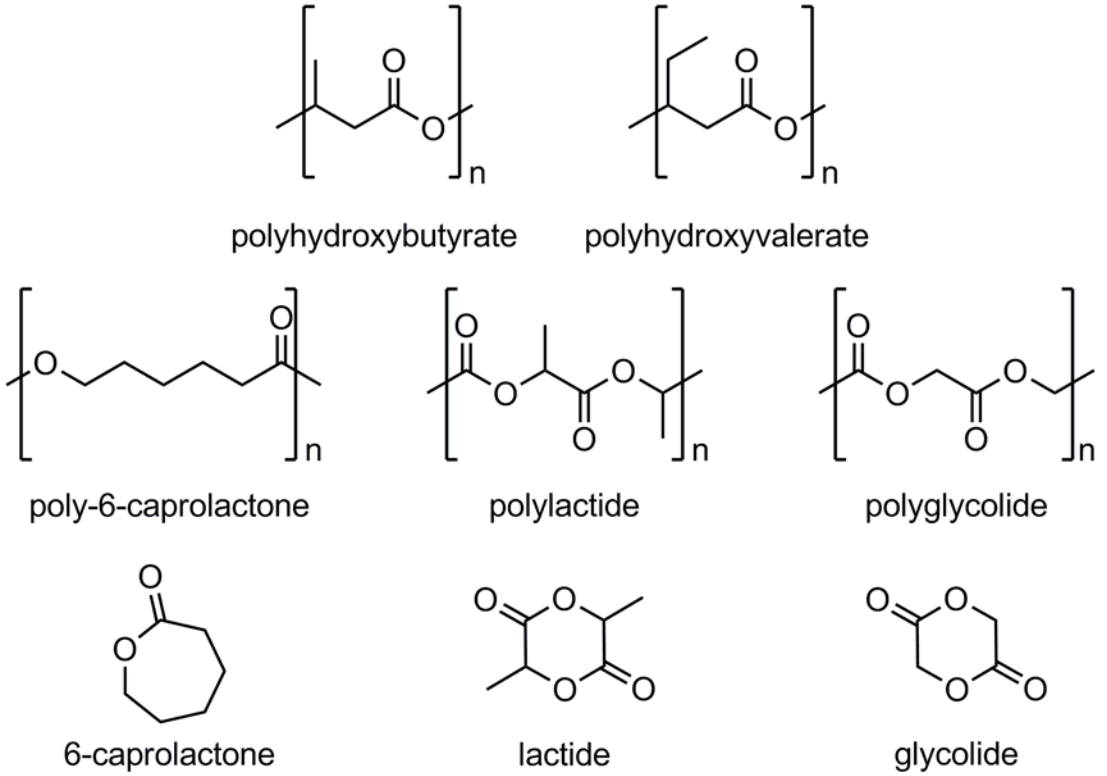

Chart 1-1: Commercially viable natural polyhydroxyalkanoates, synthetic polylactones, and lactone monomers.

Polycaprolactone (PCL) is one example of a commercially viable, biodegradable polylactone. It is sold for manufacturing purposes under the trade names CAPA[8] and PolyCLO,[9] or commercially as Shapelock (USA),[10] Friendly Plastic (USA and Canada), or Polymorph (UK).[11] It is exceptionally tough, comparable in strength to nylon or polypropylene, but has a low melting point (~60 °C: lower than both polylactide (~160 °C)[12] and polyglycolide (~220 °C)[13]), making it an excellent material for molding and manufacturing under mild conditions. The chemical structure of 6-caprolactone consists of a seven-membered ring containing a single ester functional group. Monomeric 6-

caprolactone, is produced via Baeyer-Villager oxidation[14] of cyclohexanone with peracetic acid (Scheme 1-1). Globally, three major manufacturers produce 6-caprolactone on an industrial scale: BASF (Germany),[9] Daicel (Japan),[15] and Perstorp (Belgium) – the largest global producer since acquiring all 6-caprolactone and PCL production facilities from Solvay (UK) in 2008.[8]

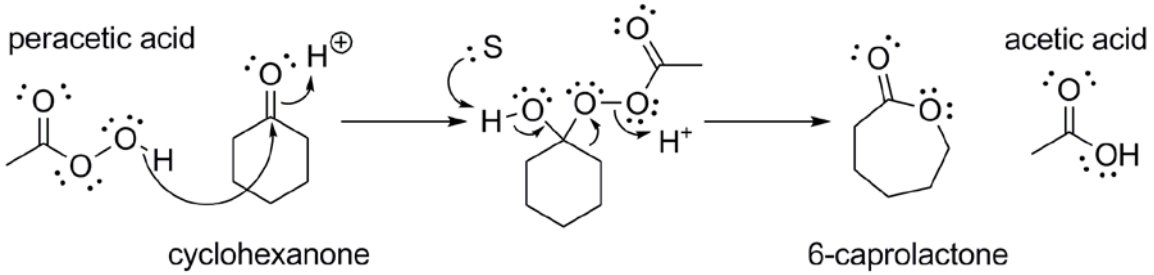

Scheme 1-1: Synthesis of 6-caprolactone via Baeyer-Villager oxidation (under acidic conditions) of cyclohexanone with peracetic acid.

Polycaprolactone was first synthesized by Wallace Carothers (an American chemist more widely known for the discovery of nylon)* in the 1930s.[16] Its production is carried out via ring-opening polymerization (ROP) of 6-caprolactone. Major industrial suppliers of polycaprolactone are Perstorp (Belgium) and BASF (Germany). Industrial catalysts most frequently employed are inorganic species based on aluminum[17] and tin[18] and require elevated temperatures for optimal polymerization activity.

Though polycaprolactone (PCL) is, strictly speaking, a non-renewable synthetic material (its precursors are derived partially from petrochemical

* Note that polycaprolactone is the lactone analogue of one nylon variety, "Nylon 6". Nylon-6 has the linear structure $[–(CH_2)_5C(O)NH–]$. Unlike the more common "Nylon-6,6", Nylon 6 is not produced by condensation polymerization, but by ring-opening polymerization of 6-caprolactam, the cyclic amide analogue of 6-caprolactone.

sources), it is biodegradable and metabolizable. PCL is readily degraded and absorbed into mammalian tissues[19] and may be degraded under ambient conditions[20] by a number of naturally-occurring microorganisms.[21,22] Although little is known about PCL depolymerases (enzymes which convert PCL into its subunits) and the mechanism by which they function, PCL degradation has been linked to many naturally occurring esterases – enzymes which degrade ester linkages in naturally occurring materials.[23]

1-2: *Mechanisms of Lactone Polymerization*

Any polymerization process may be defined by three discrete mechanistic phases; namely, initiation (the process by which polymerization begins), propagation (the process by which an oligomer extends into a larger polymer) and termination (the process by which polymerization halts and the growing terminus is converted into an end group). Biodegradable polyesters (specifically polylactide, polyglycolide, and polycaprolactone) may be isolated either by condensation polymerization (resulting in low-MW polymers) or, more controllably, by ring-opening polymerization (ROP) of monomeric lactones.[24] Lactone ROP requires the use of a polymerization initiator (Scheme 1-2) and may occur via cationic activated chain end (ACE), anionic ACE or coordination-insertion (CIN) mechanisms.

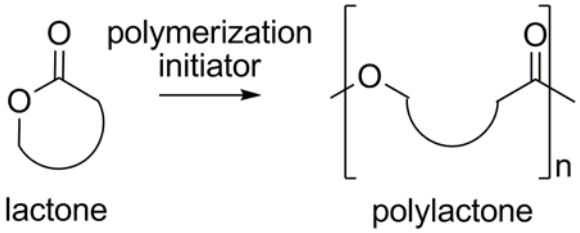

Scheme 1-2: Production of a polylactone by ROP of a lactone monomer. Non-specific structure shown throughout refers to any lactone.

Polymerization which occurs via an ACE mechanism results in the activating species becoming remote from the active site of chain growth during the propagation phase. As a result, the activating species is better described as an “initiator” (a species that is instrumental in starting a specific reaction, which then continues in the absence of any direct interaction with the initiator itself) than as a “catalyst” (which repeatedly undergoes a specific reaction without being consumed). Both cationic and anionic species may act as ACE initiators. Experimental evidence (end-group analysis and trapping of reaction intermediates) suggests that attack at the exocyclic oxygen is the dominant initiation process in cationic ACE polymerization (Scheme 1-3).[18]

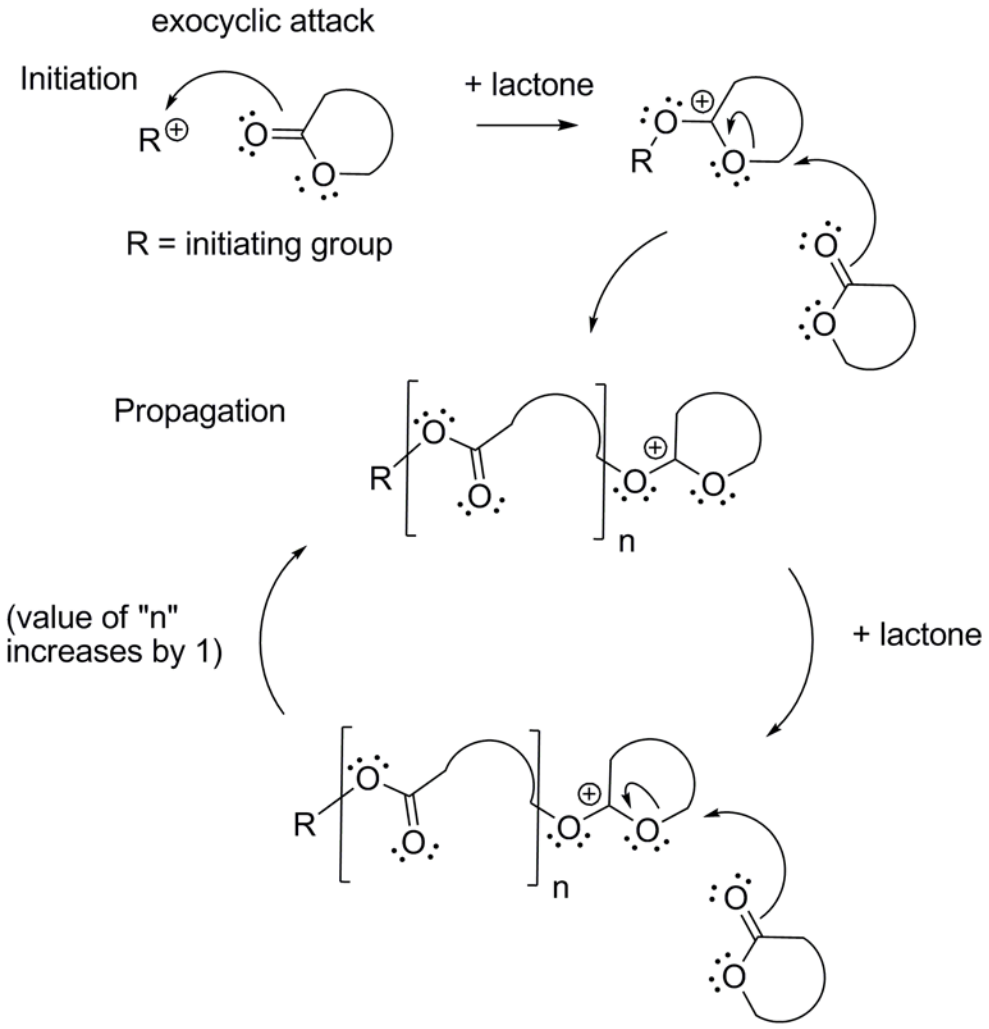

Scheme 1-3: Mechanism of cationic ACE polymerization via initial exocyclic attack on C=O. Note: First cycle shown explicitly, n = 1 (second cycle), n = 2 (third cycle), etc.

Anionic ACE polymerization takes place via a chain of nucleophilic acyl substitution reactions.[18] While anionic ACE (Scheme 1-4) is mechanistically different from cationic ACE (Scheme 1-3), both make use of an initiation process wherein the activating species remains bound to the end of the polymer opposite the active site of elongation. Systems in which either cationic or anionic ACE polymerization takes place therefore provide little opportunity to directly influence the chemical environment of the growing polymer.

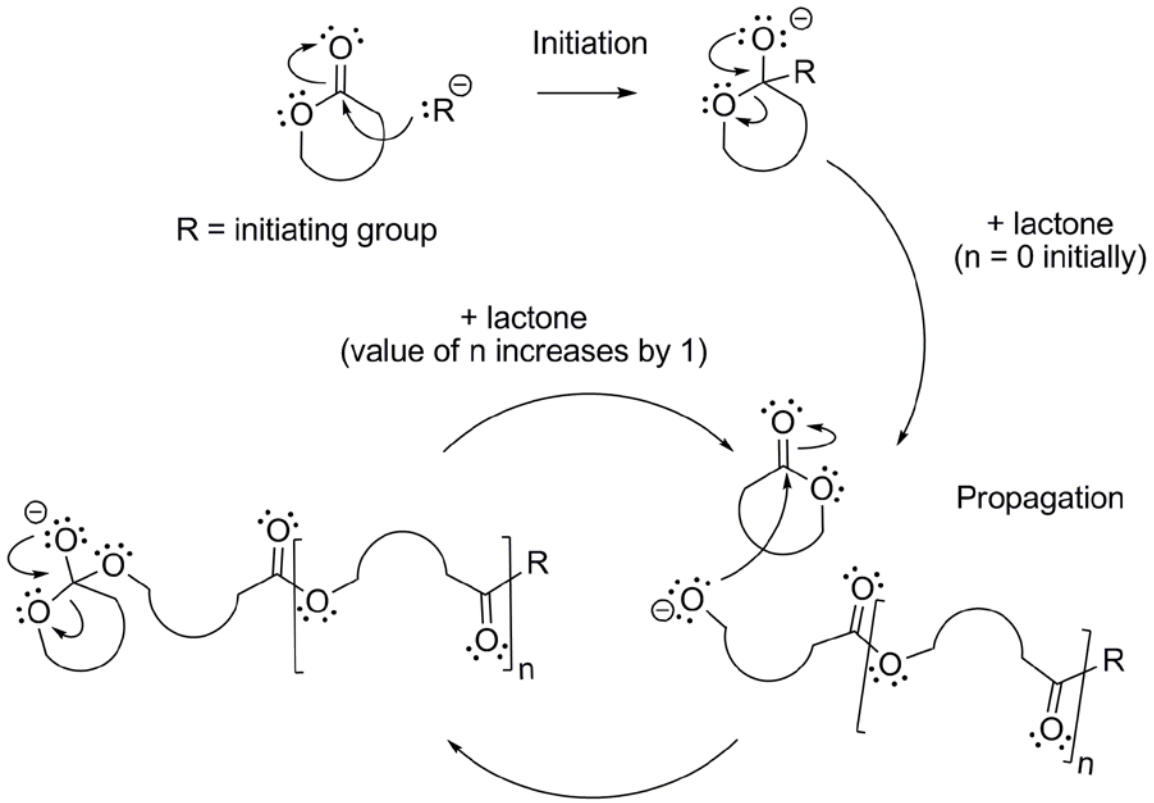

Scheme 1-4: Polymerization of lactones via an anionic ACE mechanism.

Lactone polymerization via CIN is by far the most common mechanism observed with respect to inorganic and organometallic polymerization catalysts (Scheme 1-5). Note that, strictly speaking, CIN is a special case of anionic polymerization in that the overall bonds formed and broken are identical; however, a portion of the initiating species remains bound to the propagating terminus of the growing polymer. The species bound to the propagating end is involved in the same process many times (with the obvious qualifier that the bound polymer increases by one monomer unit with each cycle) without being consumed and can thus be properly classified as a “catalyst”.

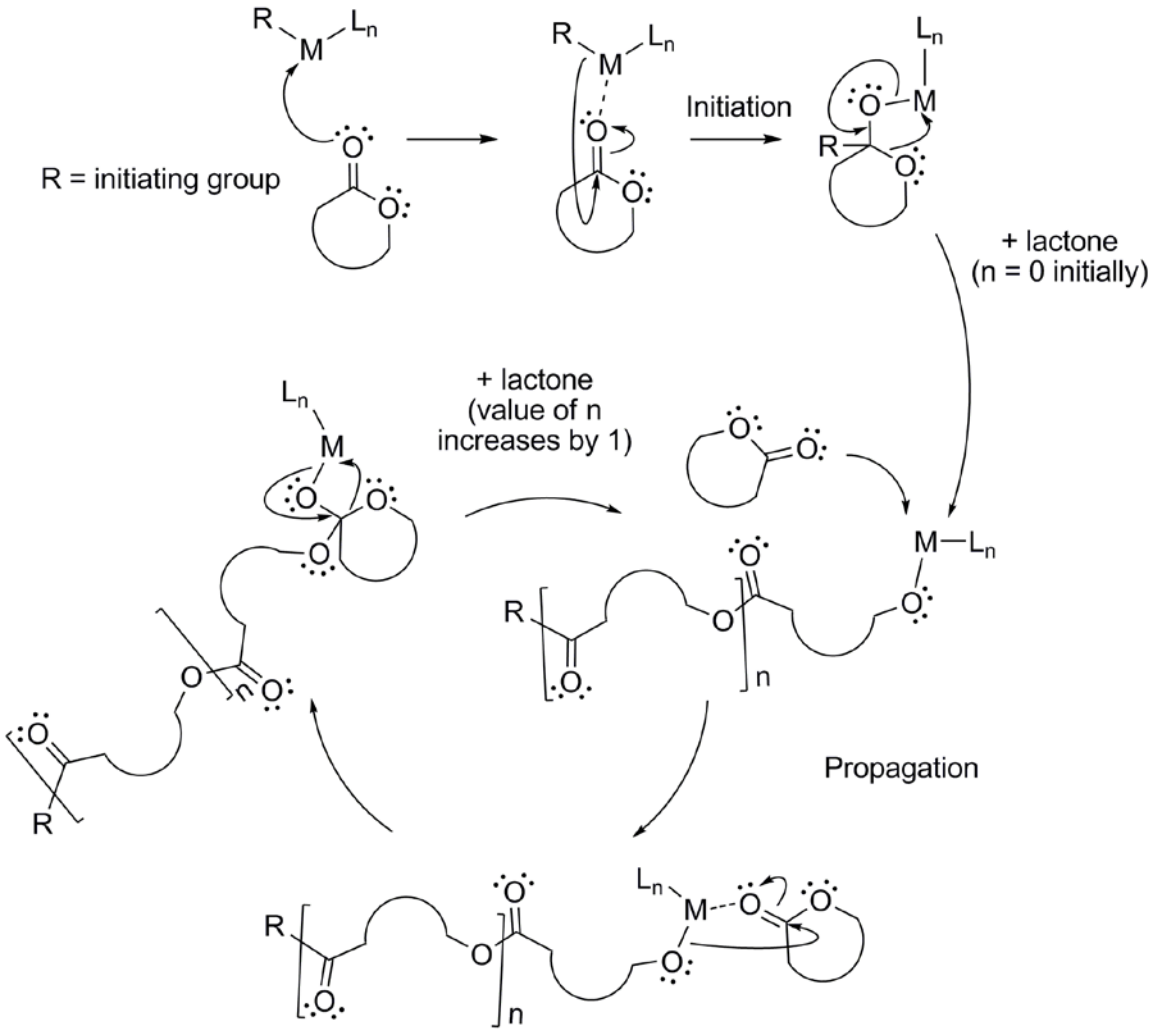

Scheme 1-5: Polymerization of a lactone via the coordination-insertion mechanism. Note: M = metal centre. L_n = unspecified ancillary.

One major benefit of CIN polymerization relative to anionic ACE polymerization is that coordination of the carbonyl group of the monomer to a metal centre decreases carbonyl electron density relative to the analogous unbound process. This promotes subsequent insertion of the nucleophilic group.[26] Higher reaction rates are thus possible in metal-catalyzed CIN polymerization than in catalyst-free anion-activated ACE polymerization. The presence of the catalytic species “M” at the propagating terminus of the chain

also presents the opportunity to directly influence the chemical environment of the growing polymer by varying the choice of metal used. Frequently, an ancillary ligand is used as it may influence the steric environment of the growing polymer, alter the electronic properties of the metal via electron donation or withdrawal, and may be easily and rationally modified provided its synthesis is modular in nature.

Termination may be induced when a polymerization reaction is quenched or may occur automatically if the propagating polymer chain undergoes deactivation. A common quenching agent, such as an alcohol, may be used to liberate the polymer from the catalyst by protonating (thereby deactivating) the propagating terminus. In principle, this process may be used to recover the catalytically active species, although success of this approach is largely dependent on the nature of the catalyst (Scheme 1-6).

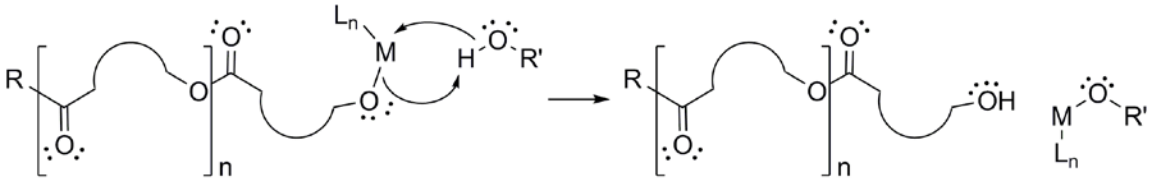

Scheme 1-6: Deactivation of lactone polymerization by a protic quenching agent such as an alcohol. L_n = unspecified ancillary.

Termination of the polymerization process may also occur by intermolecular or intramolecular transesterificaton (Scheme 1-7). Transesterification is associated with molecular weight broadening (manifested in a high PDI[†] value) and may produce low molecular weight polymers.

[†] Polydispersity index (PDI) values describe the variation in individual molecular weights of polymers defined by the ratio of the weight average to number

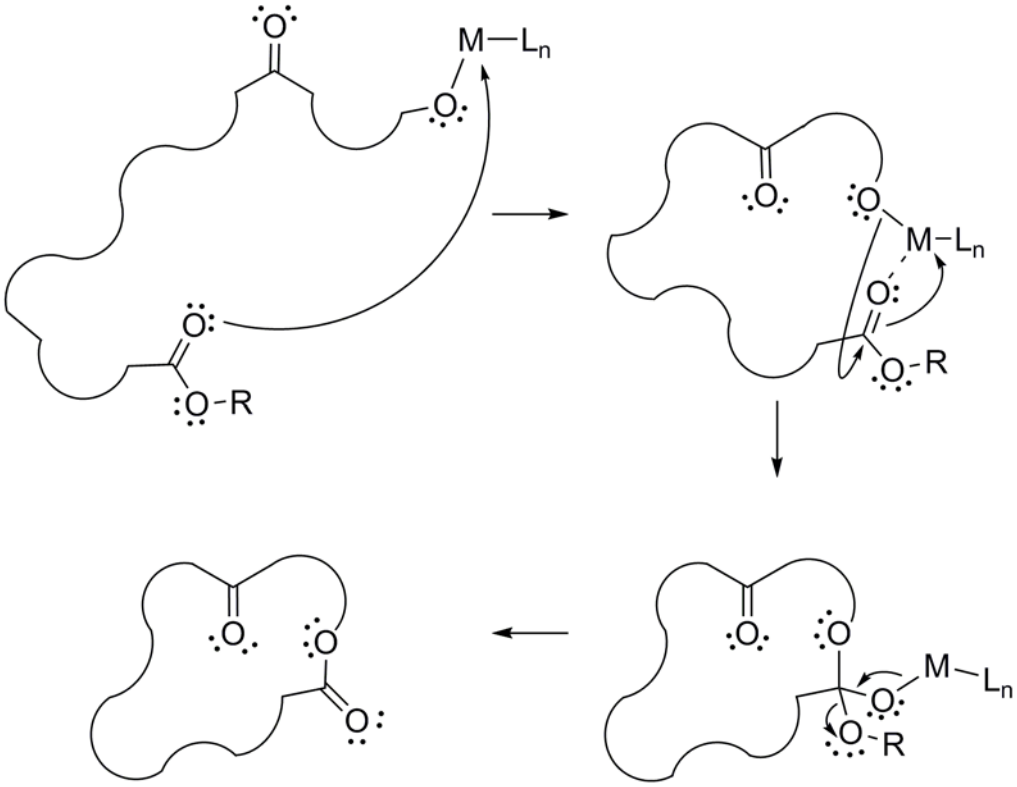

Scheme 1-7: Mechanism of intramolecular transesterification leading to termination of a CIN polymerization reaction. Note that intermolecular transesterification proceeds by a highly similar mechanism, except that the carbonyl group which undergoes substitution originates from a separate polymer chain. L_n = unspecified ancillary.

Polymerization of lactones may occur via coordination-insertion or activated chain end mechanisms although initiators which promote the CIN mechanism present greater opportunity for control over the polymerization process. As a result, novel initiator development tends to focus on inorganic or organometallic systems which make use of CIN polymerization.

---

average molecular weights (PDI = M_w/M_n). Typical values range from 1.0 (ideal) to approximately 2 or 3 but higher values are possible for poorly controlled processes. See Chapter 4-1 for additional details.

1-3: *Tin and Aluminum-Based 6-Caprolactone Polymerization Catalysts*

Historically, developers of homogeneous CIN catalysts have focused on inorganic main group species based on tin and aluminum[27] while recent work has expanded to encompass catalysts based on a wider variety of main-group, transition-metal,[28] and f-block[29] complexes as well as organocatalysts.[30] Stannous octanoate ($Sn(Oct)_2$) is one of the earliest known and most thoroughly characterized CIN polymerization catalysts for 6-caprolactone. It has demonstrated efficacy at exceptionally low catalyst loadings (< 0.005 mol%),[31] readily yielding high molecular-weight polymers (up to 1 x 10^6 g/mol).[32]

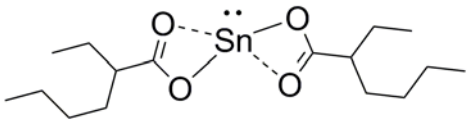

Chart 1-2: Structure of $Sn(Oct)_2$ - a prominent tin-based polymerization catalyst. (Note: monomeric structure shown. Oligomers are common in solution and extended networks exist in the solid state).

Stannous octanoate remains the most widely-used catalyst for 6-caprolactone polymerization and is particularly prominent in industrial applications as it is commercially available and considered to be highly active at elevated temperature.[33] The second-order rate constant of the polymerization of 6-caprolactone by $Sn(Oct)_2$ alone is approximately 6.7 x 10^{-5} $mol^{-1}Ls^{-1}$ at 80 ºC; however, this value may be elevated to as high as 1.3 x 10^{-2} $mol^{-1}Ls^{-1}$ (approximately 200 times) by using an alcohol-based co-initiator (^{n}butanol or benzyl alcohol are most common and are generally present in excess).[32] While the rate-enhancing influence of an alcohol co-initiator on $Sn(Oct)_2$ is well-established, it casts ambiguity onto the nature of the active catalyst. Stannous

octanoate/alcohol systems exist in equilibrium (Scheme 1-8) with substantial components of various tin-containing species, any of which may act as an initiator for lactone polymerization. Additionally, formation of tin(II) alkoxy species liberates octanoic acid, which may itself act as an ACE initiator for lactone polymerization, further convoluting the polymerization mechanism.[33] While $Sn(Oct)_2$ activation using alcohols represents a successful tactic for improving catalyst reactivity, this system presents little opportunity for rational modification as fine-tuning of the catalyst would be difficult in an environment with multiple active species.

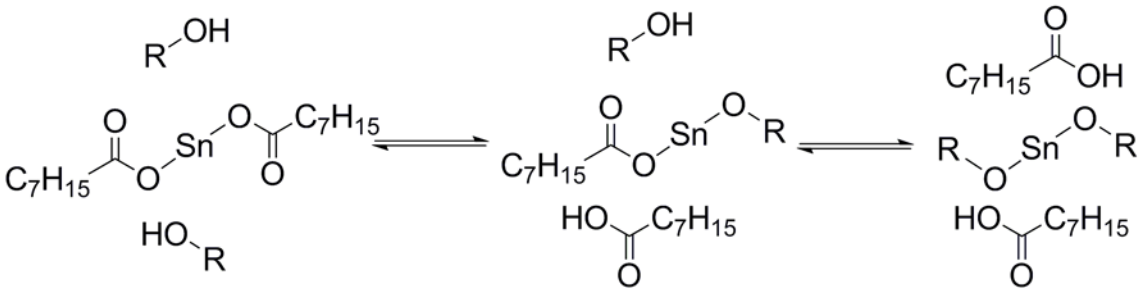

Scheme 1-8: Species present in the equilibrium of $Sn(Oct)_2$ and excess ROH (R = ^{n}butyl, CH_2Ph, etc).

Another disadvantage of $Sn(Oct)_2$ is its toxicity. The American Food and Drug Administration requires tin levels below 20 to 50 ppm for medical and food applications, although a typical polymerization procedure results in 500 to 2000 ppm tin as a result of catalyst trapped in the polymer.[31] This requires polylactone products (including polycaprolactone) to be purified before they may be distributed and used, adding time and expense to their production. A variety of analogous tin-based catalysts for lactone polymerization have been explored;

however, no alternatives have yet achieved the activity and widespread use of $Sn(Oct)_2$.[34]

Aluminum catalysts were first employed in lactone polymerization almost 50 years ago.[35] Among the most thoroughly explored catalyst types are those featuring anionic ancillary ligands which may be classified as β-ketoamino (BKA) or phenolate (PHL) species. Since only selected studies are discussed herein, the following should not be considered a comprehensive review of aluminum-based lactone polymerization catalysis.

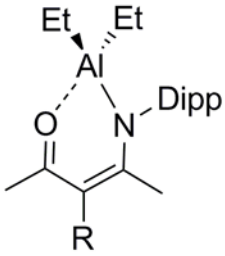

BKA-1: R = Cl
BKA-2: R = H
BKA-3: R = Ph
BKA-4: R = Me

Chart 1-3: Selected examples of organoaluminum 6-caprolactone polymerization catalysts featuring anionic BKA ligand types.

Table 1-1: Polymerization of 6-caprolactone by selected organoaluminum complexes featuring BKA ligand types (T = 60 ºC).[36]

Species	Catalyst Loading (%)	Time	Conversion (%)	M_W (x 10^4 g/mol)	PDI (M_w/M_n)
BKA-1	0.30	3 h	76.2	9.94	2.18
BKA-2	0.30	3 h	71.6	1.92	2.63
BKA-3	0.30	3 h	64.8	5.03	2.06
BKA-4	0.30	3 h	45.9	3.53	1.92

Anionic β-ketoamino ligands are known to bond strongly to a variety of metal centres and are easily modified to tune both steric and electronic properties. The series **BKA-1** to **BKA-4** (Chart 1-3) illustrates modification of catalytic activity by alteration of the ancillary ligand.[36] In terms of catalyst activity

(monomer consumption vs. time) a clear trend is defined: **BKA-1** > **BKA-2** > **BKA-3** > **BKA-4** (Table 1-1). In this series, the authors of the study suggest that the more strongly electron-withdrawing / weakly electron-donating substituents (Cl > H > Ph > Me) result in a more highly electropositive aluminum centre, activating it toward CIN polymerization. The molecular weights of polymers produced from these catalysts were inconsistent (ranging from M_w = 1.9 x 10^4 to 9.9 x 10^4 g/mol) and polydispersity was high (PDI = 1.92 to 2.63), suggesting a poorly controlled polymerization process with slow initiation relative to propagation. This study does, however, reinforce the ability of an ancillary ligand to influence the lactone polymerization process in a CIN mechanism. Furthermore, the observation of higher activity at more electrophilic centres agrees well with the known mechanism of lactone polymerization wherein electron withdrawal from the lactone carbonyl group promotes the insertion step of the polymerization process.

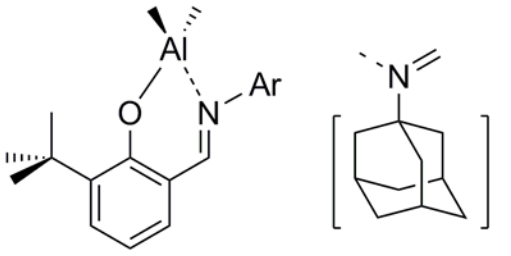

PHL-1: R = Dipp
PHL-2: R = ^{t}Bu
PHL-3: R = adamantyl
PHL-4: R = C_6F_5

Chart 1-4: Selected examples of neutral aluminum alkyl 6-caprolactone polymerization catalysts featuring anionic phenolate-derivative ligand types.

Table 1-2: Polymerization of 6-caprolactone by selected neutral aluminum alkyl and alkoxide complexes featuring PHL ligand types (**PHL-1** to **PHL-4**: T = 60 ºC, 1.0 molar equivalent BnOH co-initiator).[37]

Species	Catalyst Loading (%)	Time	Conversion (%)	M_W (x 10^4 g/mol)	PDI (M_w/M_n)
PHL-1	0.40	60 min	84	7.00	1.61
PHL-2	0.40	120 min	41	4.00	1.39
PHL-3	0.40	120 min	7.7	1.03	1.06
PHL-4	0.40	30 min	99	11.7	1.61

Anionic phenolate-based ligand systems have also been explored with respect to 6-caprolactone polymerization.[37] The series defined by **PHL-1** to **PHL-4** (Chart 1-4) clearly reinforces the ability of a chelating ancillary to modulate catalyst activity. In this series, variation of the imine-substituent illustrates the use of both steric and electronic features of the ligand to tune the activity of the catalyst. The series **PHL-4** > **PHL-1** > **PHL-2** > **PHL-3** describes the relative reactivities of these catalysts.

By comparison to **PHL-2**, polymerization using **PHL-3** is extremely slow – a likely influence of the enhanced steric bulk of the adamantyl group relative to ^{t}butyl (Table 1-2). The catalyst **PHL-1**, however, is a more active catalyst than **PHL-2**, despite possessing greater steric bulk (dipp vs. ^{t}butyl). This is likely a result of the di*iso*propylphenyl group's ability to act as an electron-withdrawing group (by resonance), rendering the metal centre more electrophilic and therefore, a more potent catalyst. This effect is even more pronounced in the enhanced activity of **PHL-4**, wherein the C_6F_5 substituent may act as a more efficient electron-withdrawing group. Note that these species are completely inert to 6-caprolactone in the absence of an alcohol co-initiator; therefore, it is likely

that analogous aluminum-alkoxy species of the form [LAl(Me)(OR)] actually act as catalysts and **PHL-1** to **PHL-4** are more accurately described as "pre-catalysts." This detail does not alter conclusions drawn on the nature of the ligand's influence on polymerization, however.

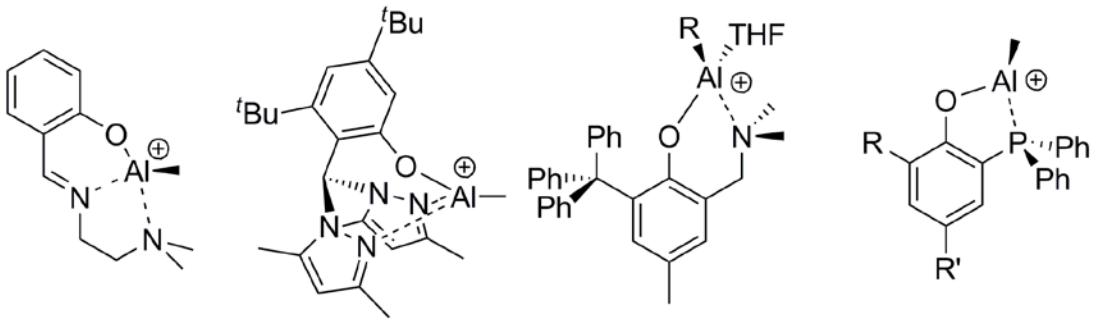

Chart 1-5: Selected examples of cationic aluminum alkyl and alkoxide complexes applied to 6-caprolactone polymerization.

Table 1-3: Polymerization of 6-caprolactone by selected cationic aluminum alkyl and alkoxide complexes featuring PHL ligand types.

Species	Catalyst Loading (%)	Time (Temp. (ºC))	Conversion (%)	M_W (x 10^4 g/mol)	PDI (M_w/M_n)	Ref.
PHL-5	2.0	1 h (40)	95	0.1-0.5	NA	38
PHL-6	0.6	2 h (50)	98	Not Reported	NA	39
PHL-7	0.83	15 min (25)	99	2.07	1.38	40
PHL-9	1.0	2 h (75)	95	5.1	1.33	41
PHL-10	1.0	2 h (75)	95	4.6	1.24	41

Phenolate-bearing aluminum complexes may be activated to form cationic species - a strategy which is extremely common in the polymerization of more conventional materials such as olefins (see Chapter 1-4), but has seen only preliminary exploration in the polymerization of lactones.[38-43] To date, very few unique examples of cationic aluminum species (or cationic species of any kind,

for that matter) have been applied to lactone polymerization, the earliest examples of which are as recent as the late 1990s.[42] The series **PHL-5** to **PHL-10** (Chart 1-5, Table 1-3) describe key examples of progress thus far. The catalysts **PHL-5**[38] and **PHL-6**[39] have been reported separately and, although they required extended periods of time at elevated temperatures to generate only low molecular-weight oligomers, represent an important initial step toward cationic 6-caprolactone polymerization catalysts. Note that **PHL-6** has been found to initiate polymerization via the anionic phenolate ligand, rather than the alkyl group, limiting its ability to exert control over the polymerization process and thus limiting potential for future exploration.

Catalyst **PHL-7** is the most active cationic aluminum-based 6-caprolactone polymerization catalyst reported to date as it is able to achieve near-quantitative polymerization of over 100 equivalents of 6-caprolactone in only 15 minutes without heating or addition of activating agents (though note that analogue **PHL-8** is completely inert to 6-caprolactone; again illustrating the importance of a suitable initiating group).[40] Although less active in polymerization than **PHL-7**, phosphine-containing species **PHL-9** and **PHL-10** are key examples as they have been found to be unambiguously *more active* than their analogous neutral precursors (of the form [L_nAlMe_2]), illustrating the promise of activation in 6-caprolactone polymerization catalysis.[41]

1-4: *Catalyst Activation Strategies*

Activating agents are well established in the field of olefin polymerization. These species are known to dramatically enhance the reactivity of catalysts.[44] Lewis or Brønsted acids may be used for this purpose, either of which has the overall effect of lowering both steric bulk and electron density at the catalytic centre.

Lewis acidic species (such as alkylaluminum reagents) are able to act as activators by abstracting anionic moieties to produce cationic species - a mechanism first postulated in the context of metallocene halide activation in the 1960s[45] and demonstrated conclusively over 20 years later.[46] The activation of $[Cp_2TiRCl]$ to form $[Cp_2TiR]^+$ is shown below (Scheme 1-9) as this species has been studied extensively to determine both the nature of the exchange mechanism[47-49] and the role of $[Cp_2TiR]^+$ as the catalytically active species in olefin polymerization.[46]

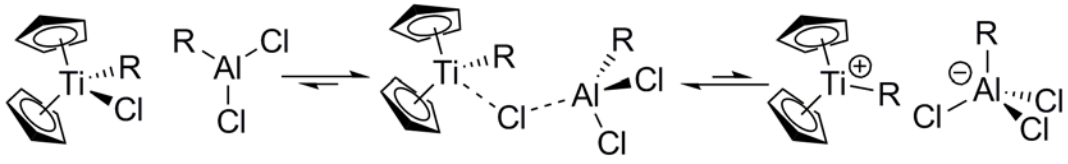

Scheme 1-9: Activation of a titanocine-based olefin polymerization catalyst by an alkylaluminum reagent.

Some of the most heavily utilized activating agents, methylaluminoxane (MAO) and its variants, may be considered a subset of alkylaluminum activators. Methylaluminoxane is prepared by controlled addition of water to $AlMe_3$[50] and was first applied to olefin polymerization in the early 1980s.[51,52] Methylaluminoxane is a heterogeneous mixture consisting of the basic subunit

$Al_4O_3Me_6$.[51,53] These combine to form assemblies of at least two subunits in active MAO. While MAO is believed to be a heterogeneous mixture of different cage structures, recent DFT studies suggest that a two-subunit cage constitutes a major portion of the material and activates olefin polymerization catalysts at two specific sites (Chart 1-6).[53]

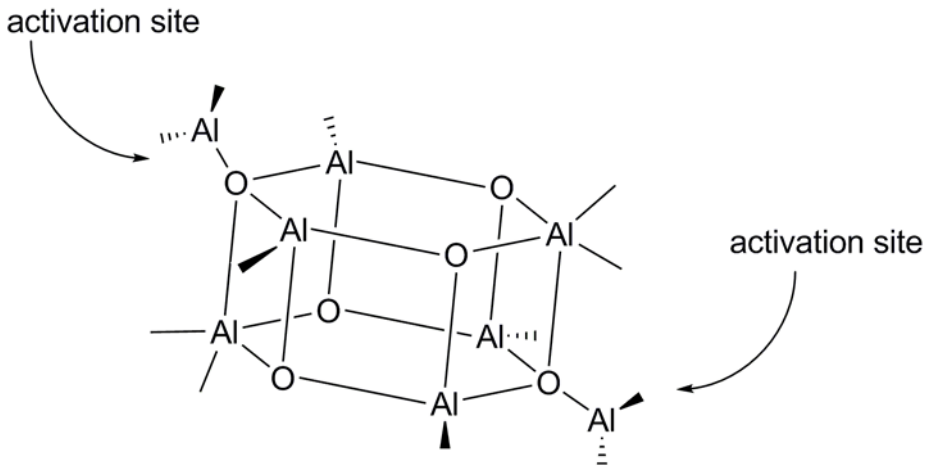

Chart 1-6: A cage structure containing two $Al_4O_3Me_6$ subunits.

The behaviour of MAO as an activator is attributed to its ability to abstract anionic functionalities from neutral complexes, as alkylaluminum reagents do. It exists in a complex equilibrium involving various side reactions and intermediate species (Scheme 1-10).[51] A vast excess of MAO is typically required to produce optimal polymerization activity for a catalyst, which may be partially attributed to this complex equilibrium, and partially to the existence of both active and inactive forms of MAO in solution.[52,53] Despite its ill-defined structure, convoluted mechanism of activation, and poor atom economy (in the sense that many equivalents of MAO are needed to activate a single equivalent of catalyst), MAO

does dramatically improve the reactivity of olefin polymerization catalysts and has thus achieved widespread use in academia and industry.[51]

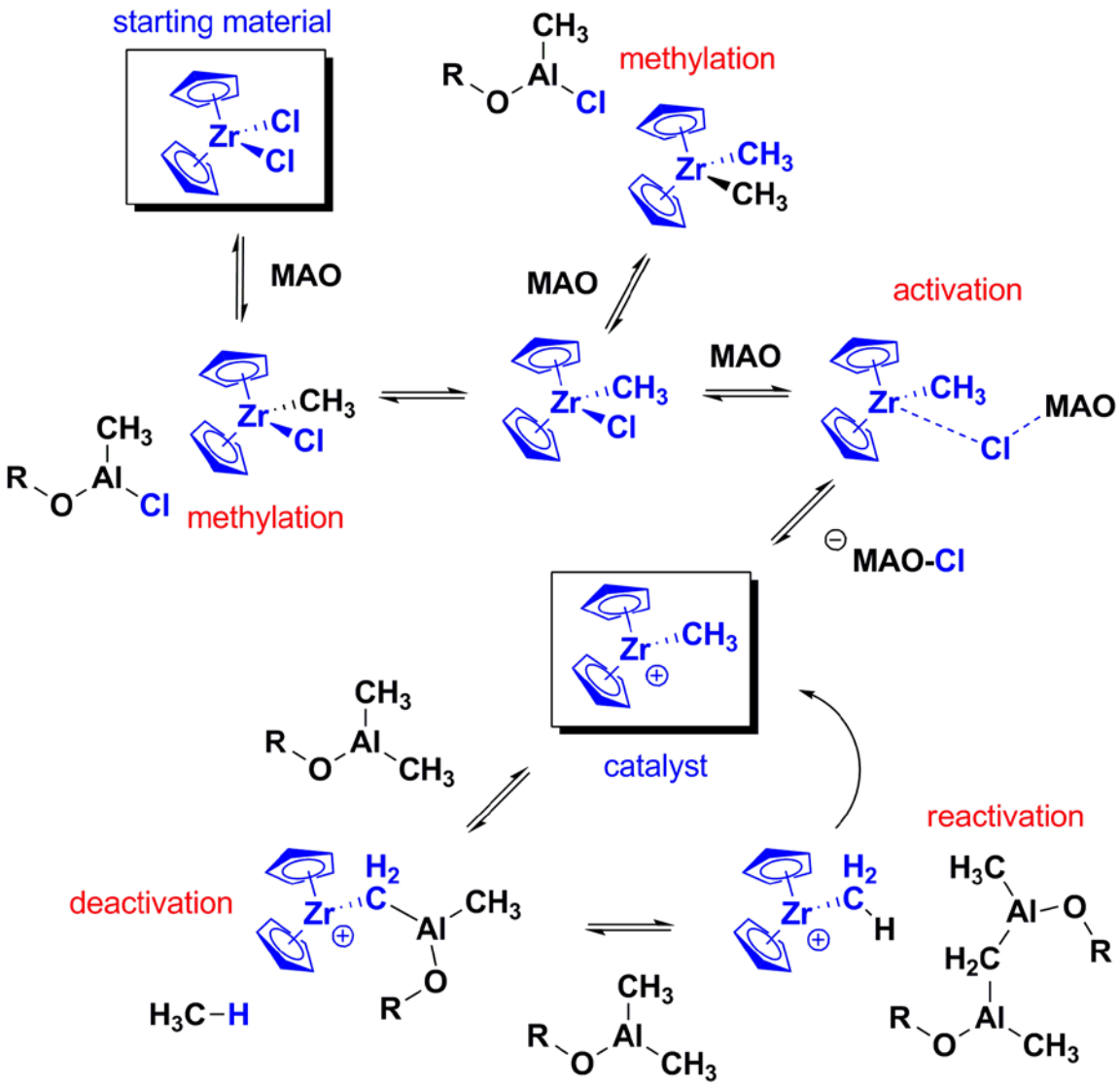

Scheme 1-10: The complex equilibrium formed in the activation of zirconocene catalysts using methylaluminoxane.

Perfluoroarylborane (FAB) activators are also among the most efficient and heavily-utilized activating reagents for olefin polymerization catalysis. Application of FAB activators to zirconocene-mediated polymerization was first

reported in the early 1990s.[54,55] Perfluoroarylborane activators function in a conceptually similar manner to alkylaluminum-based activators. They are Lewis acids and abstract alkyl moieties from the pre-catalyst to generate a formal positive charge while reducing steric bulk at the metal centre.[44]

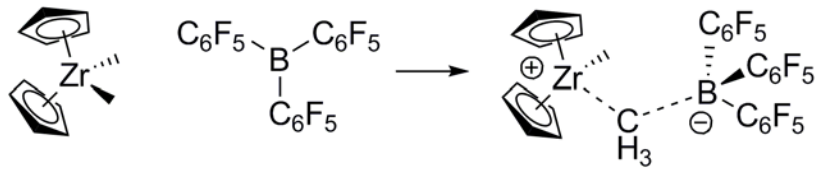

Scheme 1-11: Activation of $[Cp_2ZrMe_2]$ using a FAB activator.

Brønsted acidic species may also activate olefin polymerization catalysts by protonolysis of M–R bonds. A classic example of this approach was reported in 1986 by Bochmann *et al.* (Scheme 1-12) [56,57] in the preparation of the cationic species $[Cp_2TiMe(NH_3)]^+$. This approach has been subsequently applied to production of extremely active olefin polymerization catalysts.[58] While mechanistically quite different, Brønsted-acid activation achieves the same goal as Lewis-acid activation in that it lowers both steric bulk and electron density at the metal centre.

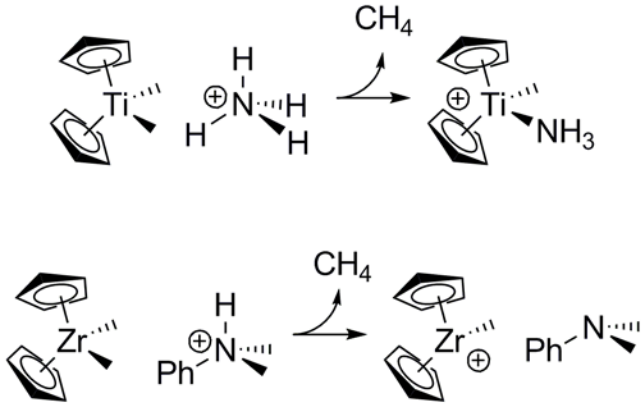

Scheme 1-12: An early example of Ti–R activation using a Brønsted acid (above) and a highly-active zirconocene-based olefin polymerization catalyst employing the same activation strategy (below).

Non-coordinating or very weakly-coordinating anions are generally used in the isolation of cationic activated complexes. This is crucial as a strongly-coordinating anion (a halide, $CF_3SO_3^-$, BF_4^-, ClO_4^-, etc.) would render the complex neutral and defeat the purpose of activation.[57,59] Arylborate derivatives are common counter-ions in this situation as they are sterically bulky (to hinder coordination), relatively soluble in organic solvents, and several variants are commercially available. The simplest example of a tetraarylborate is BPh_4^-. The BPh_4^- anion is generally considered weakly-coordinating but has been known to act as a π-donor ligand (Chart 1-7).[60] The BPh_4^- anion is also prone to phenyl transfer to a cationic centre which is undesirable in the context of catalyst activation.[59] The analogous species $B(C_6F_5)_4^-$ is often used to circumvent these issues as the C_6F_5 group is less prone to transfer and features lower π-system electron density. While $B(C_6F_5)_4^-$ is still capable of π-donation, reduced electron density results in a weaker interaction relative to BPh_4^-. The $B(C_6F_5)_4^-$ anion is also conceptually capable of coordinating to a metal via fluorine lone pairs, although evidence for this coordination mode has only been observed in rare cases and once again suggests only a very weak interaction.[61] Overall, while both BPh_4^- and $B(C_6F_5)_4^-$ may be described as “non-coordinating,” exceptions to this portrayal involving BPh_4^- are more prevalent.

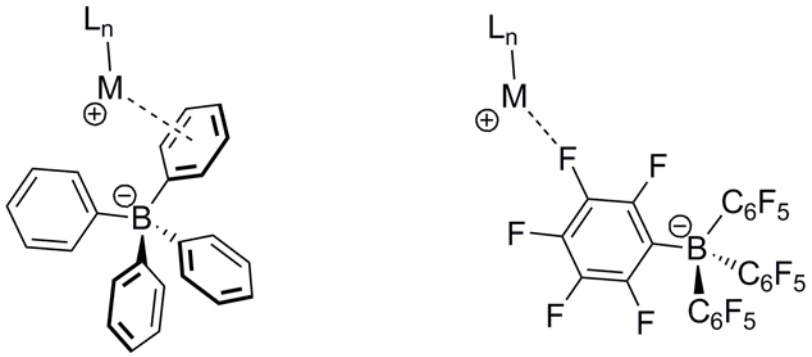

Chart 1-7: BPh_4^- as a π-donor ligand (left) and $B(C_6F_5)_4^-$ coordination through fluorine (right). M = metal centre, L_n = unspecified ancillary.

Borate anions are formed in FAB Lewis-acid activated systems, or may be introduced deliberately into Brønsted acid systems. These species are particularly convenient as ^{11}B NMR spectroscopy may be used to confirm activation of a metal centre. Neutral boranes generally resonate downfield of 0 ppm while analogous anionic borate species resonate upfield of 0 ppm, allowing for facile distinction between the two.[62] Another advantage of perfluoroarylborane anions such as $B(C_6F_5)_4^-$ is that ^{19}F NMR spectroscopy may complement ^{11}B NMR data via the gap in chemical shift between *meta* and *para* ^{19}F resonances ($\Delta\delta_{m,p}$).[63] Differences of < 4 ppm between *meta* and *para* resonances have been demonstrated to indicate a free fluoroarylborate anion, while larger values ($4 < \Delta\delta_{m,p} < 8$ ppm) are indicative of aryl group transfer, yielding a borate.[63-65]

Though a general trend toward high activity of Lewis acidic lactone polymerization catalysts suggests that they may make ideal targets for extension of established catalyst activation protocols,[66] reports of the use of activated lactone polymerization catalysts are extremely sparse in the chemical literature.[42-41] Development of activated species for the polymerization of 6-

caprolactone, lactide, glycolide, and closely related lactones therefore represents a field of enormous potential growth in the near future.

1-5: *Magnesium-Based 6-Caprolactone Polymerization Catalysts*

While tin and aluminum-based systems have traditionally dominated lactone polymerization, magnesium-based catalysts have become increasingly attractive due to low toxicity and cost coupled with high polymerization activity. Magnesium complexes featuring a anionic “heteroscorpionate” (HSC) ancillary ligand type have been successfully used in 6-caprolactone polymerization catalysis (Chart 1-8).[12] It should be noted that this complex design bears a structural resemblance to (tris(pyrazolyl)hydroborato)magnesium alkyl species first described by Parkin *et al*.[67,68] and subsequently applied to lactide polymerization.[69]

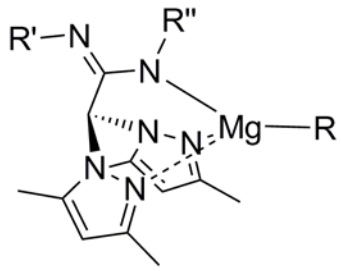

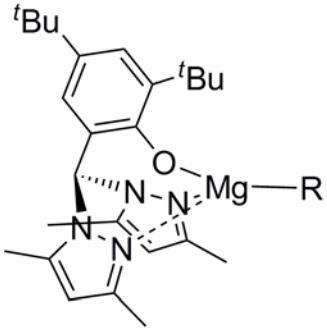

HSC-1: R = Et, R' = ^{t}Bu, R" = ^{n}Pr
HSC-2: R = Et, R' = ^{t}Bu, R" = ^{t}Bu
HSC-3: R = Et, R' = ^{t}Bu, R" = CH_2SiMe_3
HSC-4: R = R' = ^{i}Pr, R" = ^{n}Pr
HSC-5: R = R' = ^{i}Pr, R" = ^{t}Bu
HSC-6: R = R' = ^{i}Pr, R" = CH_2SiMe_3

HSC-7: R = $N(SiHMe_2)_2$
HSC-8 : R = ^{n}Bu

Chart 1-8: Selected examples of magnesium catalysts featuring HSC ligand types.

Table 1-4: Comparison of Magnesium-Based 6-caprolactone Polymerization Catalysts Featuring Heteroscorpionate Ligand Types at Ambient Temperature.

Species	Catalyst Loading (%)	Time	Conversion (%)	M_W (x 10^4 g/mol)	PDI (M_w/M_n)	Ref.
HSC-1	0.20	15 min	84	3.4	1.16	12
HSC-2	0.20	15 min	96	4.7	1.27	12
HSC-3	0.20	1 min	97	5.2	1.41	12
HSC-4	0.20	10 min	86	3.8	1.21	12
HSC-5	0.20	10 min	97	5.1	1.33	12
HSC-6	0.20	10 s	98	2.1	1.45	12
HSC-7	1.00	"immediate"	"quantitative"	8.6	2.76	70
HSC-8	1.00	"extended period"	> 10	NA	NA	70

The series **HSC-1** to **HSC-6** has been shown to be highly active in PCL production and polymers isolated from these systems are relatively monodisperse (PDI = 1.2 to 1.5), suggesting a well-controlled polymerization process. Within this series, systems with R = R' = ^{i}Pr appear consistently more active than analogous catalysts with R = Et, R' = ^{t}Bu (Table 1-4). This variation in activity was attributed to the steric demands of the ^{t}Bu group relative to ^{i}Pr in the R' position. Additionally, species with R'' = CH_2SiMe_3 showed remarkably enhanced activity relative to species with ^{n}Pr or ^{t}Bu at the R'' site. This was accompanied by a mild increase in polydispersity, suggesting a small trade-off in polymerization control.

Another set of noteworthy heteroscorpionate-derived magnesium complexes which has been found to be active in 6-caprolactone polymerization (**HSC-7** and **HSC-8**) has been reported separately.[70] This system also boasts high reactivity in the case of **HSC-7**; however, the resulting polymers were quite polydisperse in molecular weight (PDI = 2.76). This is attributed by the authors of

the study to slow initiation relative to chain propagation. The altered initiator of **HSC-8** gives rise to even slower initiation and in far lower activity than **HSC-7**. It is difficult to ascertain the influence of the ligand employed by **HSC-7** and **HSC-8** relative to **HSC-6** as the initiator group of **HSC-7** is not analogous between the two systems and seems to bear a direct influence on polymerization.

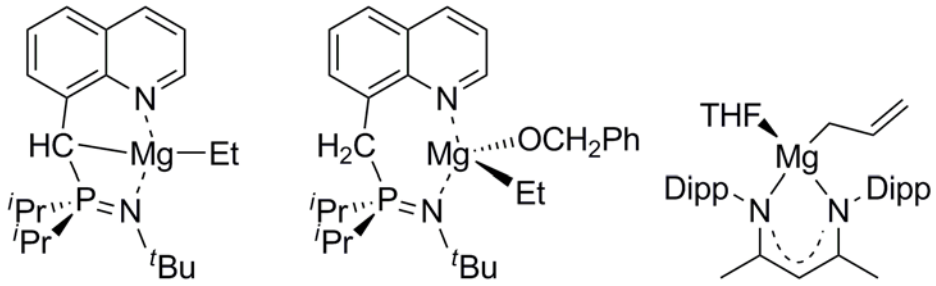

Chart 1-9: Magnesium complexes featuring the "IPQM" and "NAC" ligand types.

Table 1-5: Organomagnesium catalysts featuring "NAC" and "IPQM" ligands in the Polymerization of 6-caprolactone at 0 ºC.

Species	Catalyst Loading (%)	Time	Conversion (%)	M_W (x 10^4 g/mol)	PDI (M_w/M_n)	Ref.
IPQM-1	0.50	3 min	100	29.6	1.16	71
IPQM-2	0.50	4 min	100	16.0	1.32	71
NAC-1	0.50	6 min	92	2.75	1.4	72

Several recent examples of organomagnesium catalysts (Chart 1-9) remain highly active in 6-caprolactone polymerization even at low temperature (Table 1-5).[71,72] Examples of these species feature "Nac-Nac" and Iminophosphorano(8-quinolyl)methanide (IPQM) ligand types. The species **NAC-1** is highly active, producing polymers with molecular weights as high as 2.75 x 10^4 g/mol in minutes at 0 ºC. Catalyst **IPQM-1** is active for 6-caprolactone polymerization both in the presence and absence of an alcohol co-catalyst (the

addition of which has been found to result in the formation of **IPQM-2** *in situ*). Catalysts **IPQM-1** and **IPQM-2** display similar activity and polymerization control (PDI = 1.3 and 1.2, respectively) and produce high molecular weight polymers (up to $M_w = 29.6 \times 10^4$ g/mol).

A noteworthy cationic magnesium alkyl, $[(Et_2O)_3Mg^nBu]^+$ has been evaluated as a 6-caprolactone polymerization catalyst. It has been previously reported along with its cationic magnesium amido analogue, $[(Et_2O)_3MgN(SiMe_3)_2]^+$ and analogous zinc-containing species.[73] All species were synthesized as $[B(C_6F_5)_4]^-$ salts. While the zinc-containing analogues were found to be suitable catalysts for both 6-caprolactone and lactide polymerization, no polymerization was observed with respect to magnesium-containing species (which decomposed rapidly upon exposure to 6-caprolactone). This is attributed by the authors of the study to the magnesium complexes' higher reactivity, presumably resulting in dominant side-reactions. This negative result serves to reinforce the importance of a suitable ancillary ligand which regulates processes at the catalytic centre in order to promote desired (catalytic) over undesired (decomposition) processes.

Organomagnesium complexes have shown exceptionally high activity in the polymerization of 6-caprolactone, producing high MW polymers with low to moderate polydispersity. Unlike aluminum and tin-based systems, which typically require elevated temperatures for optimal activity, magnesium-based catalysts are often highly active at, and even below, ambient temperature. While promising results have been seen in the application of magnesium alkyl complexes to 6-

caprolactone polymerization, note that all catalytically active organomagnesium species discussed thus far have been neutral in charge. In addition to a technical challenge, synthesis of cationic organomagnesium complexes represents an opportunity to study 6-caprolactone polymerization in a new chemical environment – potentially allowing for access to even more highly active catalysts while maintaining control of the polymerization process via incorporation of an ancillary ligand.

1-6: *Thesis Outline*

The fundamental goal of the new work described herein was development of novel species which extend olefin polymerization catalyst activation strategies into the realm of lactone polymerization. The catalyst design was intended to employ highly active, inexpensive, and non-toxic metal species. By these criteria, magnesium was selected as the metal centre. An ancillary ligand design which could be readily modified to influence catalytic activity was also necessary in order to provide a means of influencing these processes. This project may be divided into three distinct phases.

1.) Design, synthesis and characterization of a novel ligand series.

2.) Synthesis and characterization of corresponding activated organometallic species to be employed as catalysts.

3.) Preliminary evaluation of catalytic efficacy and activity of these species.

A completely new series of ancillary ligands (four of which are described in Chapter 2) has been successfully synthesized and fully characterized using

multinuclear NMR spectroscopy and X-ray crystallography. Although unexpected difficulty arose in the isolation of neutral pre-catalysts, a direct route to activated cationic complexes was found and cationic organomagnesium species bearing one of the aforementioned ligand types have been successfully isolated and fully characterized. These organomagnesium species were found to be highly active in the polymerization of 6-caprolactone and preliminary evaluation of their utility as lactone polymerization catalysts has been accomplished.

Chapter 2

Synthesis and Reactivity of Phosphinimine and Bisphosphinimine Ligands

---

2-1: *Phosphinimine Chemistry and Ligand Design*

Phosphinimines‡ (species containing a formal phosphorus-nitrogen double bond) have been known since the early 20th century.[74,75] They are traditionally prepared by a Staudinger reaction (the reaction of a phosphine with an azide) although a number of alternative syntheses have since been developed.[76-79] The mechanism of the Staudinger reaction has long been thought to involve initial nucleophilic attack on the azide species by the phosphine.[80] Recent DFT computational studies strongly support a mechanism whereby nucleophilic attack first occurs at the terminal nitrogen atom, followed by formation of a cyclic transition state before the final P=N bond is introduced and dinitrogen gas is released as a byproduct (Scheme 2-1).[81]

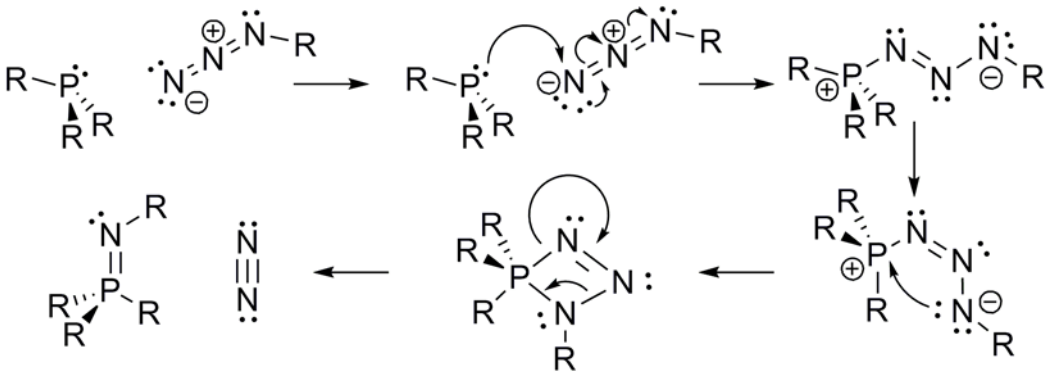

Scheme 2-1: Mechanism of the Staudinger reaction via nucleophilic attack at the terminal nitrogen atom (adapted from Wang, 2004).

‡ Note that this type of species is more accurately named "phosphoranimine," though the term "phosphinimine" is far more common in the chemical literature. "Phosphinimine" will be used throughout this work due to literature precedent.

Phosphinimines are known to behave similarly to phosphorus ylides, structurally analogous species containing a formal carbon-phosphorus double bond, particularly in their reactivity toward carbonyl-containing species. The reaction of a phosphinimine with a carbonyl functionality is analogous to the Wittig reaction, and proceeds via a similar four-membered transition state. Phosphinimines are also known to protonate at nitrogen when exposed to Brønsted acids.[80,82]

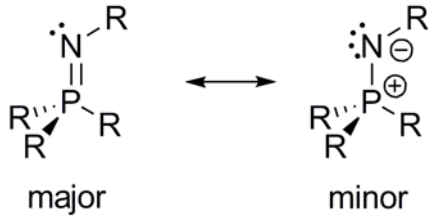

Figure 2-1: Phosphinimine resonance structures.

Phosphinimines make excellent ligands in coordination chemistry as they are able to strongly donate electron density to a metal centre (Figure 2-1). In addition, they are known to be thermally robust and may be readily assembled in a modular manner.[83-86] By virtue of the inclusion of phosphorus, phosphinimine-containing species may be characterized using ^{31}P NMR spectroscopy. This provides a useful spectroscopic handle when characterizing new phosphinimine-containing ligands and complexes, as the ^{31}P NMR resonance is sensitive to coordination, generally resulting in a downfield shift of 13 to 45 ppm upon coordination to a metal centre.[87-91,71] The first examples of well-defined metal-phosphinimine complexes emerged in the 1960s.[80] Various complexes of main-group species (aluminum,[92,93] gallium,[92,93] germanium,[94-96] indium,[93] tin,[96] antimony,[96] bismuth,[96] lead,[96] and tellurium[97]) as well as transition-metal

complexes (vanadium,[98] cobalt,[99,100] nickel,[99] copper,[99] zinc,[101] molybdenum,[102] palladium,[103] cadmium,[101,104] tungsten,[102] platinum,[105] and mercury[104]) were reported over the subsequent three decades.

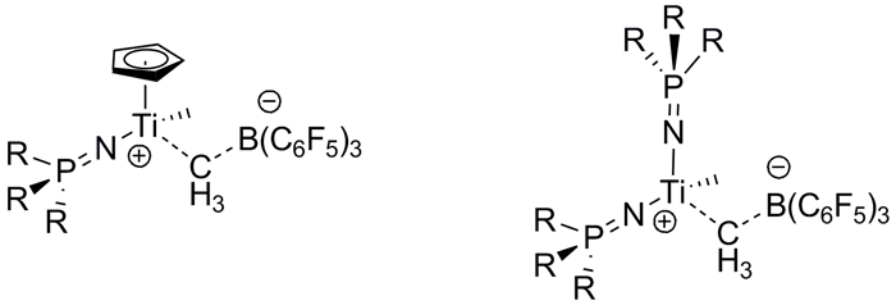

Chart 2-1: Structures of the first transition metal-phosphinimide complexes applied to olefin polymerization (R = Ph).

Arguably the most influential application of such coordination complexes was the use of early transition-metal phosphinimines and phosphinimides (closely related ligands bearing a formal negative charge on nitrogen) in the polymerization of olefins in the late 1990s.[106,107] The application was originally made using titanium-phosphinimide complexes developed in the Stephan group (Chart 2-1).[106,107] These highly active catalysts have found subsequent use in industrial olefin-polymerization protocols.

Applications of metal-phosphinimine coordination complexes to lactone polymerization include the use of *bis*phosphiniminomethane (BPM) zinc[108] complexes in lactide polymerization and zinc and magnesium phosphinimine complexes[109] in the polymerization of 6-caprolactone (Chart 2-2).

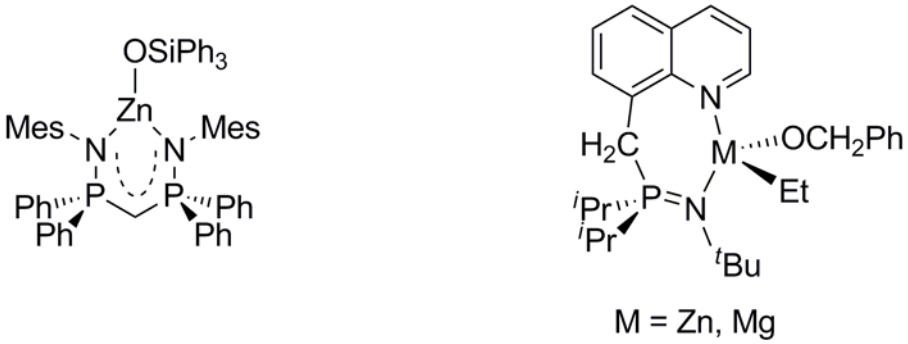

Chart 2-2: Selected phosphinimine-containing coordination complexes utilized for lactone polymerization.

As phosphinimine-containing species have shown promise in coordination chemistry and catalysis, the development of novel phosphinimine-based ligands presents the opportunity to contribute to a wide array of applications. Toward this goal, a new family of *mono* and *bis* phosphinimine species has been developed incorporating a substituted heterocyclic backbone structure. The design of these species and specific synthesis of four variants will be discussed, followed by examination of their efficacy in formation of magnesium-based complexes.

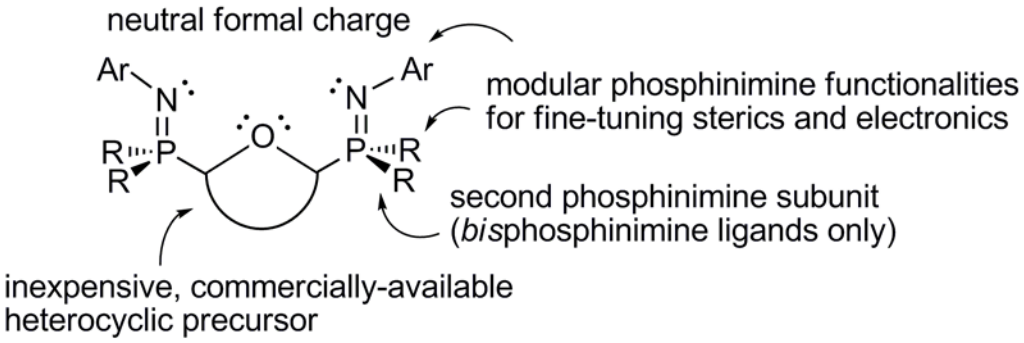

Chart 2-3: Generic ligand structure and key features targeted for synthesis.

The ligands described herein (Chart 2-3) were synthesized in a manner intended to allow for facile modification of phosphinimine substituents. In turn, this would present the opportunity to fine-tune the steric and electronic environment of resultant catalysts, granting a degree of rational control over their

behaviour. The “backbone” structures, derived from inexpensive, commercially available heterocyclic precursors, were intended to support one or two phosphinimine moieties. *Mono*phosphinimine ligand types would allow for subsequent facile installation of chiral groups; a key feature in the future development of stereospecific lactide polymerization catalysts. Symmetric *bis*phosphinimine ligands were intended to provide stronger electron donation via the incorporation of an additional coordination site. With slight modification, the employed synthetic strategy might also be used to produce asymmetric *bis*phosphinimine ligands, which would allow even greater flexibility in catalyst design.

The ligands synthesized possess an overall neutral charge. This key feature allows for use of cationic, divalent complexes in lactone polymerization as such a complex could necessarily only support one anionic moiety: the polymerization initiator (assuming a CIN polymerization mechanism). Additionally, use of a neutral ancillary would ensure that the intended initiator, not the ancillary itself, would become bound to the inactive terminus of a growing polylactone. This might help prevent circumstances such as those observed with cationic aluminum 6-caprolactone polymerization catalysts (Chapter 1-3) wherein the ancillary unintentionally acted as a polymerization initiator, eliminating its ability to exert any control whatsoever over the catalytic centre.

As these ligands were intended to provide a means of regulating processes which occur at a metal centre, their ability to attach and remain bound

to a metal is crucial to their utility. The proposed attachment scheme (Scheme 2-2) outlines the synthesis and activation of a generic organomagnesium complex.

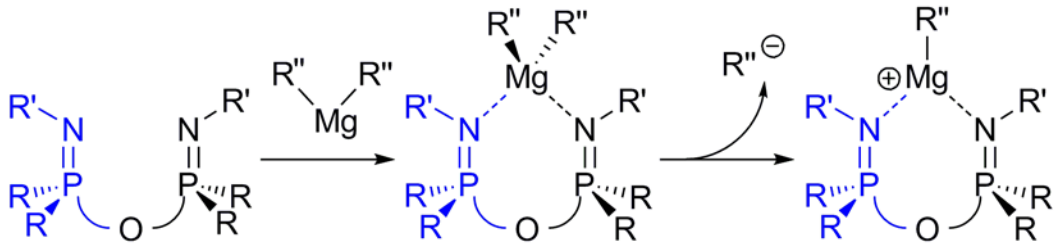

Scheme 2-2: Proposed synthesis of cationic complexes via activation of a neutral complex (Note: simplified ancillary ligand architecture. R = anionic ligand.) Blue fragments apply only to *bis*phosphinimine systems.

A series of four novel ligands (Chart 2-4) - two *mono*phosphinimine and two *bis*phosphinimine variants - will be discussed herein. The *mono*phosphinimine ligands, both dibenzofuran derivatives, are highly analogous with the exception of the nitrogen substituent group (Ar = Dipp, Mes). The ligands 4-((2,6-di*iso*propylphenyl)diphenylphosphinimino)dibenzofuran (DippN=PPh_2dbf, **L_1**) and 4-((2,4,6-trimethylphenyl)diphenylphosphinimino)dibenzofuran (MesN=PPh_2dbf, **L_2**) were synthesized as described in Chapter 2-2 and Chapter 5-2. The *bis*phosphinimine ligands consisted of one furan derivative and one dibenzofuran derivative. Synthesis of the species 2,5-*bis*((2,6-di*iso*propylphenyl)diphenylphosphinimino)furan ($(DippN=PPh_2)_2$furan, **L_3**) and 4,6-*bis*((2,4,6-trimethylphenyl)diphenylphosphinimino)dibenzofuran ($(MesN=PPh_2)_2$dbf, **L_4**) are described in Chapters 2-3 and 2-4, respectively as well as Chapter 5-2.

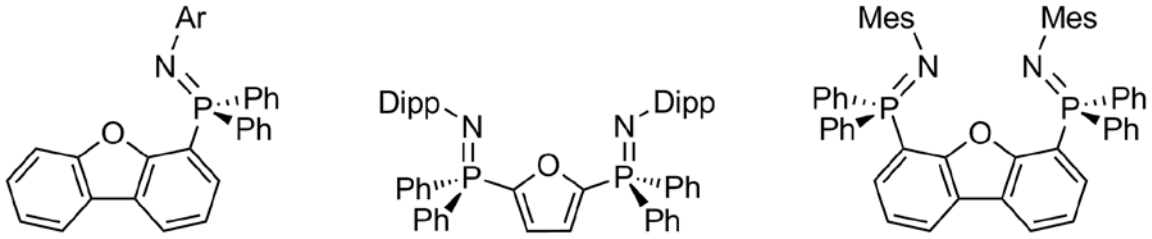

L_1: Ar = Dipp
L_2: Ar = Mes

L_3

L_4

Chart 2-4: Target *mono*phosphinimine (**L_1**, **L_2**) and *bis*phosphinimine (**L_3**, **L_4**) ligand structures synthesized. Note: Dipp = 2,6-di*iso*propylphenyl, Mes = 2,4,6-trimethylphenyl (mesityl).

2-2: *Development of Monophosphinimine Ligands*

Both **L_1** and **L_2** were synthesized using the same two-step approach (Scheme 2-3) and were isolated in high yield (92% and 69%, respectively). Selective lithiation of the "4" position of dibenzofuran was accomplished by treating it with excess ^{t}butyllithium under rigorously anaerobic conditions in diethyl ether.

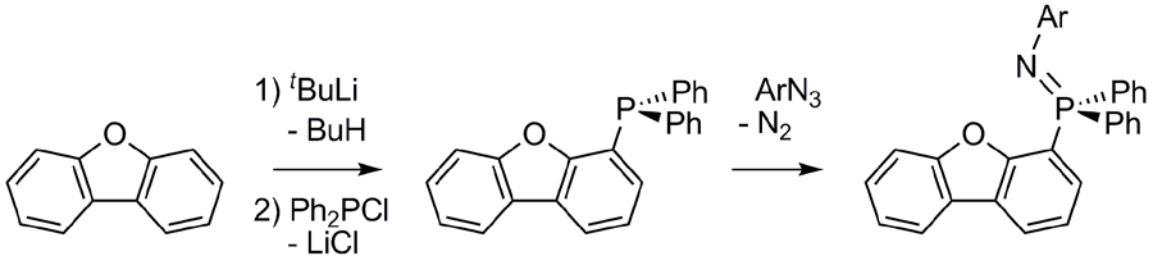

Scheme 2-3: Synthesis of **L_1** or **L_2** (Ar = Dipp, Mes) from dibenzofuran.

The reaction was initiated at low temperature (–78 ºC) by dropwise addition of a solution (in pentane) of the alkyllithium reagent, warmed slowly to ambient temperature and allowed to stir over 16 subsequent hours. The reaction was then quenched with excess Ph_2PCl at –78 ºC, warmed to ambient

temperature and allowed to stir for eight additional hours to afford the desired phosphine. Subsequently, isolated 4-$(PPh_2)_2$dibenzofuran was allowed to react with excess $DippN_3$ or $MesN_3$ in toluene over 12 hours at ambient temperature.

The ligands DippN=PPh_2dbf and MesN=PPh_2dbf were characterized using ^1H, $^{31}P\{^1H\}$, and $^{13}C\{^1H\}$ NMR spectroscopy with assignment facilitated by supporting techniques including **d**istortionless **e**nhancement by **p**olarization **t**ransfer (DEPT), **co**rrelation **s**pectroscop**y** (COSY), and **h**eteronuclear **s**ingle **q**uantum **c**oherence (HSQC). The ^{31}P NMR spectra of $\mathbf{L_1}$ and $\mathbf{L_2}$ each depicted a single resonance at –13.4 and –15.3 ppm, respectively. In both cases, the nitrogen-substituent aryl group proved to be a useful ^1H and ^{13}C NMR spectroscopic handle with well-resolved resonances. The Dipp *iso*propyl group and Mes methyl groups were particularly useful in this regard (Table 2-1).

Table 2-1: Selected NMR data for $\mathbf{L_1}$ and $\mathbf{L_2}$ (benzene-d_6).

Nucleus	Assignment	$\mathbf{L_1}$ (δ) [110]	Assignment	$\mathbf{L_2}$ (δ)
^{31}P	P	–13.4 (s)	P	–15.3 (s)
^1H	*m*-Dipp	7.18 (m)	*m*-Mes	6.88 (s)
	Dipp C***H***$(CH_3)_2$	3.68 (sp)	*p*-Mes C***H***$_3$	2.30 (s)
	Dipp CH(C***H***$_3)_2$	1.06 (d)	*o*-Mes C***H***$_3$	2.21 (s)
^{13}C	*o*-PPh_2	132.9 (d)	*o*-Ph	132.8 (d)
	m-PPh_2	132.2 (d)	*m*-Ph	132.4 (d)
	p-PPh_2	124.6 (d)	*p*-Ph	124.7 (d)
	Dipp ***C***H$(CH_3)_2$	29.5 (s)	*p*-Mes C(***C***H$_3$)	21.3 (s)
	Dipp CH(***C***H$_3)_2$	24.3 (s)	*o*-Mes C(***C***H$_3$)	22.0 (s)

Single crystals of both DippN=PPh_2dbf[110] and MesN=PPh_2dbf were obtained and X-ray crystal structures (Figure 2-2) were collected. No substantial

deviations between key bond lengths and angles (Table 2-2)[§,111] of the two were found. The phosphorus-nitrogen interatomic distances (~1.55 Å for each) were consistent with a formal bond order of two.[**87-91]

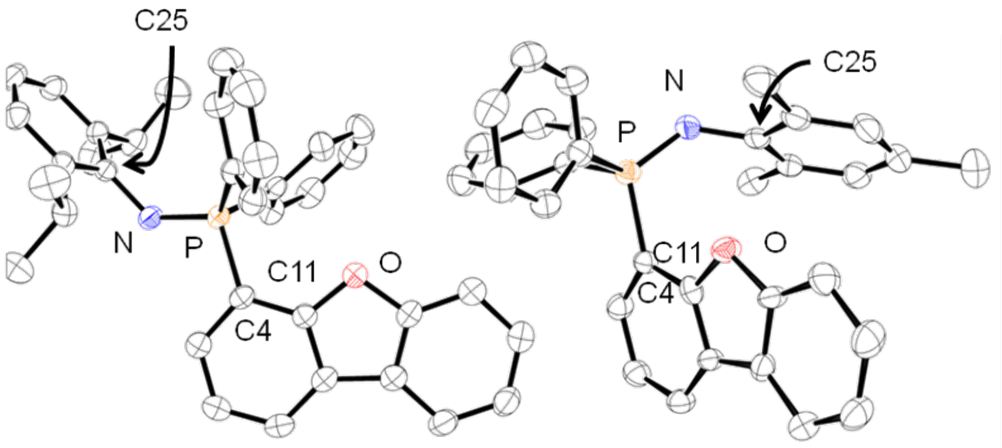

Figure 2-2: X-ray crystal structures of DippN=PPh$_2$dbf (left) and MesN=PPh$_2$dbf (right). (50% probability ellipsoids, H atoms omitted for clarity).

There was, however, a significant deviation in the orientation of the phosphinimine substructure which is evident in the corresponding torsion angles about the C4–P and P–N bonds. In the case of **L$_1$**, the aryl group was oriented away from the binding cavity (C11–C4–P–N torsion = 168.0(2)º, C4–P–N–C25 torsion = 155.7(2)º) whereas the mesityl group of **L$_2$** was situated largely within the binding cavity (C11–C4–P–N torsion = 62.6(4)º, C4–P–N–C25 torsion = 22.7(5)º). One would expect that while neither species exists in an ideal binding

§ Note that by convention, X-ray structure metrical parameters are reported such that estimated standard deviation (ESD, shown in brackets) applies to the final decimal place reported. For example 1.801(2) Å is interpreted as 1.801 Å (ESD = 0.002 Å). The standard deviation for a bond length, bond angle, or torsion angle is dependent on the standard deviations of associated atomic fractional coordinates and corresponding unit cell parameters.

** A phosphourus-nitrogen double bond length is generally 1.54 to 1.62 Å.

geometry in the solid state, either may be able to rotate in solution to accommodate coordination to a metal centre.

Table 2-2: Selected metrical data for the crystal structures of $\mathbf{L_1}$[110] and $\mathbf{L_2}$.[††]

Bond Lengths	**L_1 value(ESD)**	**L_2 value(ESD)**
C4–P	1.801(2) Å	1.816(2) Å
P–N	1.559(2) Å	1.551(2) Å
N–C25	1.409(3) Å	1.407(3) Å
Bond Angles		
C11–C4–P	123.4(2)º	119.1(2)º
C4–P–N	106.9(1)º	116.4(2)º
P–N–C25	127.2(2)º	129.8(1)º
Torsion Angles		
O–C11–C4–P	7.6(3)º	1.3(6)º
C11–C4–P–N	168.0(2)º	62.6(4)º
C4–P–N–C25	155.7(2)º	22.7(5)º

2-3: *Synthesis of (DippN=PPh_2)$_2$furan*

Of the *bis*phosphinimine ligands, (DippN=PPh_2)$_2$furan,[112] was first targeted due to the commercially available, inexpensive materials required for its synthesis. Selective lithiation of furan (C_4H_4O) at the 2 and 5 positions[113,114] was initiated at low temperature (–78 ºC) by dropwise addition of 2.1 equivalents of ^{t}BuLi (solution in pentane) under rigorously anaerobic conditions in diethylether. The reaction mixture was warmed slowly to ambient temperature and allowed to stir for 16 hours. The reaction was then cooled to –78 ºC, quenched with 2.1

[††] The unit cell of $\mathbf{L_2}$ contains two non-degenerate structures. Although not crystallographically equivalent, selected bond lengths and angles are within ESD (except torsion angles which are of opposite sign - absolute values reported). For the sake of simplicity, one has been arbitrarily chosen for discussion. See Appendix 2 for full crystallographic details.

equivalents of Ph_2PCl, warmed to ambient temperature and allowed to stir for eight additional hours to afford the desired diphosphine. Subsequent reaction of 2,5-((PPh$_2$)$_2$furan) with 2.1 equivalents of $DippN_3$ in toluene generated the requisite phosphinimine (Scheme 2-4) in 12 hours at ambient temperature.

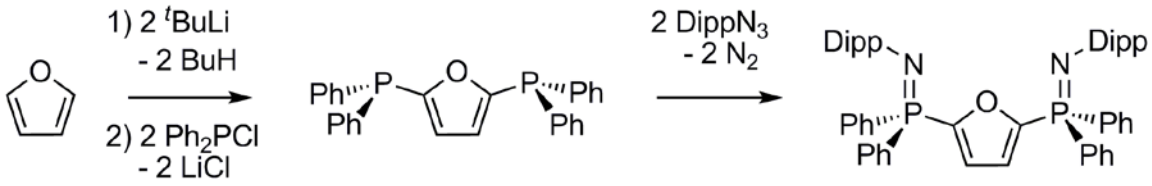

Scheme 2-4: Synthesis of **L_3** from furan.

A characteristic single ^{31}P NMR resonance at –24.9 ppm was observed, suggesting overall C_{2v} symmetry in solution. The ^{1}H and $^{13}C\{^{1}H\}$ NMR spectra were consistent with C_{2v} symmetry, most clearly illustrated by *iso*propyl methyne and methyl ^{1}H resonances at δ 3.55 and δ 1.10 ppm, respectively. Corresponding $^{13}C\{^{1}H\}$ NMR resonances were observed at 29.1 and 23.9 ppm.

Table 2-3: Selected NMR data for **L_3** (benzene-d_6).

Nucleus	Assignment	L_1 (δ)
^{31}P	P	–24.9 (s)
^{1}H	*m*-Dipp	7.23 (d)
	o-Dipp C***H***$(CH_3)_2$	3.55 (sp)
	o-Dipp CH(C***H***$_3)_2$	1.10 (d)
^{13}C	*o*-Ph	132.1 (d)
	m-Ph	120.4 (d)
	p-Ph	131.5 (d)
	Dipp ***C***$H(CH_3)_2$	29.1 (s)
	Dipp CH(***C***$H_3)_2$	23.9 (s)

Single crystals of **L_3** were grown and the X-ray crystal structure (Figure 2-3) was obtained.[112] Key bond lengths and angles of the phosphinimine moiety were similar to those observed for **L_1** and **L_2** (Table 2-2, Table 2-4). In this

structure, the P=N bonds were rotated substantially from the ideal bonding geometry (C4–P1–N1–C30 torsion = 27.0(2)º) resulting in the Dipp groups resting largely within the cavity designed to hold the metal centre. This is attributed to packing within the crystal structure.

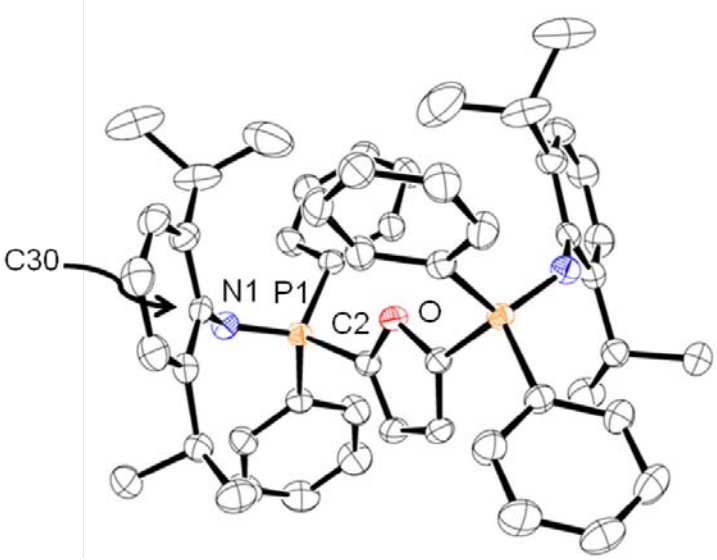

Figure 2-3: X-ray crystal structure of (DippN=PPh_2)$_2$furan (50% probability ellipsoids, H atoms omitted for clarity).

Table 2-4: Selected metrical data for the crystal structure of **L_3**.

Bond Lengths	**Value (ESD)**
C2–P1	1.806(1) Å
P1–N1	1.550(1) Å
N1–C30	1.408(2) Å
Bond Angles	
O–C2–P1	119.98(9)º
C2–P1–N1	115.37(6)º
P1–N1–C30	130.9(1)º
Torsion Angles	
O–C2–P1–N1	69.2(2)º
C2–P1–N1–C30	27.0(2)º

2-4: *Synthesis of $(MesN{=}PPh_2)_2$dibenzofuran*

A second *bis*phosphinimine was synthesized, this time derived from dibenzofuran. The ligand $(MesN{=}PPh_2)_2$dbf (**L_4**) was intended to differ from **L_3** in two ways: a decreased bite angle resultant from the altered backbone structure (Chart 2-5) and decreased steric bulk at the nitrogen substituent.

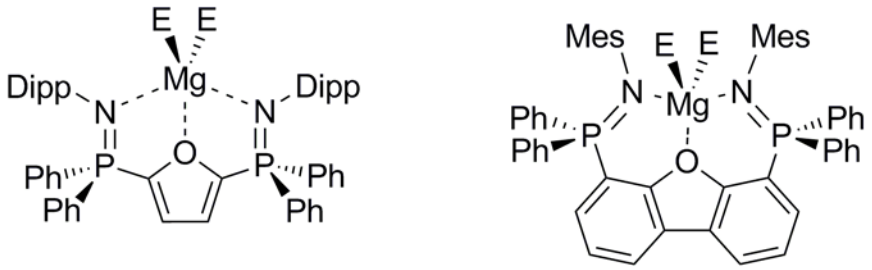

Chart 2-5: Comparison of target structures [**L_3**MgE_2] and [**L_4**MgE_2] (E = halide, alkyl, alkoxide, etc.). Note the tighter bite angle of **L_4**.

Synthesis of $(MesN{=}PPh_2)_2$dbf (Scheme 2-5) was accomplished in an analogous manner to the previously described species. Lithiation of dibenzofuran at the 4 and 6 positions was accomplished using 2.5 equivalents of ^{sec}BuLi in the presence of tetramethylethylenediamine (TMEDA).[‡‡] The reaction was initiated at low temperature (–78 ºC) by dropwise addition of the alkyllithium reagent (in pentane solution). The reaction mixture was warmed slowly to ambient temperature and stirred for eight hours. Subsequently, the reaction mixture was cooled to –78 ºC and quenched with 2.5 equivalents of Ph_2PCl and allowed to warm slowly to ambient temperature. The reaction mixture was then allowed to

[‡‡] Excess ^{t}butyllithium will produce the same phosphine as ^{sec}butyllithium; however, workup to remove the decomposition products of excess butyllithium reagents has been found to be higher-yielding in the latter case. Also note that unlike furan, dilithiation of dibenzofuran does not occur readily and requires the addition of a promoting reagent (TMEDA).

stir for 12 additional hours to afford the desired diphosphine. Subsequent reaction of the isolated diphosphine with excess $MesN_3$ in toluene was found to generate the requisite *bis*phosphinimine in 16 hours at 65 ºC.

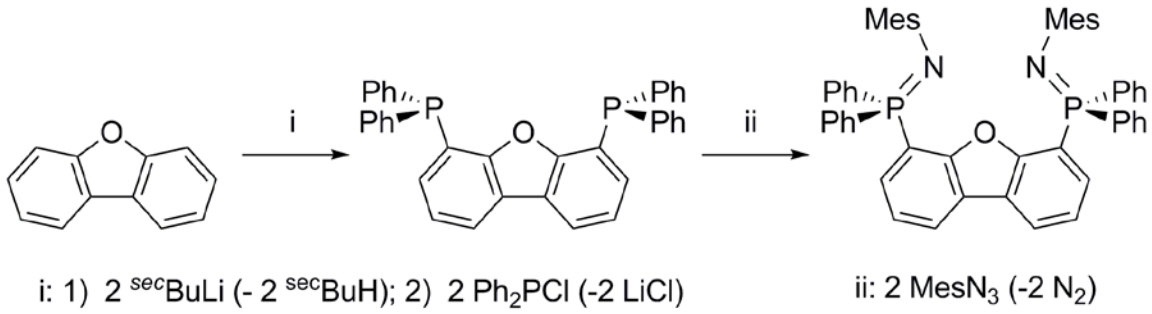

Scheme 2-5: Synthesis of $(MesN{=}PPh_2)_2$dibenzofuran from dibenzofuran.

Table 2-5: Selected NMR data for $\mathbf{L_4}$ (benzene-d_6).

Nucleus	Assignment	L_1 (δ)
^{31}P	P	–17.6 (s)
^{1}H	*m*-Mes	7.02-6.82 (ov)
	p-Mes C***H***$_3$	2.27 (s)
	o-Mes C***H***$_3$	1.93 (s)
^{13}C	*o*-Ph	132.0 (d)
	m-Ph	132.7 (d)
	p-Ph	124.0 (s)
	p-Mes C(***C***H$_3$)	21.0 (s)
	o-Mes C(***C***H$_3$)	21.1 (s)

As was the case with $\mathbf{L_3}$, NMR spectral data suggested overall C_{2v} symmetry in solution. The diagnostic $^{31}P\{^1H\}$ resonance was observed at δ –17.6 and the mesityl group again corroborated the observed symmetry with two well-resolved methyl ^1H NMR resonances at δ 2.27 and 1.93.

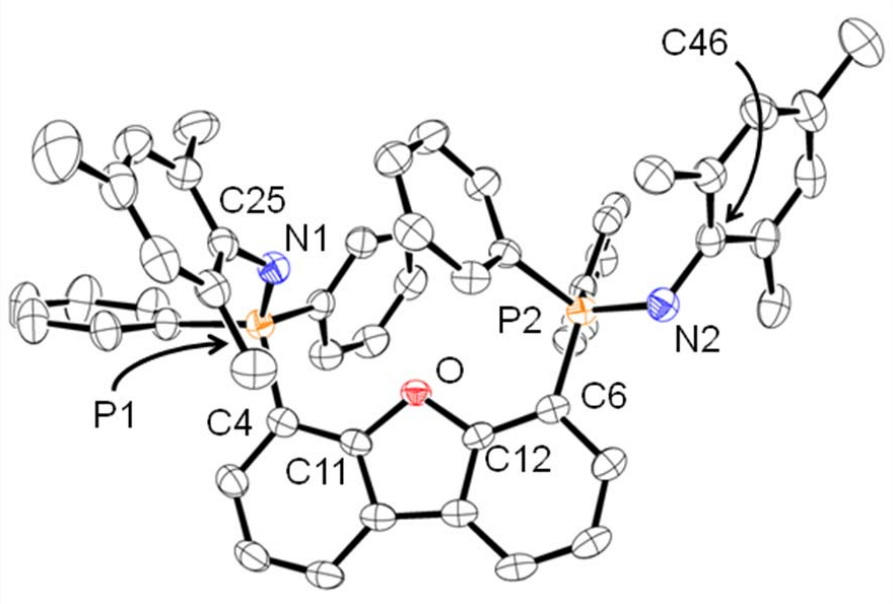

Figure 2-4: X-ray crystal structure of $(MesN{=}PPh_2)_2$dbf (50% probability ellipsoids, H atoms omitted for clarity).

Table 2-6: Selected metrical data for the crystal structure of $(MesN{=}PPh_2)_2$dibenzofuran.[110]

Bond Lengths	Value (ESD)	Bond Lengths	Value (ESD)
C4–P1	1.824(2) Å	**C6–P2**	1.807(2) Å
P1–N1	1.549(1) Å	**P2–N2**	1.565(1) Å
N1–C25	1.405(2) Å	**N2–C46**	1.413(2) Å
Bond Angles		**Bond Angles**	
C11–C4–P1	120.0(1)°	**C12–C6–P2**	126.1(1)°
C4–P1–N1	116.31(7)°	**C6–P2–N2**	105.47(7)°
P1–N1–C25	129.5(1)°	**P2–N2–C46**	112.9(1)°
Torsion Angles		**Torsion Angles**	
O–C11–C4–P1	4.7(2)°	**O–C12–C6–P2**	1.6(2)°
C11–C4–P1–N1	57.1(1)°	**C12–C6–P2–N2**	116.0(1)°
C4–P1–N1–C25	89.4(2)°	**C6–P2–N2–C46**	169.5(1)°

Single crystals of $(MesN{=}PPh_2)_2$dbf were prepared and the X-ray crystal structure (Figure 2-4) was obtained.[110] The P–N bond lengths were again

consistent with a formal bond order of two (1.549(1) Å and 1.565(1) Å). Key bond lengths and angles (Table 2-6) were comparable to those observed for **L_1**, **L_2**, and **L_3**. The structure is not bilaterally symmetric in the solid state, as one phosphinimine moiety is oriented away from the binding site due to rotation about the carbon-phosphorus bond (C12–C6–P2–N2 torsion = 116.0(1)), presumably as a result of steric interaction between mesityl groups.

2-5: *Complexation Studies*

Small-scale reactions of DippN=PPh_2dbf (**L_1**) and MesN=PPh_2dbf (**L_2**) with various magnesium halide and alkylmagnesium precursors were examined. NMR techniques (particularly $^{31}P\{^1H\}$ NMR) were used to detect the presence of new species *in situ* and track reaction progress.

The ligand DippN=PPh_2dbf (**L_1**) was found to react with [$MgBr_2(OEt_2)$] at elevated temperature in a mixture of 9:1 benzene-d_6 : tetrahydrofuran-d_8 giving rise to a product which could be readily observed by a diagnostic ^{31}P NMR resonance at δ 33.6 (~46 ppm downfield of the neutral ligand). Reaction rates were found to be extremely low, however. At 52 ºC, a stoichiometric reaction of **L_1** with [$MgBr_2(OEt_2)$] resulted in only ~35% conversion (based on relative $^{31}P\{^1H\}$ NMR peak integration) of the ligand to a single product over five days with negligible progress over three subsequent days (Figure 2-5). This suggested the establishment of an equilibrium state. Exploration of alternate temperatures (25 ºC to 80 ºC) consistently gave rise to the same product, but a substantial change in reaction rate was not observed.

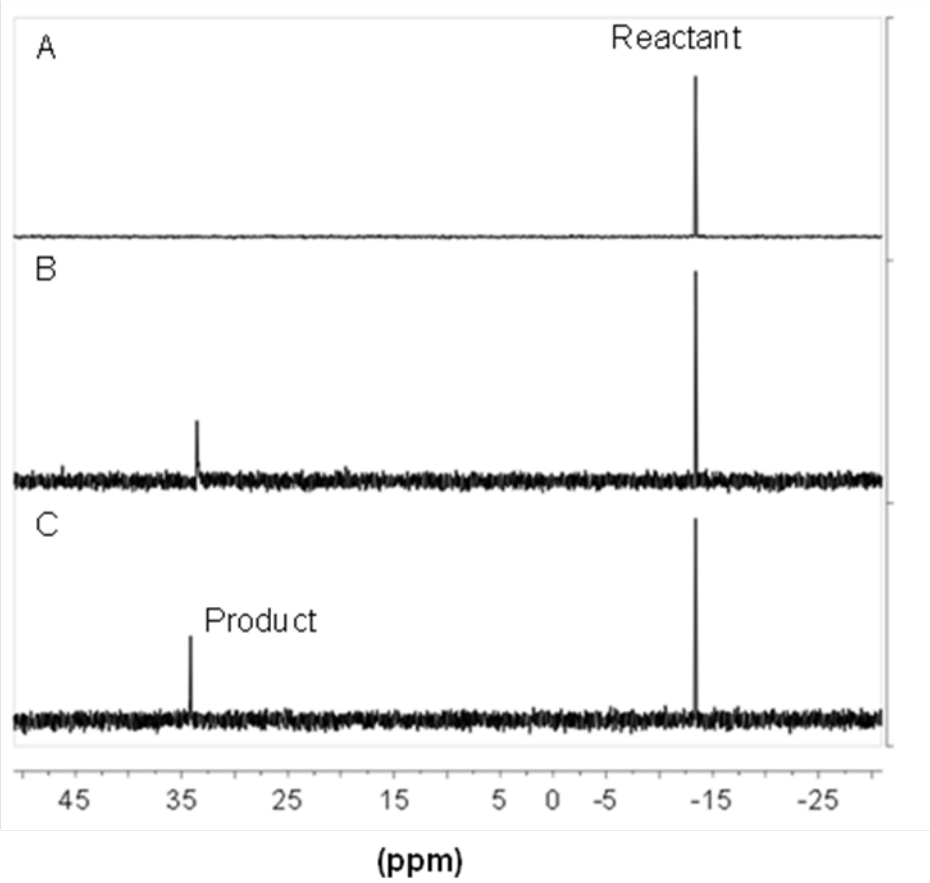

Figure 2-5: $^{31}P\{^{1}H\}$ NMR spectra illustrating the progress of a reaction of $\mathbf{L_1}$ with $[MgBr_2(OEt_2)]$ at 52 ºC in 9:1 benzene-d_6 : tetrahydrofuran-d_8 (for solubility) A.) t = 5 min. B.) t = 2 days. C.) t = 5 days. Ligand $^{31}P\{^{1}H\}$ NMR: δ –13.4. Product $^{31}P\{^{1}H\}$ NMR: δ 33.6.

The low solubility of $[MgBr_2(OEt_2)]$ in the reaction medium (benzene-d_6) necessitated the addition of a coordinating solvent (THF or tetrahydrofuran-d_8), which was suspected to compete with the neutral ligand, thereby hindering reaction progress. To test this assumption, excess THF (resulting in a 1:1 mixture of benzene-d_6 : THF) was added to an equilibrated reaction (Figure 2-5, spectrum C) resulting in quantitative conversion of the product ($^{31}P\{^{1}H\}$ NMR: δ 33.6) to the neutral ligand precursor ($^{31}P\{^{1}H\}$ NMR: δ –13.4) within minutes.

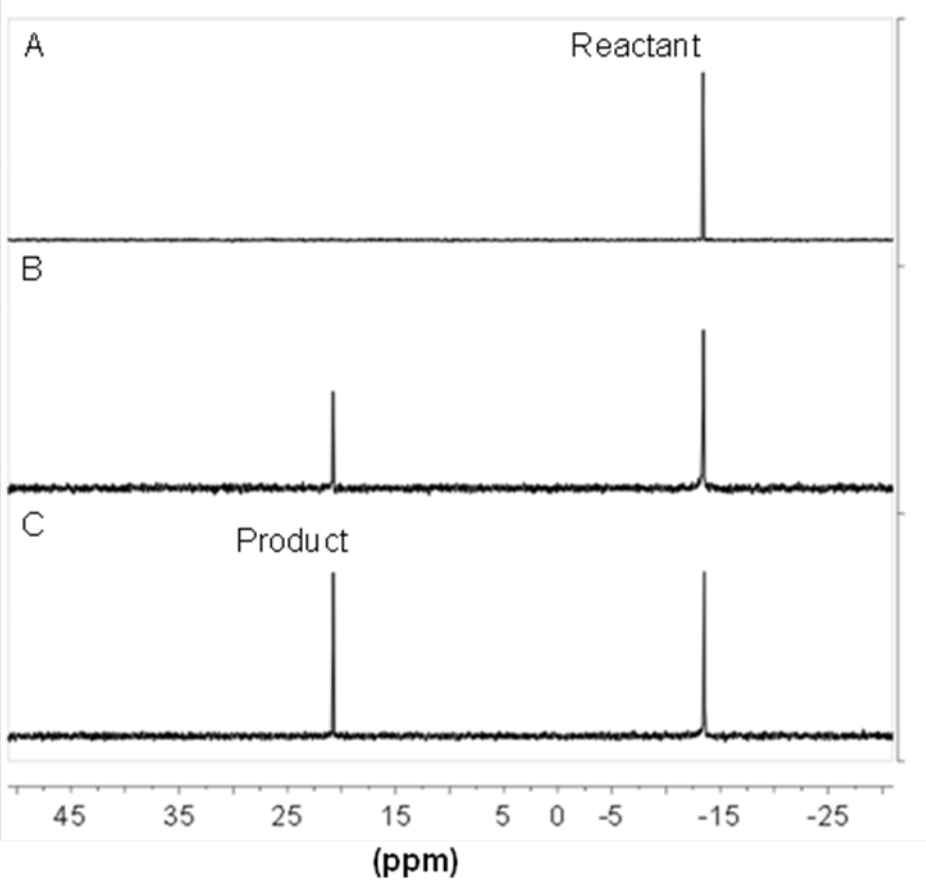

Figure 2-6: $^{31}P\{^{1}H\}$ NMR spectra illustrating the progress of the reaction of $\mathbf{L_1}$ with $[(THF)_2Mg(CH_2Ph)_2]$ at ambient temperature in benzene-d_6. A.) t = 5 minutes, B.) t = 1 day. C.) t = 7 days. $^{31}P\{^{1}H\}$ NMR: δ –13.4 ($\mathbf{L_1}$), δ 20.8 (product).

Alternate magnesium starting materials such as $[(THF)_2Mg(CH_2Ph)_2]$ were explored on the supposition that more highly soluble metal precursors may react readily in the absence of excess coordinating solvent. Results of this reaction were comparable to those observed in the reaction between $\mathbf{L_1}$ and $[MgBr_2(OEt_2)]$ in that only partial conversion to product (this time indicated by a ~34 ppm downfield shift to δ 20.8) was obtained over an extended period of time (~40% conversion over 7 days at ambient temperature, Figure 2-6). Again, exploration of alternate temperatures (25 ºC to 80 ºC) reproduced the same result without substantially altering reaction rates.

Note that while neither magnesium precursor appeared to have reacted fully, each reacted with **L_1** giving rise to a unique product with a diagnostic ^{31}P NMR resonance substantially downfield of the neutral ligand precursor. While the presence of coordinating solvents appeared to play a role in the position of equilibrium in the reaction of **L_1** with [$MgBr_2(OEt_2)$], examination of a more soluble magnesium precursor in the absence of THF still resulted in an equilibrium state.

Reactions utilizing **L_2** and [$(THF)_2Mg(CH_2Ph)_2$] were attempted under analogous conditions yielding similar results. A new product with a ^{31}P NMR resonance (δ 21.9) was observed (~37 ppm downfield from **L_2**); however, only partial conversion was obtained (~40% over 7 days at ambient temperature.) Exploration of elevated temperatures (25 ºC to 80 ºC) resulted in the formation of the same product without substantially altering the extent of conversion. The reduction in steric bulk from Dipp to Mes did not appear to substantially influence reaction rates or the position of the equilibrium.

While further investigation of reaction conditions and/or magnesium precursors may have yielded quantitative conversion of **L_1** or **L_2** to isolable, novel products, these ligands were ultimately not found to react with the examined magnesium precursors at preparatively useful rates. This suggests weak binding to the metal centre; as such, examination of the reactivity of *bis*phosphinimine ligands was pursued.

The reaction of **L_3** with [$MgBr_2(OEt_2)$] at elevated temperature (60 ºC, in a 9:1 mixture of benzene-d_6 : tetrahydrofuran-d_8) resulted in the formation of a

single product with a diagnostic ^{31}P resonance at δ 22.0, ~45 ppm downfield of the neutral ligand. While stoichiometric reactions resulted in only partial (> 50%) conversion to this species, quantitative conversion (Figure 2-7) was achieved when excess [$MgBr_2(OEt_2)$] (2.1 equivalents) was used. This reaction was observed to proceed via an asymmetric intermediate (1:1 ^{31}P resonances: δ 20.8, –23.1) and reached completion after 11 days had elapsed.

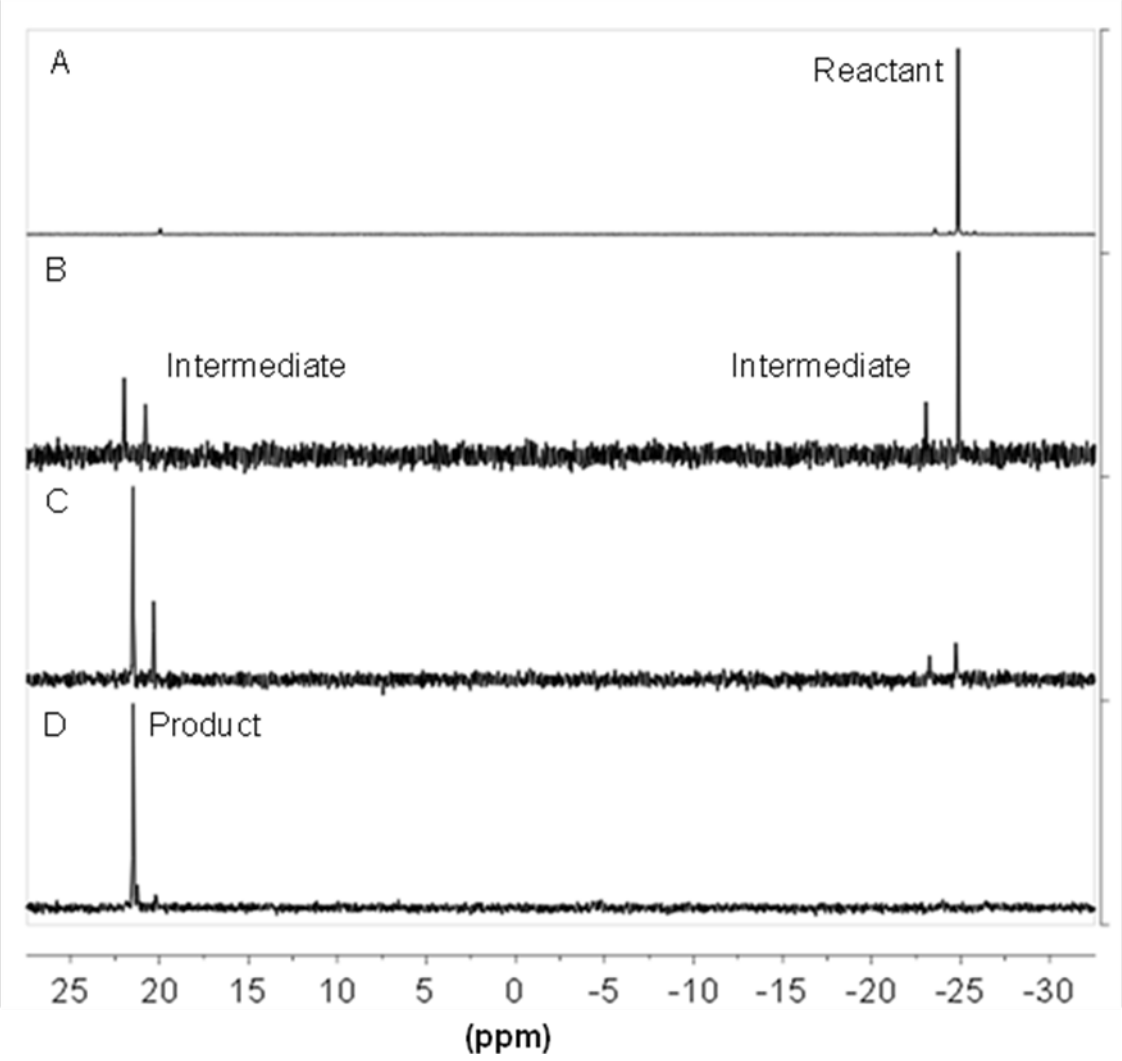

Figure 2-7: $^{31}P\{^1H\}$ NMR spectra illustrating the progress of a reaction of **L_3** with excess [$MgBr_2(OEt_2)$] (~2.1 equivalents) at 60 ºC at A.) t = 2 hours. B.) t = 3 days. C.) t = 7 days. D.) t = 11 days. Ligand $^{31}P\{^1H\}$ NMR : δ –24.9. Intermediate $^{31}P\{^1H\}$ NMR : δ 20.8, –23.1. Product $^{31}P\{^1H\}$ NMR : δ 22.0.

While the quantitative formation of a single product in this reaction was promising, the reaction rate remained exceptionally low, limiting its potential synthetic utility. Repeated attempts to scale up this reaction in order to isolate the product were unsuccessful and resulted only in intractable mixtures. The necessity of more than two equivalents of [$MgBr_2(OEt_2)$] per equivalent of ligand might be explained by an equilibrium process which favours [$\mathbf{L_3}MgBr_2$] in the presence of excess [$MgBr_2(OEt_2)$]; however, formation of the undesired complexes [$\mathbf{L_3}(MgBr_2)_2$] is also consistent with this behaviour (Scheme 2-6).

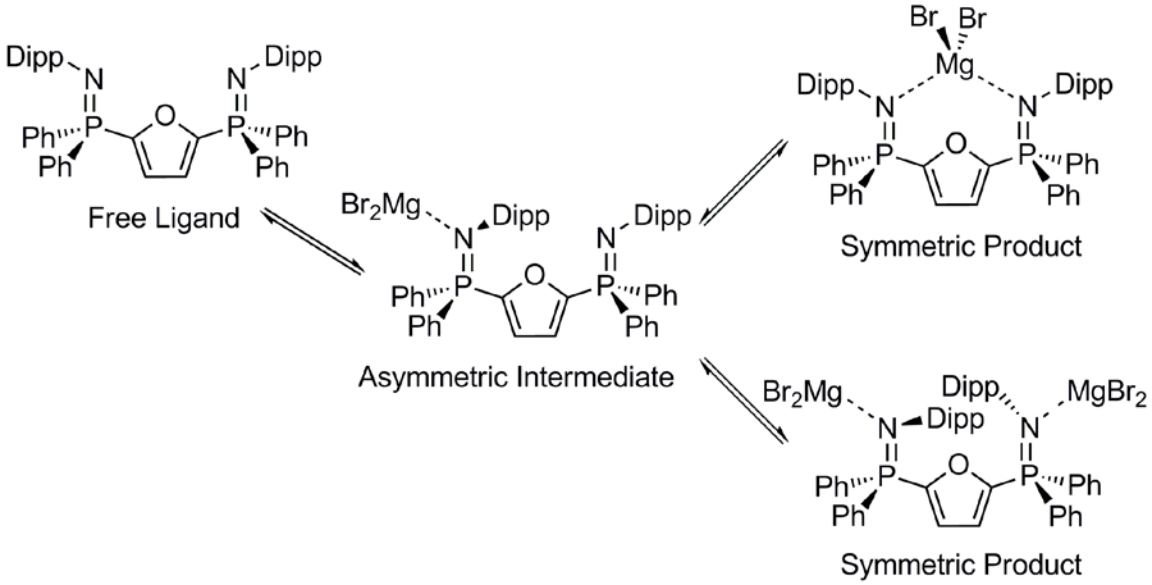

Scheme 2-6: Proposed asymmetric reaction intermediate and alternative final products for the reaction of $\mathbf{L_3}$ with [$MgBr_2(OEt_2)$].

Though impractically slow reaction rates prevented the isolation and unambiguous characterization of the product of this reaction, concurrent studies of the reactions of an analogous thiophene-based ligand system with [$AlMe_3$] resulted in the formation of [$L(AlMe_3)_2$], which has been structurally characterized.[110] This suggests that the ligand framework of $\mathbf{L_3}$ may promote

coordination to multiple metal centres and that a modified structure might facilitate the synthesis of the desired [$LMgR_2$] complexes. By comparison, **L_4** contains an additional atom within each chelate ring, potentially resulting in a narrower bite angle for the ligand as a whole (Chart 2-5). Further efforts were focused on studying the reactions of **L_4** with various magnesium-containing precursors.

Table 2-7: Diagnostic product chemical shifts observed in the reactions of **L_4** with various organomagnesium precursors.

Species/Reaction	Product ^{31}P (δ)	Time	% conversion to product
((MesN=PPh_2)$_2$dbf) (**L_4**)	–17.6	-	-
L_4 + [$(THF)_2Mg(CH_2Ph)_2$]	21.2 / 22.6 (1:1)	43 h	29
L_4 + [(^{n}Bu)Mg(OAr)]	22.9	72 h	12
L_4 + [Mg^nBu_2]	23.2	1 h	27

Small-scale reactions of **L_4** with stoichiometric amounts of magnesium-containing precursors including [$MgBr_2OEt_2$] (no result), [$(THF)_2Mg(CH_2Ph)_2$], [(^{n}Bu)Mg(OAr)] (Ar = 2,6-di^{t}butyl-4-methylphenyl), and [Mg^nBu_2] were conducted at ambient temperature. In the latter three cases, $^{31}P\{^1H\}$ NMR spectroscopy revealed new products with resonances 39 to 41 ppm downfield of the free ligand (Table 2-7). Reactions with [(^{n}Bu)Mg(OAr)] and [$(THF)_2Mg(CH_2Ph)_2$] proceeded very slowly and in the latter case resulted in decomposition without reaching full conversion. The reaction of **L_4** with [Mg^nBu_2] resulted in decomposition prior to completion, but was found to occur at a rate significantly greater than any other ligand-metal combination examined.

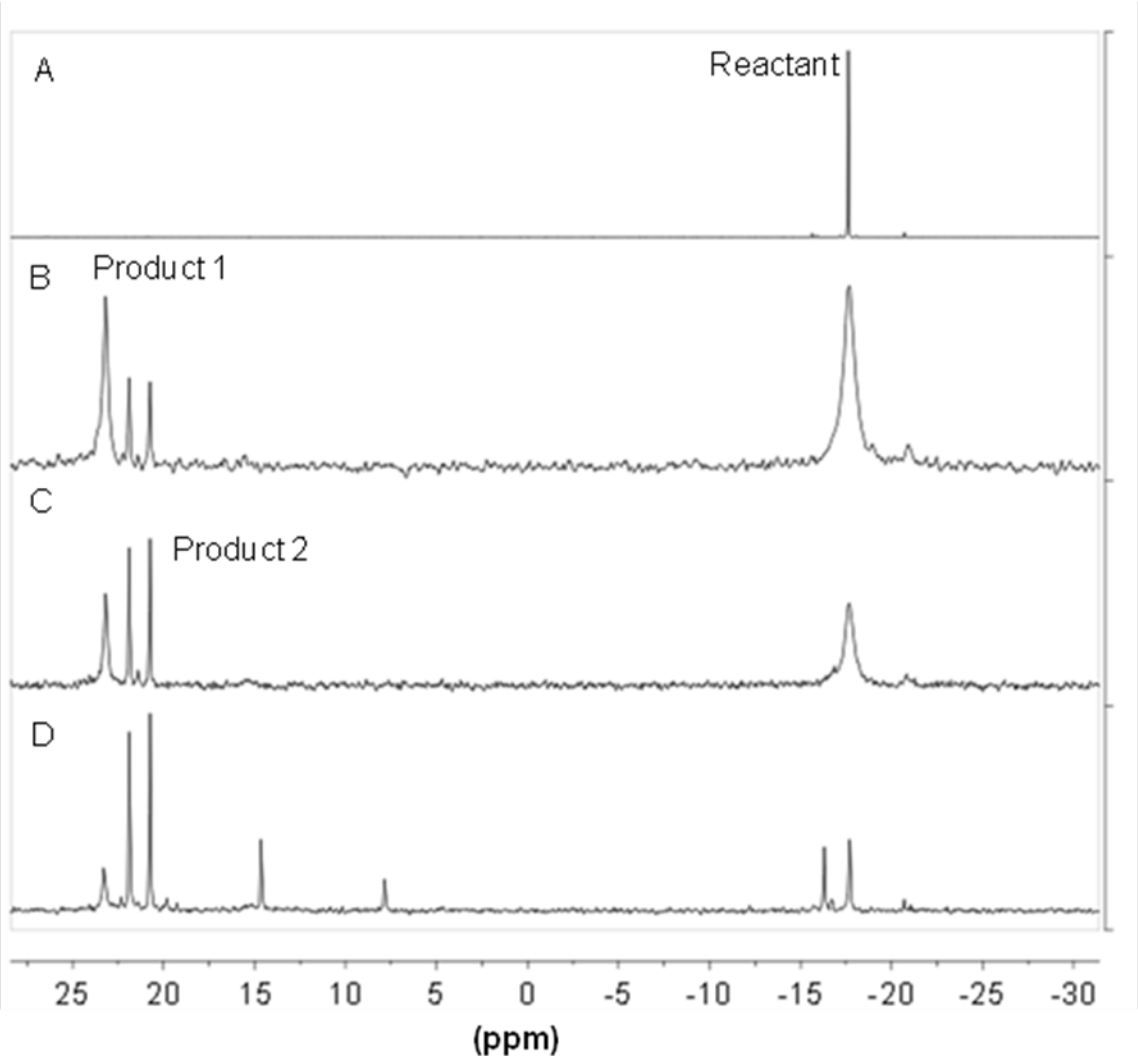

Figure 2-8: $^{31}P\{^{1}H\}$ NMR spectra (benzene-d_6) illustrating the progress of the reaction of A.) **L_4** with 1.0 equivalent [Mg^nBu_2] at ambient temperature at B.) t = 1 hour. C.) t = 4 hours D.) t = 24 hours.

Lack of product stability prevented isolation and characterization of discrete species from the reaction of **L_4** and [Mg^nBu_2]; however, NMR evidence suggested the formation of an appreciable quantity of a single, symmetric product consistent with [**L_4**Mg^nBu_2] within one hour of reaction initiation. The initial product (δ 23.2, Figure 2-8, spectrum B) appeared to decompose predominantly to form a second species giving rise to 1:1 $^{31}P\{^{1}H\}$ resonances (δ

21.9 and 20.7, Figure 2-8, spectrum C). After 24 hours, almost none of the initial product remained (Figure 2-8, spectrum D). An analogous reaction of **L_4** with two equivalents of [Mg^{n}Bu$_2$] gave rise almost exclusively to the second product (1:1 $^{31}P\{^1H\}$ resonances at δ 21.9 and 20.7) which did not decompose over 72 hours at ambient temperature. This suggested that the second product may be a relatively stable undesired complex of the form [**L_4**(Mg(^{n}Bu)$_2$)$_2$]. Note that the total integration of product 2 in Figure 2-8, spectrum D is less than the combined integration of the free ligand and the unidentified species with resonances at δ 15.0, 7.6, and –15.8. The stoicheometry of the initial reaction is therefore consistent with the formation of [**L_4**(Mg(^{n}Bu)$_2$)$_2$] provided that these unidentified species do not contain magnesium.

Though initial investigations of the reactivity of **L_1**, **L_2**, **L_3** and **L_4** did not result in the production of isolable products on a preparatively-useful timescale, a clear trend in the ^{31}P NMR data was established. In all cases where a reaction occurred, species with ^{31}P NMR chemical shifts 35 to 46 ppm downfield of the phosphinimine starting material were observed. Literature precedent suggests that coordination of a phosphinimine to a magnesium centre results in a substantial downfield shift of the ^{31}P NMR resonance, generally on the order of 30 ppm (Chart 2-6, Table 2-8).[115-119] It is therefore plausible that the species observed *in situ* are indeed magnesium-bound phosphinimines.

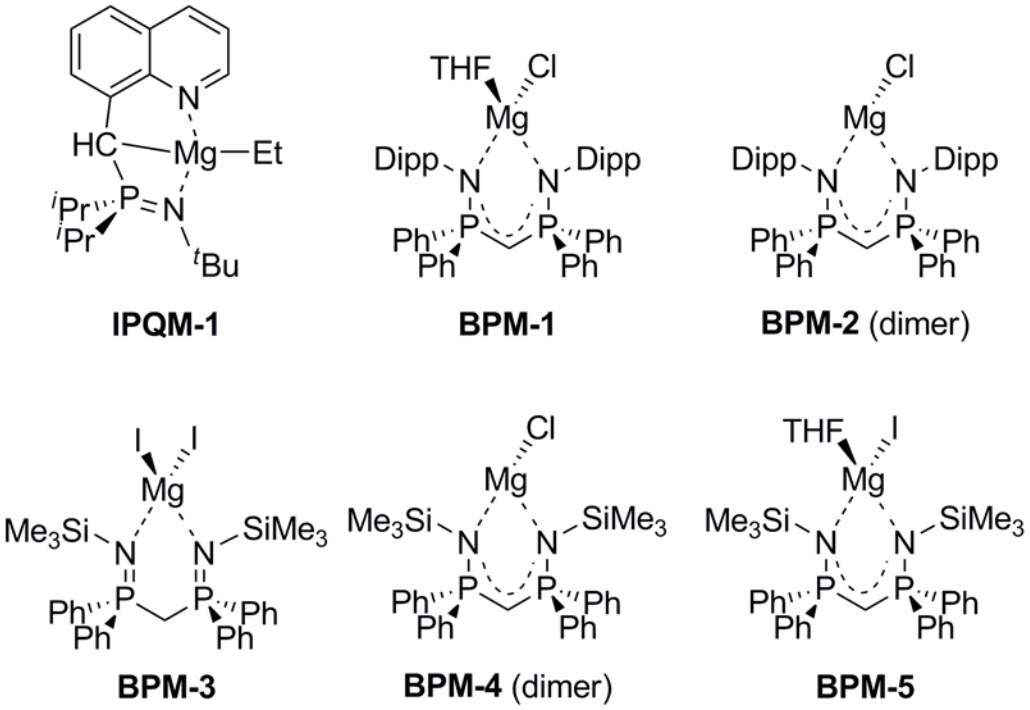

Chart 2-6: Selected literature examples of magnesium-bound phosphinimines for comparison of ^{31}P NMR spectral data.

Table 2-8: Literature examples illustrating a downfield shift in ^{31}P NMR resonance upon coordination of phosphinimines to magnesium.

Species	Free Ligand ^{31}P (δ)	Bound Ligand ^{31}P (δ)	^{31}P Downfield Shift (ppm)	Ref.
IPQM-1	9.3	34.6	25.3	71
BPM-1	–16.2	18.1	34.3	115
BPM-2	–16.2	18.1	34.3	115
BPM-3	–3.0	25.2	28.2	116
BPM-4	–3.0	25.3	28.3	116
BPM-5	–3.0	26.0	29.0	116

2-6: *Concluding Remarks*

Various neutral *mono* and *bis*phosphinimine ancillary ligands were successfully synthesized and characterized primarily using multinuclear NMR techniques and single-crystal X-ray diffraction. These species were produced with the intent of creating neutral complexes of magnesium directly, followed by

activation to produce analogous cationic species. NMR techniques, particularly ^{31}P NMR spectroscopy, were used as a preliminary tool for detecting new products. Repeated attempts to produce the requisite neutral magnesium complexes consistently gave rise to new species with ^{31}P NMR resonances 35 to 46 ppm downfield of the corresponding free ligands. Examination of the reactions of several different ligands with a variety of magnesium alkyl, alkoxide, and halide precursors under a range of reaction conditions did not reliably afford stable, isolable products on a preparatively useful timescale.

While understanding the nature of the factors giving rise to poor reactivity (thermodynamic and kinetic barriers, equilibrium states, and decomposition pathways) represented an interesting and relevant problem, the general synthetic approach applied to complex formation did not appear to offer a versatile, preparatively useful route to the synthesis of neutral magnesium complexes. An alternate approach to the original synthetic strategy (Scheme 2-2) was clearly needed for the synthesis of activated magnesium complexes for lactone polymerization. Such a strategy is described in Chapter 3.

Chapter 3

Synthesis of Cationic Organomagnesium Complexes

3-1: *Direct Synthesis of Cationic Organometallic Species*

Methods of directly producing cationic organomagnesium complexes are exceedingly rare in the chemical literature. One noteworthy preparation method is the reaction of dialkylmagnesium precursors with azacrown macrocycles (AEMs).[120] A recent, structurally characterized example of this approach is **AEM-1** (Scheme 3-1).[121] This strategy is not general as analogous reactions with [RMgOR'] precursors generated only neutral [(AEM)Mg(R)(OR')] complexes. Although no applications have been reported for **AEM-1**, it is one of few examples of discrete, isolable, cationic magnesium complexes reported to date.

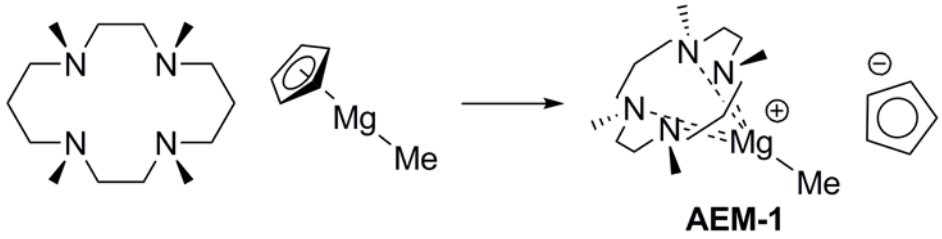

Scheme 3-1: Synthesis of **AEM-1** from [CpMgMe] and a neutral macrocyclic precursor.

A particularly promising, direct synthetic route to cationic complexes was first suggested by Bochmann *et al.* in 2002 for the production of cationic zinc and cadmium species bearing *bis*imine ancillary ligands (Scheme 3-2).[122,123] Conceptually, this approach is similar to the use of Brønsted acids in olefin polymerization catalyst activation (Chapter 1-4) with the exception that the chelating ancillary ligand itself is able to act as the activating species. In this

case, the protonated conjugate acid of the desired *bis*imine ligand was first synthesized and isolated. The protonated ligand was then allowed to react with neutral organozinc or organocadmium precursors, resulting in alkide or amide abstraction to generate corresponding cationic organometallic complexes bearing neutral *bis*imine ligands. These species were collected as salts with sterically bulky $B(C_6F_5)_4^-$ counter-ions which are generally weakly-coordinating; a feature which may be readily confirmed by ^{11}B and ^{19}F NMR spectroscopy.[63-62,59]

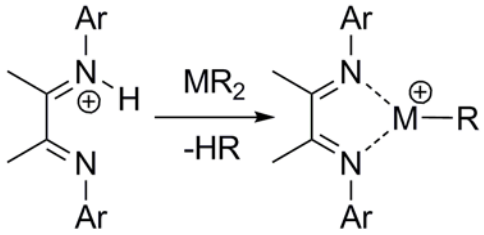

Scheme 3-2: Synthesis of cationic complexes by reaction of neutral metal-containing precursors with protonated *bis*imine ancillary ligands. This approach has been applied to the synthesis of the following: A.) M = Zn, Ar = Dipp, R = Et, B.) M = Zn, Ar = Dipp, R = OH, C.) M = Zn, Ar = 2,6-$Ph_2C_6H_3$, R = Me, D.) M = Zn, Ar = 2,6-$Ph_2C_6H_3$, R = $N(SiMe_3)_2$, E.) M = Cd, Ar = Dipp, R = $N(SiMe_3)_2$, F.) M = Cd, Ar = 2,6-$Ph_2C_6H_3$, R = $N(SiMe_3)_2$.

As this approach has been utilized successfully in the synthesis of *bis*imine-bound cationic organometallic species, an analogous strategy may be useful in the synthesis of cationic *bis*phosphinimine complexes containing **L_3**, or **L_4** (Scheme 3-3). The reaction of protonated derivatives of *bis*phosphinimines therefore presents an alternative to isolation of neutral precatalysts followed by activation using conventional Lewis or Brønsted acids (Chapter 1-4).

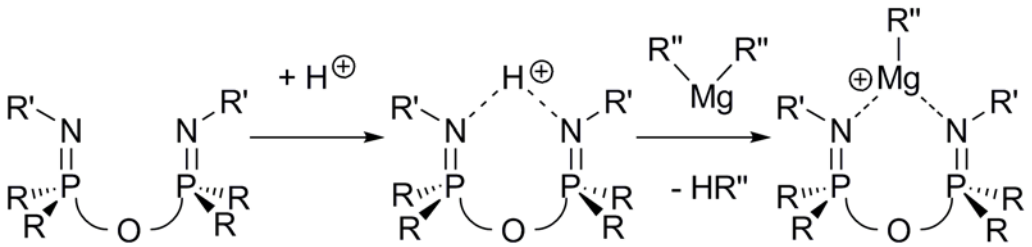

Scheme 3-3: Proposed synthesis of cationic organomagnesium complexes via a protonated ancillary ligand (Simplified ligand architecture. R = anionic ligand.)

3-2: *Synthesis of [H(MesN=PPh$_2$)$_2$dbf]$^+$[BR$_4$]$^-$ Analogues*

Inspired by the previous work of Bochmann *et al.*, efforts were directed at producing cationic organomagnesium species by reaction of neutral organomagnesium precursors with protonated analogues of the novel ligand series reported in Chapter 2. Initially, synthesis of an **L$_4$** derivative activator with the weakly-coordinating $B(C_6F_5)_4^-$ anion was targeted. This was accomplished by direct reaction of **L$_4$** with the Brønsted acid activator $[HNMe_2Ph]^+[B(C_6F_5)_4]^-$ to afford a mixture of $[\mathbf{L_4}H]^+[B(C_6F_5)_4]^-$ (**A$_1$**) and dimethylaniline. The reaction was quite rapid, reaching completion in under 10 minutes at ambient temperature in benzene. Subsequent removal of dimethylaniline by washing with pentane and drying *in vacuo* afforded **A$_1$** as an analytically pure light yellow solid in 80% yield.

In order to reduce the cost associated with producing "$[\mathbf{L_4}H]^+$" and provide an analogue for comparison of spectral data, $[\mathbf{L_4}H]^+[BPh_4]^-$ (**A$_2$**) was prepared by reaction of **L$_4$** with $NaBPh_4$ and a Brønsted acid. While this reaction may be performed using HCl as the acid,[110] in its absence water alone will act as a suitable proton donor. Solutions of **L$_4$** in benzene and $NaBPh_4$ in distilled water

were thoroughly mixed for 25 minutes and the organic phase was dried *in vacuo* to afford $[\mathbf{L_4}H]^+[BPh_4]^-$ in 86 % yield as an analytically pure light yellow solid.

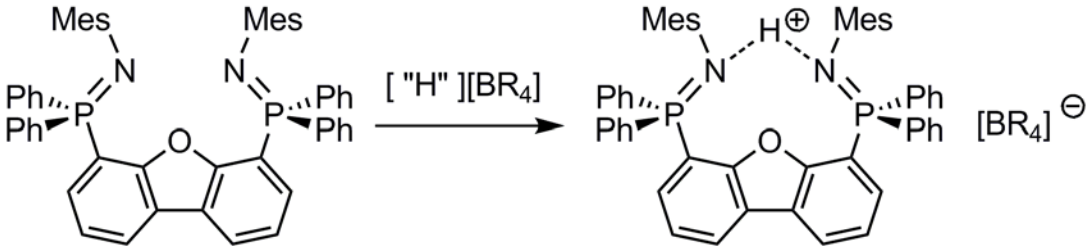

Scheme 3-4: Synthesis of $[\mathbf{L_4}H]^+[B(C_6F_5)_4]^-$ (**A_1**) and $[\mathbf{L_4}H]^+[BPh_4]^-$ (**A_2**) by reaction of $\mathbf{L_4}$ with Brønsted acids. Balanced reactions: $\mathbf{L_4}$ + $[HNMe_2Ph]^+[B(C_6F_5)_4]^- \rightarrow [\mathbf{L_4}H]^+[B(C_6F_5)_4]^-$ + Me_2NPh; $\mathbf{L_4}$ + $NaBPh_4$ + $H_2O \rightarrow [\mathbf{L_4}H]^+[BPh_4]^-$ + NaOH.

With the exception of BR_4^- resonances, the ^1H, $^{31}P\{^1H\}$, and $^{13}C\{^1H\}$ NMR NMR spectra of **A_1** and **A_2** (Table 3-1) were not significantly different. Diagnostic ^{31}P NMR resonances for **A_1** and **A_2** were virtually identical appearing as singlets at δ 9.4 and 9.5, respectively. The overall C_{2v} symmetry was corroborated by key mesityl methyl ^1H NMR (δ 2.2 and 1.6) and ^{13}C NMR (δ 21 and 20) resonances. The symmetry of $\mathbf{L_4}H^+$ could be explained by a rapidly (relative to the NMR time scale) exchanging NH proton.

Table 3-1: Comparison of selected NMR for $[\mathbf{L_4}H]^+[BR_4]^-$ (R = C_6F_5 (**A_1**), Ph (**A_2**)) in chloroform-*d*.

Nucleus	Assignment	A_1 (δ)	A_2 (δ)
^{31}P	P	9.4 (s)	9.5 (s)
^1H	*m*-Mes	6.58 (s)	6.58 (s)
	N-***H***	5.72 (br s)	5.69 (br s)
	p-Mes C***H***$_3$	2.17 (s)	2.18 (s)
	o-Mes C***H***$_3$	1.55 (s)	1.56 (s)
^{13}C	dbf-C_2	134.6 (d)	134.5 (s)
	o-Ph	132.6 (d)	132.5 (d)
	dbf-C_1	127.1 (s)	127.4 (s)
	p-Mes C(***C***H$_3$)	20.8 (s)	20.8 (s)
	o-Mes C(***C***H$_3$)	20.1 (s)	20.2 (s)

Additionally, ^{11}B NMR resonances were observed upfield of δ 0 (at δ –16.7 for **A_1** and δ –6.5 for **A_2**), consistent with free BR_4^- (R = C_6F_5, Ph) anions (Chapter 1-4).[63-62] This was corroborated by the difference between *meta* and *para* ^{19}F NMR resonances ($\Delta\delta_{m,p}$) of **A_1** which, at 3.8 ppm, is also consistent with free $B(C_6F_5)_4^-$ (Chapter 1-4). Collectively, this implies minimal interaction between ionic components in both **A_1** and **A_2**.

While repeated attempts to produce single crystals of **A_1** and **A_2** were not successful, a closely related species, $[\mathbf{L_4}H_2]^{2+}[BPh_4]^-_2$ (**A_3**), has been isolated and structurally characterized by X-ray crystallography.[110] Elongation of the P–N bonds (**L_4**: P1–N1 = 1.549(1) Å, **A_3**: P1–N1 = 1.639(2) Å) was consistent with weakening of the π bonds due to protonation at nitrogen. As expected, the BPh_4^- counter-ions of **A_3** were found to be dissociated from LH^+ in the solid state.

3-3: *Synthesis of Cationic Magnesium Complexes*

Cationic magnesium complexes $[\mathbf{L_4}Mg^nBu]^+[B(C_6F_5)_4]^-$ (**C_1**) and $[\mathbf{L_4}Mg^nBu]^+[BPh_4]^-$ (**C_2**) were readily obtained using the approach outlined in Scheme 3-5. Specifically, benzene solutions of **A_1** and **A_2** were prepared under anaerobic conditions and one stoichiometric equivalent of $[Mg(^nBu)_2]$ (solution in heptane) was added to each. In both cases, evolution of a colourless gas was observed. Reactions reached completion in less than one hour and removal of solvents afforded air-sensitive solids in 73% (**C_1**) and 91% yields (**C_2**).

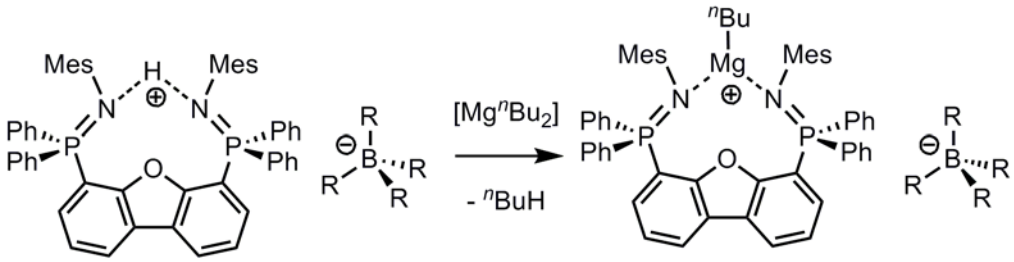

Scheme 3-5: Synthesis of [**L$_4$**Mg^{n}Bu]$^+$[BR$_4$]$^-$ (R = C_6F_5, Ph) from [**L$_4$**H]$^+$[BR$_4$]$^-$ and [Mg^{n}Bu$_2$].

Single ^{31}P{^{1}H} NMR resonances of **C$_1$** and **C$_2$** were observed at δ 23.0 and 23.2, respectively, ~41 ppm downfield of free **L$_4$** (–17.6 ppm, Figure 3-1). An NMR-scale synthesis of **C$_1$** in benzene-*d$_6$* was performed resulting in observation of very weak signals at δ 1.95 and 1.10 (consistent with trace ^{n}butane)[124] which disappeared upon exposure of the sample to vacuum. The presence of a single remaining ^{n}butyl group was corroborated by ^{1}H NMR spectroscopy (Figure 3-2). Integration of ^{n}butyl signals (Mg–C***H***$_2$ (δ –0.1), Mg–(CH$_2$)$_3$–C***H***$_3$ (δ 1.0)) relative to ligand-derivative resonances (*p*-Mes C(C***H***$_3$) (δ 2.0), *o*-Mes C(C***H***$_3$) (δ 1.5)) were particularly useful in this regard (Table 3-2).

The ^{1}H, ^{31}P{^{1}H}, and ^{13}C{^{1}H} NMR spectra of [**L$_4$**Mg^{n}Bu]$^+$[BR$_4$]$^-$ analogues were virtually identical with the exception of anion resonances. The ^{11}B NMR spectra of **C$_1$** and **C$_2$** were highly similar to those of **A$_1$** and **A$_2$**, respectively. The ^{11}B NMR resonances were observed upfield of 0 ppm (δ –15.8 for B(C_6F_5)$_4^-$ and δ –5.6 for BPh_4^-). The ^{19}F NMR spectrum of **C$_1$** was similar to that of **A$_1$** giving a $\Delta\delta_{m,p}$ value of 3.8 ppm. Collectively, these data indicate a non-coordinating (or extremely weakly-coordinating) BR_4^- anion in each case.

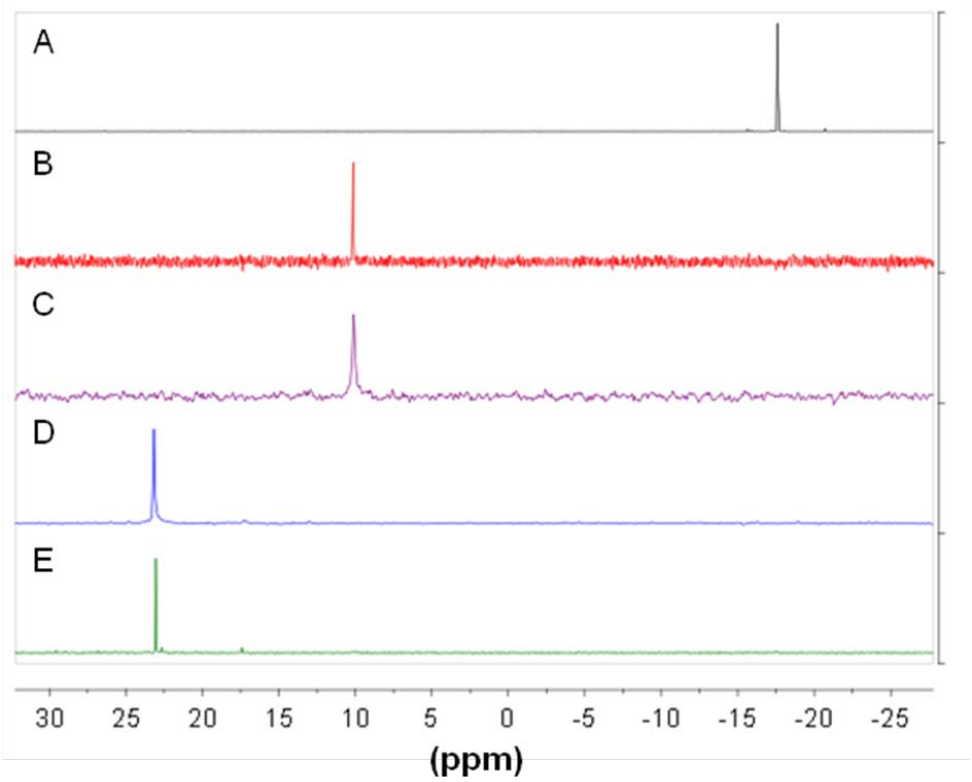

Figure 3-1: Diagnostic $^{31}P\{^{1}H\}$ NMR spectra (benzene-d_6) of cationic magnesium complexes $[\mathbf{L_4}Mg^{n}Bu]^{+}[BR_4]^{-}$ (R = C_6F_5 (**C_1**), Ph (**C_2**)) and their synthetic precursors. A) **L_4** δ –17.6. B) **A_1** δ 10.1. C) **A_2** δ 10.1. D) **C_1** δ 23.0. E) **C_2** δ 23.2.

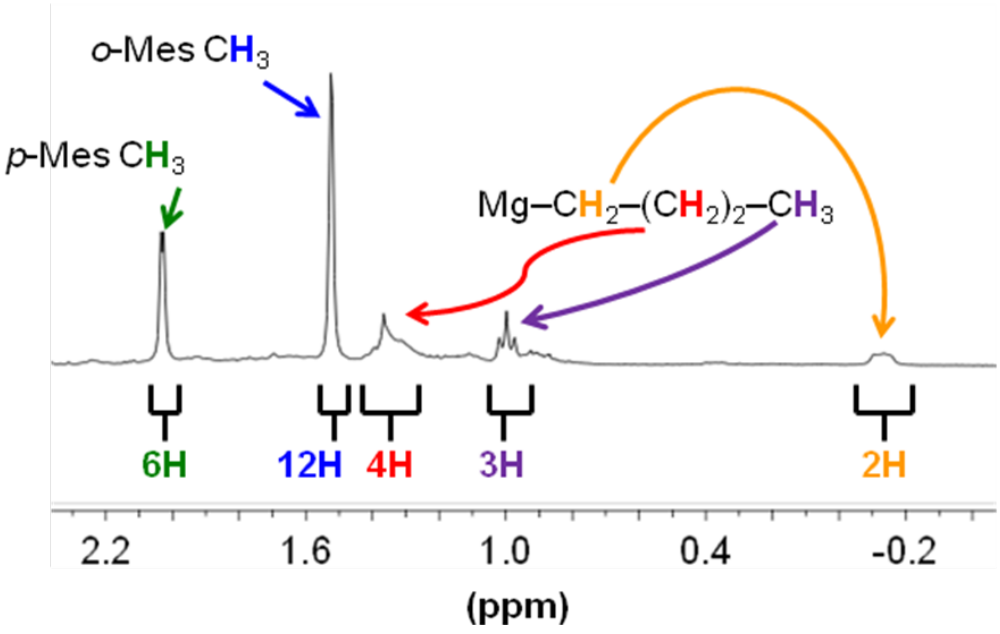

Figure 3-2: Expansion of the ^{1}H NMR spectrum (benzene-d_6) of **C_2**.

Table 3-2: Comparison of selected NMR data for $[\mathbf{L_4}Mg^{n}Bu]^{+}[BR_4]^{-}$ (R = C_6F_5 (**C_1**), Ph (**C_2**)) in benzene-d_6.

Nucleus	Assignment	C_1 (δ)	C_2 (δ)
^{31}P	P	23.0 (s)	23.2 (s)
^{1}H	*m*-Mes	6.36 (s)	6.35 (s)
	p-Mes C***H***$_3$	2.04 (s)	2.03 (s)
	o-Mes C***H***$_3$	1.50 (s)	1.52 (s)
	Mg–$(CH_2)_3$–C***H***$_3$	0.99 (t)	0.99 (t)
	Mg–C***H***$_2$–	–0.13 (t)	–0.13 (t)
^{13}C	*o*-Ph	134.1 (d)	133.9 (ov m)
	p-Mes C(***C***H_3)	20.6 (s)	20.6 (s)
	o-Mes C(***C***H_3)	20.1 (s)	20.3 (s)
	Mg–$(CH_2)_3$–***C***H_3	14.1 (s)	14.0 (s)
	Mg–***C***H_2–	12.0 (s)	11.9 (s)

X-ray quality single crystals of $[\mathbf{L_4}Mg^{n}Bu]^{+}[BPh_4]^{-}$ were obtained and the molecular structure was confirmed by crystallography (Figure 3-3, Table 3-3).[110] The interatomic distance between magnesium and oxygen was 3.233(5) Å, indicating no significant bonding interaction (sum of van der Waals radii (O + Mg): 3.25 Å[125]). Interatomic distances between magnesium and nitrogen were found to be ~2.08 Å (bond lengths: N1–Mg 2.086(6) Å, N2– Mg 2.077(5) Å, sum of van der Waals radii (N + Mg): 3.28 Å[125]) suggesting a strong bonding interaction. The Mg–N bond lengths were consistent with literature values for analogous structures[71,72,115-117] (Chart 3-2, Table 3-4) which range from 2.04 Å to 2.19 Å (Table 3-4). The local geometry about magnesium is trigonal planar (sum of angles = 360º) and the phosphorus-nitrogen bonds were established to be ~1.60 Å (Bond lengths: P1–N1 1.602(5) Å, P2–N2 1.601(5) Å), which is also consistent with literature values (Table 3-4).[71,72,115-117] The P–N bonds of **C_2** are elongated by ~0.05 Å relative to the structure of **L_4** (Bond lengths: P1–N1

1.549(1) Å, P2–N2 1.565(1) Å). This suggests that the phosphorus-nitrogen bond weakens slightly upon coordination to magnesium.

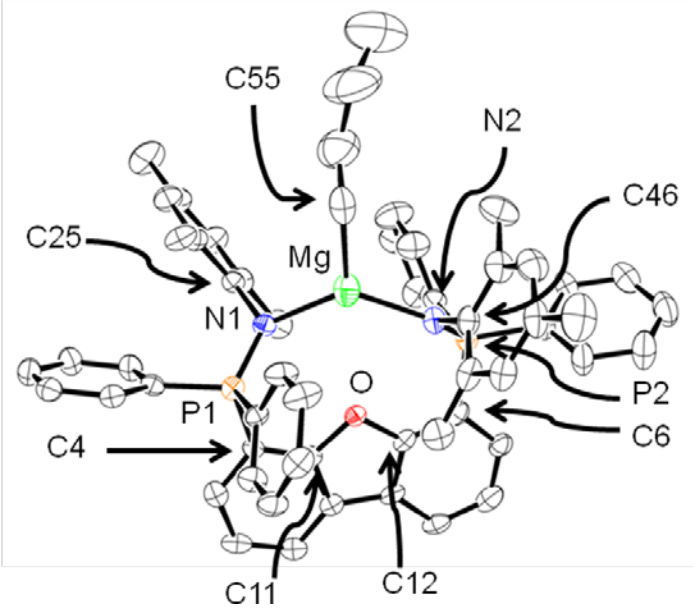

Figure 3-3: X-ray crystal structure of **C_2** (30% probability ellipsoids, H atoms and BPh_4^- counter-ion removed for clarity).

Table 3-3: Selected metrical data for the crystal structure[110] of $[\mathbf{L_4}Mg^nBu]^+[BPh_4]^-$

Bond Lengths	Value (ESD)	Bond Lengths	Value (ESD)
C4–P1	1.803(7) Å	**C6–P2**	1.797(7) Å
P1–N1	1.602(5) Å	**P2–N2**	1.601(5) Å
N1–C25	1.440(7) Å	**N2–C46**	1.454(8) Å
Mg–N1	2.086(6) Å	**Mg–N2**	2.077(5) Å
Mg–C55	2.13(1) Å		
Bond Angles		**Bond Angles**	
C11–C4–P1	120.5(4)º	**C12–C6–P2**	121.0(5)º
C4–P1–N1	116.1(3)º	**C6–P2–N2**	115.3(3)º
P1–N1–C25	119.8(4)º	**P2–N2–C46**	119.9(4)º
P1–N1–Mg	129.6(3)º	**P2–N2–Mg**	130.7(3)º
N1–Mg–C55	115.0(3)º	**N2–Mg–C55**	112.3(3)º
N1–Mg–N2	132.6(2)º		
Torsion Angles		**Torsion Angles**	
C11–C4–P1–N1	42.3(6)º	**C12–C6–P2–N2**	44.5(6)º
C4–P1–N1–C25	98.7(5)º	**C6–P2–N2–C46**	94.2(5)º

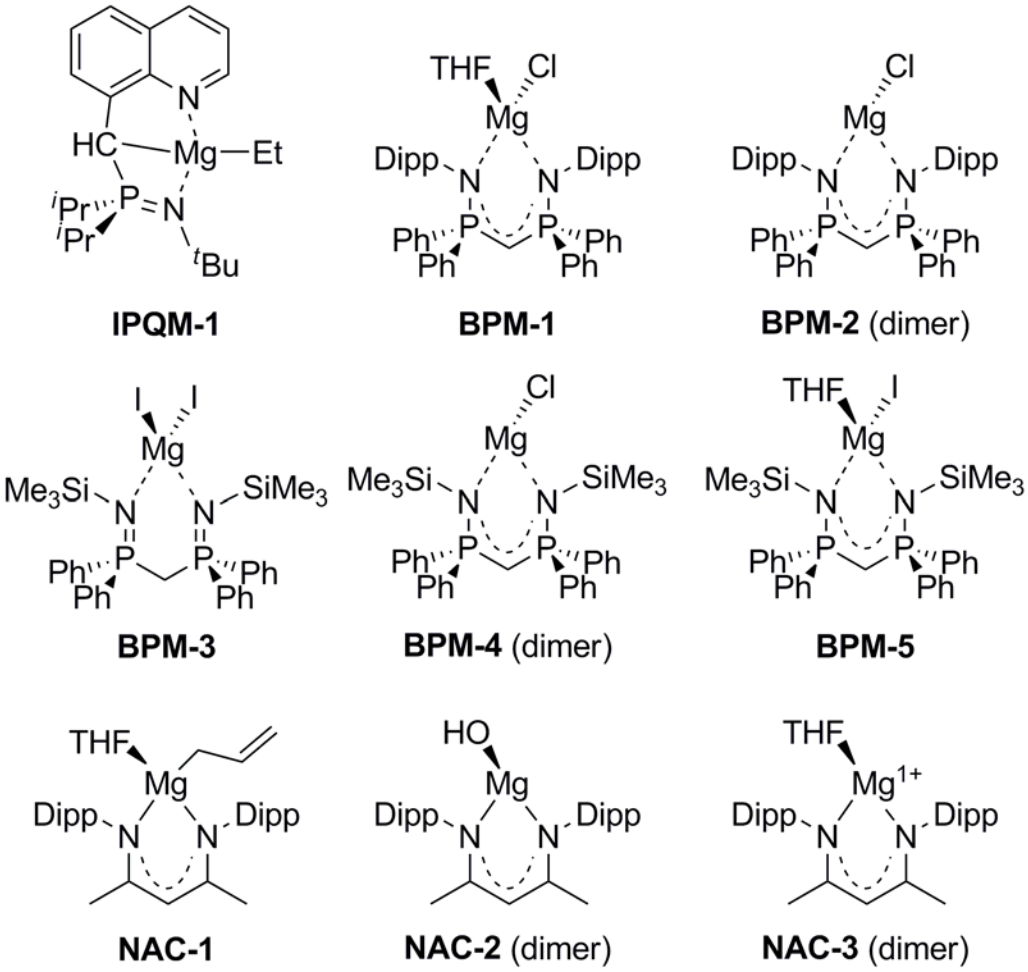

Chart 3-1: Selected literature examples for comparison of structural data. Indicated species are dimeric in the solid state.

Table 3-4: Magnesium-nitrogen and phosphorus-nitrogen (P=N) bond lengths of selected literature compounds.

Species	Mg–N Bond Lengths (Å)	P=N Bond Lengths (Å)	Ref.
IPQM-1	2.108(3) (P–**N–Mg**)	1.633(3)	71
BPM-1	2.045(3)	1.617(3)	115
	2.040(2)	1.706(2)	
BPM-2	2.067(3)	1.618(3)	115
	2.070(2)	1.715(2)	
BPM-3	2.111(5)	1.584(5)	116
	2.112(5)	1.587(4)	
BPM-4	2.104(7)	1.610(7)	116
	2.163(7)	1.606(7)	
BPM-5	2.099(5)	1.606(5)	116
	2.121(5)	1.609(4)	
NAC-1	2.052(2)	NA	72
	2.050(2)	NA	
NAC-2	2.169(2)	NA	72
NAC-3	2.159(NR)	NA	117

The shortest contact between magnesium and a non-hydrogen BPh_4^- atom was 6.265(5) Å between Mg and C79 (Figure 3-4); therefore, the crystal structure of $\mathbf{C_2}$ clearly indicates no coordination of BPh_4^- to the magnesium centre. While repeated attempts to obtain X-ray quality crystals of $\mathbf{C_1}$ were not successful, it has been well established that the $B(C_6F_5)_4^-$ counter-ion generally does not coordinate as strongly to a metal centre as BPh_4^-.[59] Since BPh_4^- is clearly non-coordinating in the case of $\mathbf{C_2}$, it is reasonable to suggest that both $\mathbf{C_1}$ and $\mathbf{C_2}$ are non-coordinating ion pairs. This conclusion is corroborated by the similar NMR spectral properties of $[\mathbf{L_4}Mg^nBu]^+$ in $\mathbf{C_1}$ and $\mathbf{C_2}$.

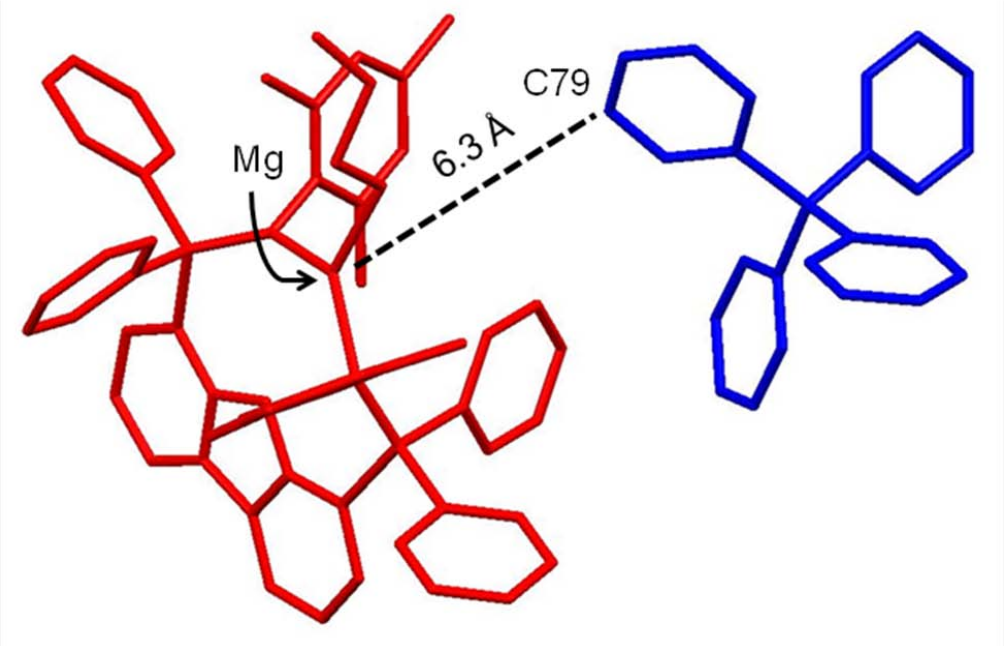

Figure 3-4: Interatomic distances between magnesium and the closest atom in the crystal structure of **C_2** (H atoms omitted for clarity).

The large downfield shift in the $^{31}P\{^{1}H\}$ NMR resonances upon coordination of **L_4** to the magnesium centre was consistent with the trend established by literature examples **IPQM-1**, **BPM-1** to **BPM-5** (see Chapter 2-5).[115-119] The ~41 ppm shift also agrees with and observations made upon reaction of **L_1**, **L_2**, **L_3**, and **L_4** with neutral magnesium precursors (Chapter 2-5), which resulted in products with ^{31}P NMR resonances 35-46 ppm downfield of the corresponding neutral ligands. While the aforementioned neutral complexes of **L_1** to **L_4** were only observed *in situ* and never fully characterized, the similar chemical environments for phosphorus support the hypothesis that these species were, in fact, magnesium-bound phosphinimines.

3-4: *Concluding Remarks*

The protonated analogue of **L_4**, [**L_4**H]$^+$ was isolated as a salt with both $B(C_6F_5)_4^-$ (**A_1**) and BPh_4^- (**A_2**) anions. Treatment of [**L_4**H]$^+$ with [Mg^{n}Bu$_2$] was found to produce a cationic organomagnesium species of the form [**L_4**Mg^{n}Bu]$^+$. Comparison of NMR data of [**L_4**Mg^{n}Bu]$^+$[$B(C_6F_5)_4$]$^-$ (**C_1**) and [**L_4**Mg^{n}Bu]$^+$[BPh_4]$^-$ (**C_2**) did not reveal any evidence of substantial cation-anion interactions, nor was any interaction observed in the X-ray structure of **C_2**. Species **C_1** and **C_2** are best described as non-coordinating ion pairs. The catalytic efficacy of [**L_4**Mg^{n}Bu]$^+$ in the polymerization of lactones will be described in Chapter 4.

Chapter 4

From Complex to Catalyst: Polymerization of 6-caprolactone

4-1: *Characterization of Polymer Samples*

The molecular weight (MW) distribution of a polymer sample plays a key role in determining its macroscopic properties. Polymers are composed of mixtures of nearly-identical species which vary in the number of repeating monomer units and therefore vary in molecular weight. Several definitions of molecular weight are used in practice with number average (M_n) and weight-average (M_w) being most prevalent.[18]

Number-average molecular weight (M_n) is defined as:

$$M_n = \Sigma\, N_x \bullet M_x \qquad (4\text{-}1)$$

wherein N_x = the molar fraction of polymer chains with a given molecular weight (*number* of polymer chains with MW = M_x / total *number* of polymer chains in sample) and M_x = the corresponding molecular weight. The sum is taken for all polymer weights present (all values of "x"). Number-average molecular weight may be determined experimentally by measurement of colligative properties using techniques such as vapour pressure osmometry or membrane osmometry.[18] The value of M_n may be thought of as an arithmetic average of the MW values of individual units in a polymer sample.

Weight-average molecular weight (M_w) is defined as follows:

$$M_w = \Sigma\, w_x \bullet M_x \qquad (4\text{-}2)$$

Wherein w_x = the weight fraction of polymer chains with a given molecular weight (total *mass* of polymer chains with MW = M_x / total *mass* of sample). Weight-average MW values may be measured by light-scattering methods.

If a polymer sample were completely monodisperse, only one molecular weight would be present and represent 100% of the material. Consider a hypothetical polymer (sample 1) composed completely of polymer chains possessing MW = 10 000 g/mol. In this situation:

$M_{n1} = \Sigma N_x \bullet M_x = (1)(10\ 000\ g/mol) = 10\ 000\ g/mol$

$M_{w1} = \Sigma w_x \bullet M_x = (1)(10\ 000\ g/mol) = 10\ 000\ g/mol$

$M_{n1} = M_{w1}$

Now consider two simple mixtures: one composed of polymers possessing near-uniform molecular weight of 10 000 g/mol contaminated with a small amount (10.00 mol%, 1.10 mass%) of oligomers with MW = 1 000 g/mol (sample 2) and the other composed of primarily 1 000 g/mol oligomers with 10.00 mol% (52.63 mass%) of polymers (MW = 10 000 g/mol) - sample 3. For these examples:

$M_{n2} = \Sigma N_x \bullet M_x = (0.1000)(1\ 000\ g/mol) + (0.9000)(10\ 000\ g/mol) = 9\ 100\ g/mol.$

$M_{w2} = \Sigma w_x \bullet M_x = (0.0110)(1\ 000\ g/mol) + (0.9890)(10\ 000\ g/mol) = 9\ 901 g/mol.$

$M_{n3} = \Sigma N_x \bullet M_x = (0.9000)(1\ 000\ g/mol) + (0.1000)(10\ 000\ g/mol) = 1\ 900\ g/mol.$

$M_{w3} = \Sigma w_x \bullet M_x = (0.4737)(1\ 000\ g/mol) + (0.5263)(10\ 000\ g/mol) = 5\ 701 g/mol.$

While these examples are clearly simplified by comparison to a real polymer mixture, they do illustrate one key relationship between different methods of reporting MW. Namely: As M_w gives greater emphasis to heavier components,

any polymer sample containing two or more different MW components will satisfy the relationship $M_w > M_n$. It follows that the more a sample deviates from a perfectly monodisperse molecular weight, the greater will be the difference between M_n and M_w.

It is not sufficient to simply report M_n or M_w as a measure of polymer molecular weight; however, as neither one alone gives any indication of the distribution of polymer molecular weights within a given sample. As M_w and M_n vary more for highly polydisperse samples, the ratio between them provides a useful metric for quantifying polydispersity. This is referred to as the polydispersity index (PDI), defined as follows:

$$PDI = M_w/M_n \tag{4-3}$$

Considering our hypothetical polymer samples from before:

$PDI_1 = M_{w1}/M_{n1}$ = 10 000 g/mol / 10 000 g/mol = 1.0000

$PDI_2 = M_{w2}/M_{n2}$ = 9 901 g/mol / 9 100 g/mol = 1.088

$PDI_3 = M_{w3}/M_{n3}$ = 5 701 g/mol / 1 900 g/mol = 3.001

Therefore, in a perfectly monodisperse system, PDI = 1. As the relationship $M_w > M_n$ is always true in a polydisperse sample, PDI > 1 must also be true. Recall that a greater deviation from perfectly monodisperse results in a greater difference between M_w and M_n. As a result, a sample with a broad MW distribution would possess a greater value of PDI. As M_w is more strongly influenced by high molecular weight components, PDI is as well ($PDI_3 > PDI_2$).

Though the use of M_w as a method for reporting average molecular weight may seem less intuitive than using M_n (essentially an arithmetic average), M_w is

considered preferable as the macroscopic properties of polymers are more heavily influenced by their higher-MW components.[18] In practice, either M_n or M_w may be reported along with PDI; therefore, it is necessary to determine both M_n and M_w to properly describe a polymer sample's MW distribution.

Gel-permeation chromatography (GPC), also known as size-exclusion chromatography (SEC), is a powerful technique for characterizing the molecular weight distribution of a polymer sample. In GPC, a separation column is packed with porous beads of varying pore size. A polymer sample is then introduced within a solvent phase which moves through the column. Large polymers are not able to fit within the pores of most SEC beads, spend proportionally more time within the mobile phase, and therefore elute more quickly. Relatively small polymers are able to permeate the SEC beads more readily and spend relatively less time within the mobile phase. They therefore elute more slowly. As a result, polymers are separated based on size (which, of course, is closely related to molecular weight) and the GPC column may be coupled to an appropriate detector (such as a light-scattering detector) to quantify the eluting polymer as a function of elution volume.[2] Provided that the relationship between MW and elution volume is known (determined by running standards of known MW either in series or in parallel with unknown samples), this will directly give rise to a distribution of MW values which may be used to calculate both M_n and M_w.[18]

If polymer composition and MW distribution are known, the final question to be addressed concerns the identity of the end groups of a polymer chain. While the end groups of large polymers impart little influence on the macroscopic

properties of the materials themselves, they may provide opportunity for functionalization or block copolymerization depending on the nature of the functional groups involved.[18] In the case of ring-opening polymerization, end groups are necessarily involved in the first and last steps of the polymerization process; thus, knowledge of the identity of end groups may provide insight into the polymerization mechanism. In the case that a low MW polymer is being observed (< ~100 repeat units) this may be conveniently accomplished by NMR techniques, provided that resonances of the polymer and end groups are well-resolved from each other.[2] If larger polymers are being analyzed (making low-intensity end group NMR resonances difficult to resolve) or if polymer and end group resonances overlap, end group analysis must be achieved by other means (generally MALDI-TOF mass spectrometry)[126] or inferred from prior knowledge of the polymerization mechanism.[1,2]

4-2: *Cationic Organomagnesium Catalysts in Lactone Polymerization*

Both [$\mathbf{L_4}$Mg^{n}Bu]$^+$[B(C_6F_5)$_4$]$^-$ ($\mathbf{C_1}$) and [LMg^{n}Bu]$^+$[BPh_4]$^-$ ($\mathbf{C_2}$) were tested for efficacy in the polymerization of 6-caprolactone. Preliminary studies were conducted using ^{1}H NMR spectroscopy as ^{1}H resonances arising from the ε methylene protons (–C(O)–OC$\boldsymbol{H}_2$–, Figure 4-1) of 6-caprolactone and polycaprolactone (PCL) are known to be well resolved from each other with monomer and polymer signals at 3.6 ppm and 4.0 ppm, respectively (benzene-d_6).[127] Initial NMR-scale polymerization reactions were examined in benzene-d_6 at catalyst loadings below 1% (over 100 equivalents monomer: catalyst) at

ambient temperature. Catalysts $\mathbf{C_1}$ and $\mathbf{C_2}$ were examined at a concentration of ~4 mmol/L and a catalyst loading of ~0.8 mol%. Both were found to be highly active catalysts, giving > 90% conversion of monomer to polymer within four minutes at ambient temperature. The observed results place $\mathbf{C_1}$ and $\mathbf{C_2}$ amongst the most active catalysts for 6-caprolactone polymerization reported to date (Table 1-4, Table 1-5).

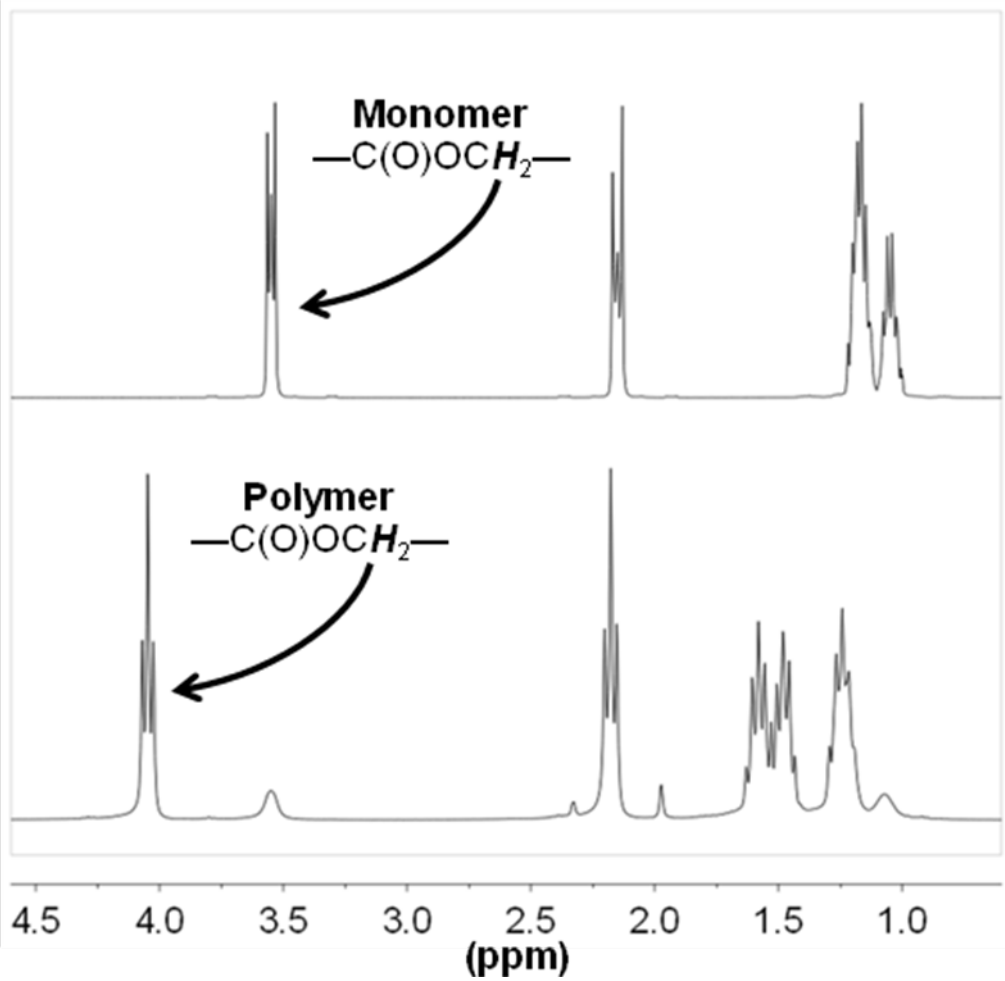

Figure 4-1: Comparison of the ^{1}H NMR spectra of the 6-caprolactone monomer and polymer produced by reaction of 6-caprolactone with $\mathbf{C_1}$ ([catalyst] = 0.42 mmol/L in benzene-d_6, catalyst loading = 0.77%, elapsed time = ~4 min).

Results of initial studies revealed similar catalytic activity of **C_1** and **C_2**. No evidence for interactions between $[\mathbf{L_4}Mg^{n}Bu]^{+}$ and $[BR_4]^{-}$ (R = C_6F_5, Ph) was observed (Chapter 3-3); therefore, the reactivity of $[\mathbf{L_4}Mg^{n}Bu]^{+}$ is expected to be similar for each species. In subsequent studies, $[\mathbf{L_4}Mg^{n}Bu]^{+}[BPh_4]^{-}$ was considered as a model system for polymerization of 6-caprolactone by $[\mathbf{L_4}Mg^{n}Bu]^{+}$. Although initial screening confirmed the efficacy of the catalysts, data collection did not provide more than a crude estimate of activity as catalysis had essentially reached completion before observation could be made.

Three strategies were explored to slow the polymerization to an observable rate: reduction of concentration, reduction of the catalyst loading, and reduction of the reaction temperature. A variety of concentration and catalyst loading conditions were explored at ambient temperature (Table 4-1, entries 1 to 4) and catalyst **C_2** was found to retain appreciable activity at both decreased concentration (as low as 0.40 mmol/L) and catalyst loading (as low as 0.20%), although in all cases the majority of polymerization activity was complete before any observations could be made. At lower concentration (Table 4-1, entry 4), catalytic activity was noted (9% conversion over 4 min) but no substantial reaction progress was observed beyond the first few minutes. The loss of polymerization activity suggested that in high dilution, decomposition of $[\mathbf{L_4}Mg(–O–(CH_2)_5–C(O))_n–^{n}Bu]$ might compete with catalytic propagation of the polymer chain. This established an operating minimum catalyst concentration for subsequent work (~0.40 mM).

Table 4-1: $[\mathbf{L_4}Mg^nBu]^+[B(C_6F_5)_4]^-$ and $[\mathbf{L_4}Mg^nBu]^+[BPh_4]^-$ as catalysts for 6-caprolactone polymerization. (conversion % within 4 minutes of initiation determined by relative ^{1}H NMR integration).

Entry	Catalyst	[Catalyst]	Catalyst Loading	Conversion (%)
1	$\mathbf{C_1}$	4.2 mM	0.77%	95
2	$\mathbf{C_2}$	4.4 mM	0.77%	90
3	$\mathbf{C_2}$	0.40 mM	0.20%	75
4	$\mathbf{C_2}$	0.05 mM	0.2%	9
5	$\mathbf{C_2}$ (at 0ºC)	2.1 mM	0.56%	73

Toward the goal of slowing the polymerization rate, low-temperatures conditions were subsequently examined. Polymerization of 6-caprolactone (~50% to ~90% completion over 15 minutes, Figure 4-2, Figure 4-3[§§]) was observed at 0 ºC using $\mathbf{C_2}$ as a catalyst. Analogous reactions were attempted with temperatures ranging from –20 ºC to –40 ºC (in toluene-d_8); however, these were found to yield poor conversion (between 15% and 70% over 30 minutes). Incomplete conversion at low temperature may be attributed to precipitation of PCL which resulted in a highly viscous (effectively solidified between –20 ºC and –40 ºC) reaction medium.

[§§] The estimated error associated with ^{1}H NMR integration was manually calculated according to examination of raw data with emphasis on ^{1}H integration accuracy. All acquisitions were made over 20 s intervals. Data points have been assigned to the midpoint of each interval.

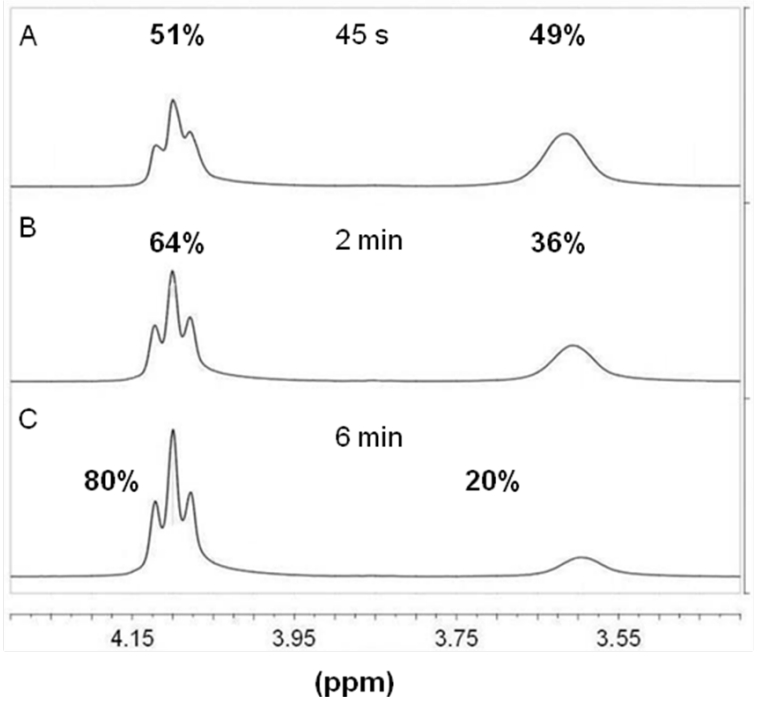

Figure 4-2: Selected ^{1}H NMR spectra illustrating the conversion of 6-caprolactone to PCL. A.) t = 45 s, 51% conversion, B.) t = 2 min 15 s, 64% conversion C.) t = 6 min 10 s, 80% conversion. [$\mathbf{C_2}$] = 2.1 mmol/L, catalyst loading = 0.56%, T = 0 ºC.

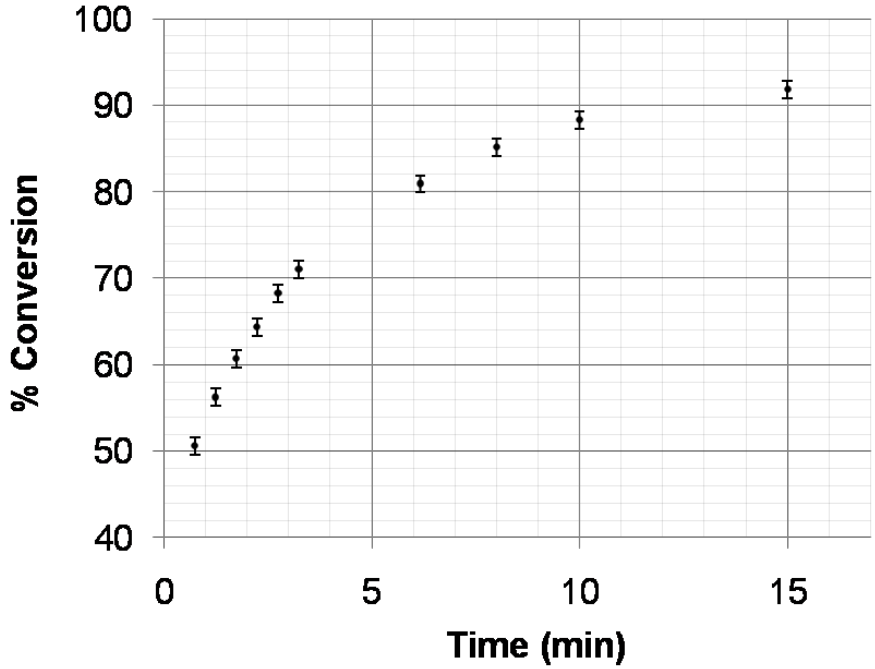

Figure 4-3: Polymerization of 6-caprolactone at 0 ºC using $\mathbf{C_2}$ as a catalyst. Conversion determined by relative ^{1}H NMR integration. [$\mathbf{C_2}$] = 2.1 mmol/L, catalyst loading = 0.56%. Error bars denote estimated error in % conversion.

Having established catalytic activity of **C_1** and **C_2** for 6-caprolactone polymerization, characterization of resultant polymers was of interest. Under anaerobic conditions, a solution of **C_2** in benzene (2.76 mmol/L) was prepared and neat 6-caprolactone was rapidly injected (catalyst loading: 0.255%), resulting in the immediate formation of a thick gel. Under aerobic conditions, the gel was then injected into a vast excess of methanol to quench the polymerization reaction. This resulted in the immediate precipitation of polycaprolactone as a white solid. The molecular weights of polymers in the sample were determined by GPC analysis to be over 1×10^5 g/mol ($M_w = 2.00 \times 10^5$ g/mol, $M_n = 1.28 \times 10^5$ g/mol). This is higher than the predicted value of $M_n = 4.47 \times 10^4$ g/mol, based on the assumption that each equivalent of catalyst should ideally produce a single polymer chain of uniform length. Heightened molecular weights could be explained by slow initiation relative to propagation in the polymerization mechanism, which would result in a fraction of the catalyst generating high molecular-weight polymers while the remainder produced only low MW oligomers (which may not have precipitated during the quenching step.) The polydispersity of this sample (PDI = 1.56) was notably higher than ideal, corroborating the notion that polymer propagation was rapid relative to initiation resulting in a broadened distribution of polymer molecular weights.

4-3: *Concluding Remarks*

A preliminary examination of the activity of $\mathbf{C_1}$ and $\mathbf{C_2}$ in the polymerization of 6-caprolactone has been accomplished. Both species appear to be highly active in the production of polycaprolactone and display similar reactivity. The use of ^{1}H NMR spectroscopy allows for facile distinction between monomer and polymer present in solution. Though not rapid enough to allow for direct observation of lactone polymerization at ambient temperature, this spectroscopic tool has been used successfully to observe the polymerization process under low-temperature conditions.

Chapter 5

Thesis Conclusions

5-1: *Future Directions*

While the results described herein establish both efficacy and very high activity for **C_1** and **C_2** in the polymerization of 6-caprolactone, a more comprehensive understanding of polymerization kinetics would be desirable. Observation of the polymerization process at reduced temperature may provide a good starting point for a more thorough kinetic study. While the temperature range in which catalysis proceeds slowly enough that it may be observed before reaching completion without generating an exceptionally viscous reaction medium appears fairly narrow (between 0 ºC and 23 ºC), it may be sufficient to establish the temperature-dependence of the rate constant, allowing for calculation of activation parameters ($\Delta H^{\ddagger}$ and $\Delta S^{\ddagger}$ via an Eyring plot).[128] Alternately, adaptation of more rapid experimental techniques (such as stopped-flow kinetics)[129] or development of less reactive systems may be appropriate.

Mechanistic study of the polymerization process would also be desirable. End groups of polymers were not directly observed by ^{1}H NMR spectroscopy due to the overwhelming relative intensity of polymer signals. Confirmation of ^{n}Bu insertion might be achieved by examination of stoichiometric reactions of **C_1** or **C_2** with 6-caprolactone. The lower operating catalyst concentration limit (Table 4-1, entry 4) suggests that in high dilution, decomposition of the active species may hinder its ability to participate in the polymerization process. Stoichiometric study

of 6-caprolactone oligomerization may also provide insight into such a decomposition mechanism. This would in turn provide valuable insight for future generations of this catalyst design.

While the cationic alkylmagnesium catalysts described herein are able to initiate 6-caprolactone polymerization, alkoxides have generally been established as superior lactone polymerization initiators to alkyl groups (Chapter 1-3, Chapter 1-5).[24] Catalysts of the form $[\mathbf{L_4}Mg(OR)]^+[BR'_4]^-$ might increase overall activity while lowering polydispersity of PCL produced, as polymer initiation rates might exceed propagation rates. Synthesis of magnesium akoxides by reaction of magnesium alkyls with alcohols has been established;[130,131] thus, preparation of magnesium alkoxides from $\mathbf{C_1}$ or $\mathbf{C_2}$ is expected to be relatively facile.

Only one ligand architecture has been examined in active 6-caprolactone polymerization catalysts; however, the design provides the opportunity to examine a range of steric and electronic environments by variation of the phosphinimine substituent groups. Modulation of steric bulk could be most easily established by varying the nitrogen-substituent group ("Mes" in the case of $\mathbf{L_4}$). Suitable targets might include phenyl, 4-*iso*propylphenyl, 2,6-di*iso*propylphenyl, or 2,4,6-tri(*tert*butyl)phenyl ("supermesityl") groups. Electronic donation could be modulated by including electron withdrawing or donating groups in either phosphorus or nitrogen substituents. Alteration of the ancillary ligand architecture may provide a means of modulating catalyst reactivity, either to increase the polymerization rates to even higher levels, or slow them sufficiently to produce a model system for the aforementioned kinetic and mechanistic studies.

While efficacy of $\mathbf{C_1}$ and $\mathbf{C_2}$ for 6-caprolactone polymerization has been established, their application to the polymerization of other lactones remains largely unexplored. Extension to the polymerization and copolymerization of other lactones such as lactide or glycolide would also be worthwhile.

5-2: *Conclusion*

The results described herein constitute an initial foray into the use of phosphinimine-bound cationic organomagnesium catalysts for the polymerization of 6-caprolactone. A novel series of neutral, *mono* and *bis* phosphinimines has been successfully prepared by the Staudinger reaction of requisite phosphines with aryl azides. While unforeseen difficulty arose in the initially targeted preparation of neutral magnesium complexes, an alternate route to cationic organomagnesium species was found by reaction of a protonated ligand with a dialkylmagnesium precursor. This gave rise to the desired cationic organomagnesium species which were isolated with non-coordinating tetraarylborane counter-ions.

The novel cationic organomagnesium species synthesized were found to be exceptionally active in the polymerization of 6-caprolactone. Representative polymer samples were characterized by GPC analysis, revealing the molecular weights to be exceptionally high ($> 1 \times 10^5$ g/mol). Preliminary catalytic profiling has been accomplished and thorough kinetic and mechanistic study of these catalysts may provide valuable information for the design of future generations of this highly active system.

Chapter 6

Experimental Details

6-1: *General Methods*

Standard Techniques

All manipulations of air-sensitive materials and reagents were performed using a double-manifold high-vacuum line and standard techniques[132] or under a purified argon or nitrogen atmosphere in a glove box (MBraun Labmaster 130) unless otherwise noted. Specialty glassware including swivel-frit assemblies and thick-walled glass bombs were dried at 110 ºC for no less than 10 hours prior to use, assembled, and evacuated while hot. Liquid nitrogen (–196 ºC), dry ice/acetone (–78 ºC), and ice/water (0 ºC) baths were used for cooling receiving flasks during vacuum transfers of solvents and distillations, as well as maintaining low-temperature conditions. Heated oil baths were allowed to equilibrate prior to use in order to maintain constant temperature (25 to 80 ºC). Heated mixtures were stirred rapidly and temperatures were controlled with the aid of an appropriately heated oil bath.

Solvents

Benzene, toluene, pentane, heptane, tetrahydrofuran and diethylether used in air-sensitive reactions and workup steps were purified using an MBraun solvent purification system (MB-SPS). Stock solvents were stored in a glove box or within teflon-sealed glass bombs over sodium with benzophenone ketyl

indicator (tetrahydrofuran and diethylether) or titanocene indicator (benzene, toluene, pentane, heptane). Solvents were introduced directly from glass bombs into reaction or storage vessels by condensation at –78 ºC. Solvents used in air-stable reactions and workup steps were obtained from commercial sources and used without further purification. Deuterated solvents (Cambridge Isotopes) were dried with sodium over benzophenone ketyl indicator (benzene-d_6, tetrahydrofuran-d_8) or with calcium hydride (toluene-d_8, chloroform-d), vacuum transferred, and stored under an inert atmosphere in a glove box prior to use.

Starting Materials

Phosphines (2,5-*bis*(diphenylphosphino)furan,[112] 4-diphenylphosphinodibenzofuran,[133] 4,6-*bis*(diphenylphosphino)dibenzofuran[134]) and azides ($DippN_3$, $MesN_3$)[135-137] used in the synthesis of the ligand series (**L_1** to **L_4**) were prepared by established procedures. In the preparation of **L_1** and **L_3**, removal of LiCl produced during phosphine formation was found to be higher-yielding following phosphinimine synthesis. In these cases, “crude” masses refer to the combined masses of phosphine and LiCl used. Magnesium-containing precursors were synthesized according to established procedures ($[(THF)_2Mg(CH_2Ph)_2]$,[138] $[Mg(OAr)_2]$ (Ar = 2,6-di^{t}butyl-4-methylphenyl),[130] $[(^nBu)Mg(OAr)]$[131]) or purchased from commercial sources ($[Mg^nBu_2]$, $[MgBr_2(OEt_2)]$, $[MgBr_2]$, $[MgCl_2]$, $[CH_3MgBr]$, $[(PhCH_2)MgCl]$). 6-caprolactone was dried over CaH_2, distilled, and stored under an inert atmosphere prior to use. All

other materials were obtained in high purity (Sigma-Aldrich, Fischer) and used without additional purification.

Nuclear Magnetic Resonance (NMR) Spectroscopy

NMR spectra (^{1}H (300.13 MHz), ^{13}C{^{1}H} (75.47 MHz), ^{31}P{^{1}H} (121.48 MHz), ^{19}F (282.42 MHz), and ^{11}B (96.29 MHz)) were collected using a Bruker Avance II NMR spectrometer equipped with a variable-temperature unit (VTU). NMR spectra were collected at ambient temperature except where otherwise noted and referenced to residual protio solvent resonances (^{1}H), solvent ^{13}C resonances (^{13}C{^{1}H}), or an external standard[139] (triphenylphosphine (^{31}P{^{1}H}: δ –5.1 in benzene-d_6), trifluorotoluene (^{19}F: δ –65.8 in dichloroethane-d_4), trifluoroborane diethyletherate (^{11}B: δ 0 neat)) depending on the nucleus of interest. All ^{1}H and ^{13}C NMR peak assignments were facilitated by DEPT-45, DEPT-90, DEPT-135, COSY, and HSQC experiments. Analyses of spectra were conducted using Bruker Topspin (version 1.3, 2005) or MestreNova (trial version 5.21, 2009) software suites.

Except where otherwise noted, NMR samples and NMR-scale reactions were prepared in a glovebox and sealed with rubber septa. Sample procedures are described in the appropriate sections. Ambient temperature reactions requiring extended observation were stored under an inert atmosphere except when collecting NMR spectra. Reactivity studies requiring heat for short periods of time (<24 hours) were sealed with Parafilm^{TM} and heated in an oil bath. Reactions requiring heat for longer periods of time were transferred to J. Young

tubes to minimize the risk of atmospheric contamination and similarly heated in an oil bath.

Other Instrumentation and Analysis

Single crystals were coated in paratone oil and X-ray crystal structures were collected at –100 ºC using a Bruker AXS SMART APEX II single crystal X-ray diffractometer by Mr. Craig A. Wheaton of this department (**L_1**, **L_4**, **C_2**) or by the author (**L_2**, **L_3**, Appendix 2). Crystal structures were solved with the SHELXTL (Version 6.10) software suite[140] using direct methods and refined on F^2. All non-hydrogen atoms were refined anisotropically and hydrogen atom positions were calculated and refined using a riding model. For structures with extensive solvent disorder (**L_3**, **C_2**), a SQUEEZE data filter was applied to remove solvent electron density using PLATON (Version 60709).

Elemental analyses were performed using an Elementar Vario Microcube by Mr. Craig A. Wheaton of this department or by the author. Samples for elemental analysis were packed and sealed in tin capsules in a glove box.

GPC analysis of polymer samples was conducted by Dr. Andrew McWilliams (Ryerson University) using a Viscotek Triple Detector GPC System outfitted with a model 270 Dual Detector Platform (four capillary viscometer and light scattering detector) and a Refractive Index Detector. Samples were run in THF (1 mg/mL) against polystyrene standards.

Sonication was performed using a VWR 75HT bath where indicated.

6-2: *Experimental Details Pertaining to Chapter 2*

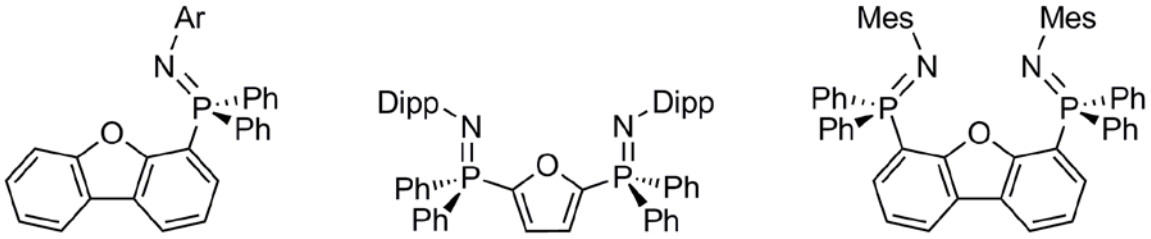

$\mathbf{L_1}$: Ar = Dipp
$\mathbf{L_2}$: Ar = Mes

$\mathbf{L_3}$

$\mathbf{L_4}$

Chart 6-1: Novel species discussed in Chapter 2.

*Synthesis of 4-(DippN=PPh$_2$)dibenzofuran (**L$_1$**):*

A two–neck 100 mL round–bottom flask attached to a swivel frit apparatus was charged with 4-(diphenylphosphino)dibenzofuran (0.7634 g crude, ~0.68 g pure, 1.9 mmol). Toluene (~35 mL) was added by vacuum transfer followed by injection of excess $DippN_3$ (0.4634 g, 2.279 mmol). Within minutes of initiating the reaction, evolution of a colourless gas was observed. The reaction mixture was stirred for 12 h at ambient temperature producing a cloudy yellow solution. Filtration to remove residual LiCl yielded a clear yellow solution, which in turn yielded an oily yellow solid upon removal of toluene *in vacuo*. Approximately 60 mL of pentane was added by vacuum transfer to the crude product and the mixture was sonicated for approximately 2 min and vigorously stirred for 2 h. Filtration of the resulting suspension afforded **L$_1$** as a white powder which was washed three times with 10 mL portions of pentane and dried *in vacuo*. Total yield was 92% (0.922 g, 1.75 mmol). $^{31}P\{^1H\}$ NMR (benzene-d_6): δ –13.4 (s). ^1H NMR (benzene-d_6): δ 7.89–7.80 (ov m, 5H, *o*-PPh_2 + dbf), 7.61 (d, 1H, $^3J_{HH}$ = 6.0

Hz, dbf), 7.51 (m, 1H, dbf), 7.18 (ov d, 2H, *m*-Dipp), 7.08–6.93 (br ov m, 11 H, *m*-PPh_2, *p*-PPh_2, *p*-Dipp, dbf x 4), 3.68 (sp, 2H, $^3J_{HH}$ = 6.9 Hz, Dipp C***H***$(CH_3)_2$), 1.06 (d, 12H, $^3J_{HH}$ = 6.9 Hz, Dipp CH(C***H***$_3)_2$). $^{13}C\{^1H\}$ NMR (benzene-d_6): δ 157.3 (d, $^2J_{CP}$ = 3.0 Hz, dbf-quaternary), 156.9 (s, dbf-quaternary), 145.1 (s, dbf-quaternary), 143.2 (d, $^2J_{CP}$ = 6.8 Hz, *ipso*-Dipp), 134.7 (s, *o*-Dipp ***C***–^{i}Pr) 133.7 (d, $^1J_{CP}$ = 107 Hz, dbf-C_4), 132.9 (d, $^2J_{CP}$ = 10.6 Hz, *o*-PPh_2), 132.2 (d, $^3J_{CP}$ = 5.3 Hz, *m*-PPh_2), 131.6 (d, $^3J_{CP}$ = 3.0 Hz, dbf-C_2), 128.8 (d, $^2J_{CP}$ = 12.8 Hz, dbf-C_3), 128.7 (s, *p*-Dipp), 125.5 (s, dbf-quaternary), 124.6 (d, $^4J_{CP}$ = 2.3 Hz, *p*-PPh_2), 123.6 (s, dbf), 123.5 (s, dbf), 123.3 (s, dbf), 121.1 (s, dbf), 120.5 (s, *m*-Dipp), 118.7 (d, $^1J_{CP}$ = 92.1 Hz, *ipso*-PPh_2), 112.4 (s, dbf), 29.5 (s, Dipp ***C***H$(CH_3)_2$), 24.3 (s, Dipp CH(***C***$H_3)_2$). Anal. Calcd. (%) for $C_{36}H_{34}NOP$: C: 81.95; H: 6.50; N: 2.65; found: C: 81.54; H: 6.75; N: 2.56. X-ray quality single crystals[110] of **L_1** were grown by slow evaporation of a saturated solution of the compound in a toluene and pentane mixture.

*Synthesis of 4-(MesN=PPh_2)dibenzofuran (**L_2**):*

Synthesis of **L_2** was analogous to the aforementioned synthesis of **L_1**. Masses of 4-(diphenylphosphino)dibenzofuran and $MesN_3$ used were 0.6703 g (1.9022 mmol) and 0.8590g (5.3278 mmol), respectively. The product was isolated as a white powder in 68.92% (0.6371 g, 1.311 mmol) yield. $^{31}P\{^1H\}$ NMR (benzene-d_6): δ –15.3 (s). ^1H NMR (benzene-d_6): δ 8.02 (dd, $^2J_{HP}$ = 12.1 Hz, $^3J_{HH}$ = 6.0 Hz, 1H, dbf-C_3), 7.91 (dd, $^3J_{HP}$ = 11.3 Hz, $^3J_{HH}$ = 5.8 Hz, 4H, *o*-PPh_2), 7.61 (d, $^3J_{HH}$ = 6.9 Hz, 1H, dbf), 7.49 (m, 1H, dbf), 7.08-6.93 (br ov m, 10H, *m*-PPh_2,

p-PPh_2, dbf x 4), 6.88 (s, 2H, *m*-Mes), 2.30 (s, 6H, *o*-Mes), 2.21 (s, 3H, *p*-Mes). $^{13}C\{^1H\}$ NMR (benzene-d_6): δ 157.1 (d, $^2J_{CP}$ = 3.0 Hz, dbf-quaternary), 156.8 (s, dbf-quaternary), 145.6 (s, dbf-quaternary), 134.7 (d, $^1J_{CP}$ = 105 Hz, dbf-C_4), 132.8 (d, $^2J_{CP}$ = 9.1 Hz, *o*-PPh_2), 132.7 (s, *p*-Mes ***C***CH_3), 132.4 (d, $^3J_{CP}$ = 6.0 Hz, *m*-PPh_2), 131.5 (d, $^3J_{CP}$ = 3.0 Hz, dbf-C_2), 129.7 (s, *o*-Mes ***C***CH_3), 129.5 (s, *m*-Mes) 128.8 (d, $^2J_{CP}$ = 12.1 Hz, dbf-C_3), 127.7 (s, *ipso*-Mes), 125.4 (s, dbf-quaternary), 124.7 (d, $^4J_{CP}$ = 2.4 Hz, *p*-PPh_2), 123.5 (s, dbf), 123.5 (s, dbf), 123.4 (s, dbf), 121.2 (s, dbf), 119.3 (d, $^1J_{CP}$ = 96.6 Hz, *ipso*-PPh_2), 112.4 (s, dbf), 22.0 (s, *o*-Mes C(***C***H_3)), 21.3 (s, *p*-Mes C(***C***H_3)). Anal. Calcd. (%) for $C_{33}H_{28}NOP$: C: 81.65; H: 5.81; N: 2.88; found: C: 81.16; H: 6.15; N: 2.94. X-ray quality single crystals of **L_2** were grown from a saturated solution in toluene at –35 ºC.

*Synthesis of 2,5-(DippN=PPh_2)$_2$furan (**L_3**):*

A 2-neck 100 mL round-bottom flask attached to a swivel frit apparatus was charged with crude 2,5-*bis*(diphenylphosphino)furan (0.67 g crude, 0.61 g, 1.4 mmol) to which approximately 20 mL of toluene was added. Excess neat $DippN_3$ (0.66 g, 3.3 mmol) was added dropwise and evolution of a colourless gas was observed within minutes. The mixture was allowed to stir for 12 h under an inert atmosphere at ambient temperature then filtered to remove residual LiCl. The filtrate was dried *in vacuo* affording an oily brown solid which was washed with four 10 mL portions of heptane. The product was isolated as a light brown solid in moderate yield (0.52 g, 0.66 mmol, 47%). $^{31}P\{^1H\}$ NMR (benzene-d_6): δ –24.85 (s). $^{31}P\{^1H\}$ NMR (chloroform-*d*): δ –20.71 (s). ^1H NMR (benzene-d_6): δ

7.62 (dd, $^{3}J_{HP}$ = 12.8 Hz, $^{3}J_{HH}$ = 6.9 Hz, 8H, *o*-PPh_2), 7.23 (d, $^{3}J_{HH}$ = 7.8 Hz, 4H, *m*-Dipp), 7.14 – 6.88 (br ov m, 14H, *m*-PPh_2, *p*-PPh_2, *p*-Dipp), 6.63 (s, 2H, furan-C_3***H***), 3.55 (sp, $^{3}J_{HH}$ = 6.8 Hz, 4H, Dipp C***H***$(CH_3)_2$), 1.10 (d, $^{3}J_{HH}$ = 6.8 Hz, 24H, Dipp CH(C***H***$_3)_2$). $^{13}C\{^{1}H\}$ NMR (benzene-d_6): δ 143.5 (s, *o*-Dipp ***C***–^{i}Pr), 142.7 (d, $^{1}J_{CP}$ = 11.9 Hz, furan-C_2), 133.7 (s, *ipso*-Dipp), 132.8 (d, $^{1}J_{CP}$ = 112 Hz, *ipso*-PPh_2), 132.1 (d, $^{2}J_{CP}$ = 8.3 Hz, *o*-PPh_2), 131.5 (d, $^{4}J_{CP}$ = 2.9 Hz, *p*-PPh_2), 128.3 (s, *p*-Dipp), 123.2 (s, *m*-Dipp), 122.7 (dd, $^{3}J_{CP}$ = 14.1 Hz, $^{2}J_{CP}$ = 7.5 Hz, furan-C_3), 120.4 (d, $^{3}J_{CP}$ = 3.1 Hz, *m*-PPh_2), 29.1 (s, Dipp ***C***H$(CH_3)_2$), 23.9 (s, Dipp CH(***C***$H_3)_2$). Anal. Calcd. (%) for $C_{52}H_{56}N_2OP_2$: C: 79.36; H: 7.17; N: 3.56; found: C: 78.81; H: 7.09; N: 3.26. X-ray quality single crystals of **L_3** were grown from a saturated solution in toluene at –35 ºC.

*Synthesis of 4,6-(MesN=$PPh_2)_2$dibenzofuran (**L_4**):*

A 500 mL glass bomb[***] was charged with 5.7732 g (10.760 mmol) of 4,6-*bis*diphenylphosphinodibenzofuran which dissolved fully in 110 mL of toluene. Excess neat $MesN_3$ (4.255 g, 26.39 mmol) was added. Evolution of a colorless gas was noted within 5 min and the solution was allowed to stir at ambient temperature, with occasional venting, for 60 min. The temperature was then gradually raised to 65 °C and the solution was stirred for 16 h, over which time

[***] Note that use of a sealed glass bomb is not necessary in this procedure. While it does provide excellent protection from atmospheric exposure, and the specialty glassware is capable of handling high pressure, use of a heated, sealed system could be considered an unnecessary safety hazard. This may be avoided by using a round-bottom flask equipped with a water condenser under an argon atmosphere.

the color changed from yellow to light brown. An additional 0.459 g (2.85 mmol) of neat $MesN_3$ was added and the reaction mixture was allowed to stir at 65 °C until the ^{31}P NMR spectrum of crude reaction mixture aliquots indicated that the reaction had reached completion (approximately 2 additional h). The solution was cooled to ambient temperature and transferred to a 100 mL round-bottom flask in two fractions of approximately 60 mL each. The solvent was removed *in vacuo* between fractions and after the full volume had been transferred, yielding an oily yellow solid. All subsequent manipulations were conducted under aerobic conditions. The product was washed five times with 50 mL fractions of hexane. During each washing procedure, the mixture was sonicated and vigorously stirred for 5 min prior to filtration. The product was collected as a white powder and dried *in vacuo*. Total yield was 93.9% (8.10 g, 10.1 mmol). $^{31}P\{^1H\}$ NMR (benzene-d_6): δ –17.6 (s). ^1H NMR (benzene-d_6): δ 7.82 (dd, $^3J_{HP}$ = 12.3 Hz, $^3J_{HH}$ = 9.2 Hz, 2H, dbf-$C_{3/7}$***H***), 7.71 – 7.60 (m, 8H, *o*-PPh_2), 7.57 (m, 2H, dbf-$C_{1/9}$***H***), 7.02 – 6.82 (br ov m, 18H, dbf-$C_{2/8}$***H*** + *m*-PPh_2 + *p*-PPh_2 + *m*-Mes), 2.27 (s, 6H, *p*-Mes), 1.93 (s, 12H, *o*-Mes). $^{13}C\{^1H\}$ NMR (benzene-d_6): δ 157.0 (s, dbf-quaternary), 145.2 (s, dbf-quaternary), 133.0 (s, *p*-Mes ***C***CH_3), 132.7 (d, $^3J_{CP}$ = 7.5 Hz, *m*-PPh_2), 132.0 (d, $^2J_{CP}$ = 10.6 Hz, *o*-PPh_2), 131.9 (d, $^1J_{CP}$ = 50.6 Hz, dbf-$C_{4/6}$), 131.3 (s, dbf-$C_{1/9}$), 129.0 (s, dbf-$C_{2/8}$), 128.6 (s, *m*-Mes), 127.0 (d, $^3J_{CP}$ = 3.0 Hz, *o*-Mes ***C***CH_3), 124.5 (d, $^2J_{CP}$ = 6.8 Hz, *ipso*-Mes), 124.0 (s, *p*-PPh_2), 123.1 (d, $^2J_{CP}$ = 9.8 Hz, dbf-$C_{3/7}$), 121.5 (d, $^1J_{CP}$ = 93.6 Hz, *ipso*-PPh_2), 21.1 (s, *o*-Mes C***C***H_3), 21.0 (s, *p*-Mes C***C***H_3). Anal. Calcd. (%) for $C_{54}H_{48}N_2OP_2$: C, 80.76; H, 6.04; N, 3.48. Found: C, 80.46; H, 6.03; N, 3.49. X-ray quality single

crystals[110] of **L_4** were grown by slow evaporation of a saturated solution of the compound in a toluene and pentane mixture.

Reactivity studies utilizing neutral ligands:

A wide variety of reactions between neutral ligands (**L_1**, **L_2**, **L_3**, **L_4**) and neutral magenesium-containing precursors ([Mg^{n}Bu$_2$], [MgBr$_2$(OEt$_2$)], [MgBr$_2$], [MgCl$_2$], [CH$_3$MgBr], [(PhCH$_2$)MgCl], [(THF)$_2$Mg(CH$_2$Ph)$_2$], [Mg(OAr)$_2$] (Ar = 2,6-di^{t}butyl-4-methylphenyl), [(^{n}Bu)Mg(OAr)]) were explored. Typically, these reactions were performed on a scale of 1 to 10 mg (masses known to +/- 0.1 mg) of the ligand of interest with 0.8 to 1.2 molar equivalents magnesium precursor (except where noted otherwise) in approximately 0.5 mL of a deuteurated solvent (C_6D_6 or ~10:1 C_6D_6:THF). Reactions were performed analogously to the following procedure:

An NMR tube was charged with 0.0057 g (0.0071 mmol) of **L_4** and 0.0024 g (0.0068 mmol) [(PhCH$_2$)$_2$Mg(THF)$_2$] which fully dissolved upon addition of 0.5 mL of benzene-*d_6*. The reaction was monitored by collecting ^{31}P{^{1}H} and ^{1}H NMR spectra at 4 h intervals for the first 12 h, then at least once per 24 h interval until no further progress was noted (approximately 72 h).

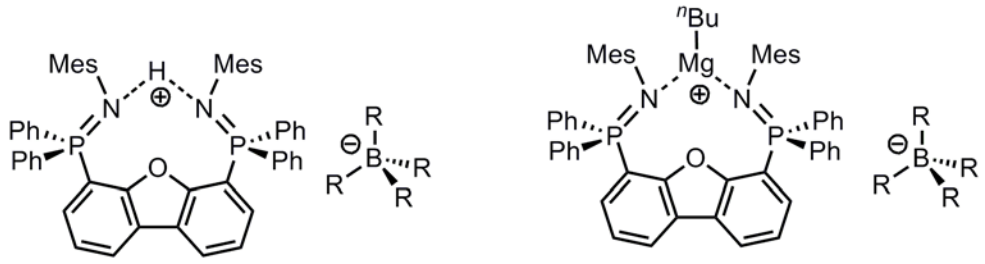

A_1: R = C_6F_5
A_2: R = Ph

C_1: R = C_6F_5
C_2: R = Ph

Chart 6-2: Novel species discussed in Chapter 3.

*Synthesis of [H-4,6-(MesN=PPh$_2$)$_2$dibenzofuran]$^+$[B(C$_6$F$_5$)$_4$]$^-$ (**A$_1$**):*

A 50 mL round-bottom flask was charged with 0.2710 g (0.3375 mmol) of **L$_4$**, 0.2659 g (0.3319 mmol) of [HNMe$_2$Ph]$^+$[B(C$_6$F$_5$)$_4$]$^-$ and 10 mL of benzene. The solution was stirred for 10 min and the benzene was removed *in vacuo* affording an oily, light yellow solid containing the desired product and Me$_2$NPh. The flask was attached to a swivel frit apparatus and the solid was washed three times with 10 mL portions of pentane. During each washing procedure, the mixture was sonicated and stirred for several minutes before filtration. The resultant light yellow solid was dried *in vacuo* for 20 h. A total of 0.3945 g (0.2660 mmol) of **A_1** was recovered as an analytically pure light yellow solid (80.1% yield). ^{31}P{^{1}H} NMR (benzene-*d*$_6$): δ 10.1 (s). ^{31}P{^{1}H} NMR (chloroform-*d*): δ 9.4 (s). ^{1}H NMR (chloroform-*d*): δ 8.30 (d, $^3J_{HH}$ = 6.0 Hz, 2H, dbf-C$_{1/9}$***H***), 7.57 – 7.21 (br ov m, 24H, dbf-C$_{2/8}$***H*** + dbf-C$_{3/7}$***H*** + *o*-PPh$_2$ + *m*-PPh$_2$ + *p*-PPh$_2$), 6.58 (s, 4H, *m*-Mes), 5.72 (br s, 1H, N***H***), 2.17 (s, 6H, *p*-Mes), 1.55 (s, 12H, *o*-Mes). ^{13}C{^{1}H} NMR (chloroform-*d*): δ 157.2 (s, dbf-quaternary), 134.6 (d, $^3J_{CP}$ = 5.3 Hz, dbf-

$C_{2/8}$), 134.0 (s), 133.4 (s), 132.6 (d, $^{2}J_{CP}$ = 10.6 Hz, *o*-PPh_2), 131.2 (s), 130.0 (s, *p*-PPh_2), 129.8 (s, *m*-PPh_2), 129.5 (s, *m*-Mes), 127.1 (s, dbf-$C_{1/9}$), 125.4 (s), 124.0 (s), 123.3 (s), 20.8 (s, *p*-Mes C***C***H_3), 20.1 (s, *o*-Mes C***C***H_3). $B(C_6F_5)_4^-$ resonances not reported. *Ipso*-PPh_2 not observed. ^{19}F NMR (chloroform-*d*): δ –131.7 (br d, $^{3}J_{FF}$ = 10 Hz, 8F, *o*-C_6F_5), –162.4 (t, $^{3}J_{FF}$ = 22 Hz, 4F, *p*-C_6F_5), –166.0 (m, 8F, *m*-C_6F_5). ^{19}F NMR (benzene-d_6): δ –130.8 (br d, $^{3}J_{FF}$ = 11 Hz, 8F, *o*-C_6F_5), –161.7 (t, $^{3}J_{FF}$ = 22 Hz, 4F, *p*-C_6F_5), –165.5 (m, 8F, *m*-C_6F_5). ^{11}B NMR (chloroform-*d*): δ –16.7 (br s). Anal. Calcd. (%) for $C_{78}H_{49}BF_{20}N_2OP_2$: C, 63.17; H, 3.34; N, 1.89. Found: C, 63.34; H, 3.37; N, 1.95.

*Synthesis of [H-4,6-(MesN=PPh_2)$_2$dibenzofuran]$^+$[BPh_4]$^-$ (**A$_2$**):*

Under aerobic conditions, two solutions: one containing 1.0531 g (1.3115 mmol) of previously prepared **L$_4$** in 125 mL of benzene, the other containing 0.4418 g (1.291 mmol) of $NaBPh_4$ in 75 mL of distilled water, were prepared. The aqueous solution was added to the organic solution in a 500 mL round-bottom flask and the mixture was stirred vigorously for 25 min. The organic layer was decanted and washed with three 50 mL portions of distilled water. The organic layer was then thoroughly dried *in vacuo* for 14 h, yielding the desired product as an analytically-pure light yellow solid in high yield (1.2508 g, 1.1136 mmol, 86.26%). ^{31}P{^{1}H} NMR (benzene-d_6): δ 10.1 (s). ^{31}P{^{1}H} NMR (chloroform-*d*): δ 9.5 (s). ^{1}H NMR (chloroform-*d*): δ 8.14 (d, $^{3}J_{HH}$ = 6.3 Hz, 2H, dbf-$C_{1/9}$***H***), 7.46 – 7.31 (ov m, 24H, dbf-$C_{2/8}$***H*** + dbf-$C_{3/7}$***H*** + *o*-PPh_2 + *p*-PPh_2 + *o*-BPh_4^-),

7.30 – 7.19 (m, 8H, *m*-PPh_2), 6.95 (dd, $^3J_{HH}$ = 7.4 Hz, $^3J_{HH}$ = 6.1 Hz, 8H, *m*-BPh_4^-), 6.82 (t, $^3J_{HH}$ = 7.4 Hz, 4H, *p*-BPh_4^-), 6.58 (s, 4H, *m*-Mes), 5.69 (br s, 1H, N***H***), 2.18 (s, 6H, *p*-Mes), 1.56 (s, 12H, *o*-Mes). $^{13}C\{^1H\}$ NMR (chloroform-*d*): δ 164.4 (1:1:1:1 q, $^1J_{CB}$ = 49.1 Hz, *ipso*-BPh_4^-), 157.0 (s, dbf-quaternary), 136.5 (s, *o*-BPh_4^-), 134.5 (s, dbf-$C_{2/8}$), 133.9 (s), 133.6 (s), 132.5 (d, $^2J_{CP}$ = 9.8 Hz, *o*-PPh_2), 131.2 (s), 129.6 (s, *p*-PPh_2), 129.3 (s, *m*-PPh_2), 128.5 (s, *m*-Mes), 127.4 (s, dbf-$C_{1/9}$), 125.5 (s, *m*-BPh_4^-), 125.1 (s) 124.2 (d, $^2J_{CP}$ = 6.0 Hz, dbf-$C_{3/7}$), 123.4 (s), 121.6 (s, *p*-BPh_4^-), 20.8 (s, *o*-Mes C***C***H_3), 20.2 (s, *p*-Mes C***C***H_3). *Ipso*-PPh_2 not observed. ^{11}B NMR (chloroform-*d*): δ –6.5 (br s). Anal. Calcd. (%) for $C_{78}H_{69}BN_2OP_2$: C, 83.39; H, 6.20; N, 2.49. Found: C, 83.24; H, 6.11; N, 2.51.

*Synthesis of [4,6-(MesN=PPh_2)$_2$dibenzofuran·MgBu]$^+$[$B(C_6F_5)_4$]$^-$ (**C_1**):*

Under argon, a 50 mL round-bottom flask was charged with 0.1791 g (0.1207 mmol) of **A_1** to which 12 mL of benzene was added. Di(^{n}butyl)magnesium (0.112 mL of 1.0 M solution in heptane, 0.11 mmol) was slowly injected and evolution of a colorless gas was noted. The solution was stirred for 50 min then benzene was removed *in vacuo*. This afforded the desired product as a pale yellow solid in 73% yield (0.1286 g, 0.08226 mmol). $^{31}P\{^1H\}$ NMR (benzene-d_6): δ 23.0 (s). ^1H NMR (benzene-d_6): δ 7.80 (d, $^3J_{HH}$ = 6.0 Hz, 2H, dbf-$C_{1/9}$***H***), 7.28 (dd, $^3J_{HP}$ = 12 Hz, $^3J_{HH}$ = 9.2 Hz, 8H, *o*-PPh_2), 7.09 – 6.97 (br ov m, 6H, dbf-$C_{2/8}$***H*** + *p*-PPh_2), 6.97 – 6.80 (br ov m, 10H, dbf-$C_{3/7}$***H*** + *m*-PPh_2), 6.36 (s, 4H, *m*-Mes), 2.04 (s, 6H, *p*-Mes), 1.50 (s, 12H, *o*-Mes), 1.38 – 1.32 (ov m, 4H, $MgCH_2C$***H***$_2C$***H***$_2CH_3$), 0.99 (t, $^3J_{HH}$ = 7.3 Hz, 3H, $MgCH_2CH_2CH_2C$***H***$_3$),

–0.13 (t, $^{3}J_{HH}$ = 9.2 Hz, 2H, MgC***H***$_2$CH$_2$CH$_2$CH$_3$). ^{13}C{^{1}H} NMR (benzene-d_6): δ 156.8 (s, dbf-quaternary), 137.3 (s, *p*-Mes ***C***CH$_3$), 135.6 (d, $^{2}J_{CP}$ = 6.8 Hz, dbf-quaternary), 134.1 (d, $^{2}J_{CP}$ = 9.1 Hz, *o*-PPh$_2$), 133.9 (s), 133.7 (d, $^{1}J_{CP}$ = 45.5 Hz, dbf-C$_{4/6}$), 133.1 (d, $^{2}J_{CP}$ = 9.8 Hz, dbf-C$_{3/7}$), 130.0 (s, *m*-Mes), 129.6 (s), 129.4 (s), 128.1 (s), 126.4 (s), 125.3 (d, J_{CP} = 8.3 Hz), 112.7 (d, $^{1}J_{CP}$ = 106 Hz, *ipso*-PPh$_2$), 32.0, 30.2 (s, MgCH$_2$***C***H$_2$***C***H$_2$CH$_3$), 20.6 (s, *p*-Mes C***C***H$_3$), 20.1 (s, *o*-Mes C***C***H$_3$), 14.1 (s, MgCH$_2$CH$_2$CH$_2$***C***H$_3$), 12.0 (s, Mg***C***H$_2$CH$_2$CH$_2$CH$_3$). B(C$_6$F$_5$)$_4^-$ resonances not reported. ^{19}F NMR (benzene-d_6): δ –130.7 (d, $^{3}J_{FF}$ = 11 Hz, 8F, *o*-C$_6$F$_5$), –161.7 (t, $^{3}J_{FF}$ = 22 Hz, 4F, *p*-C$_6$F$_5$), –165.5 (m, 8F, *m*-C$_6$F$_5$). ^{11}B NMR (benzene-d_6): δ –15.8 (br s). Anal. Calcd. (%) for C$_{82}$H$_{57}$BF$_{20}$MgN$_2$OP$_2$: C, 62.99; H, 3.68; N, 1.79. Found: C, 62.17; H, 3.86; N, 1.84.

*Synthesis of [4,6-(MesN=PPh$_2$)$_2$dibenzofuran·MgBu]$^+$[BPh$_4$]$^-$ (**C$_2$**):*

Under argon, a 100 mL round-bottom flask was charged with 0.7422 g (0.6608 mmol) of **A$_2$** to which 40 mL of benzene was added. A solution of Di(^{n}butyl)magnesium (0.66 mL of 1.0 M solution in heptane, 0.66 mmol) in 4 mL of benzene was slowly injected. Evolution of a gas was noted, followed by a color change from yellow to pale pink as the reaction mixture was allowed to stir for 30 min at ambient temperature. The solvent was removed *in vacuo* yielding the desired material as a pale pink solid (0.7242 g, 0.6017 mmol, 91.07%). ^{31}P{^{1}H} NMR (benzene-d_6): δ 23.2 (s). ^{1}H NMR (benzene-d_6): δ 8.09 – 8.01 (br m, 8H, *o*-BPh$_4^-$), 7.64 (d, $^{3}J_{HH}$ = 6.0 Hz, 2H, dbf-C$_{1/9}$***H***), 7.26 (dd, $^{3}J_{HP}$ = 12 Hz, $^{3}J_{HH}$ = 9.1 Hz, 8H, *o*-PPh$_2$), 7.19 (ov t, $^{3}J_{HH}$ = 7.4 Hz, 4H, *p*-BPh$_4^-$), 7.09 – 6.97 (br ov m,

14H, dbf-$C_{2/8}$***H*** + *p*-PPh_2 + *m*-BPh_4^-), 6.97 – 6.84 (br ov m, 10H, dbf-$C_{3/7}$***H*** + *m*-PPh_2), 6.35 (s, 4H, *m*-Mes), 2.03 (s, 6H, *p*-Mes), 1.52 (s, 12H, *o*-Mes), 1.38 – 1.32 (ov m, 4H, $MgCH_2C\boldsymbol{H}_2C\boldsymbol{H}_2CH_3$), 0.99 (t, $^3J_{HH}$ = 7.3 Hz, 3H, $MgCH_2CH_2CH_2C\boldsymbol{H}_3$), –0.13 (t, $^3J_{HH}$ = 9.2 Hz, 2H, $MgC\boldsymbol{H}_2CH_2CH_2CH_3$). $^{13}C\{^1H\}$ NMR (benzene-d_6): δ 165.4 (1:1:1:1 q, $^1J_{CB}$ = 48.3 Hz, *ipso*-BPh_4^-), 156.6 (s, dbf-quaternary), 137.5 (s, *m*-BPh_4^-), 137.2 (s), 135.7 (d, $^2J_{CP}$ = 6.8 Hz, dbf-quaternary), 133.9 (ov m, *o*-PPh_2), 133.8 (s), 133.1 (d, $^2J_{CP}$ = 9.1 Hz, dbf-$C_{3/7}$), 129.9 (s, *m*-Mes), 129.7 (s), 129.5 (s), 128.1 (s), 126.5 (s), 126.2 (s, *o*-BPh_4^-), 125.4 (d, J_{CP} = 8.3 Hz), 122.2 (s, *p*-BPh_4^-), 112.2 (d, $^1J_{CP}$ = 107 Hz, *ipso*--PPh_2), 32.0, 30.2 (s, $MgCH_2\boldsymbol{C}H_2\boldsymbol{C}H_2CH_3$), 20.6 (s, *p*-Mes C$\boldsymbol{C}H_3$), 20.3 (s, *o*-Mes C$\boldsymbol{C}H_3$), 14.0 (s, $MgCH_2CH_2CH_2\boldsymbol{C}H_3$), 11.9 (s, Mg$\boldsymbol{C}H_2CH_2CH_2CH_3$). Dbf-$C_{4/6}$ not observed. ^{11}B NMR (benzene-d_6): δ –5.6 (br s). Anal. Calcd. (%)[110] for $C_{82}H_{77}BMgN_2OP_2$: C, 81.81; H, 6.46; N, 2.33. Found: C, 80.85; H, 6.33; N, 2.72. X-ray quality single crystals of **C_2**[110] were grown by diffusion of heptane into a benzene solution of the compound.

6-4: *Experimental Details Pertaining to Chapter 4*

Monitoring Polymerization Using NMR Spectroscopy:

A representative procedure for the polymerization of 6-caprolactone by **C_2** (monitored by NMR spectroscopy) is described herein. All NMR-scale polymerization procedures using **C_1** and **C_2** made use of similar methods. An NMR tube was charged with 0.0010 g (0.00083 mmol) of **C_2**, to which 2.2 mL of benzene-d_6 was added. The tube was capped with a rubber NMR tube septum

which was then wrapped in parafilm and shaken vigorously. Dry, distilled 6-caprolactone (48 µL, 0.43 mmol, 5.2 x 10^2 equiv.) was measured under an inert atmosphere into a 100.0 µL gastight microsyringe which was sealed by inserting the needle into a rubber septum until just before addition to the catalyst. Prior to monomer injection, all appropriate instrumental parameters were set and NMR spectra ($^{31}P\{^1H\}$ and ^1H) of the catalyst were collected. The sample was then removed from the spectrometer, injected with the monomer, shaken, and reinserted into the NMR spectrometer. Collection of NMR data began within 60 seconds of injection of the monomer. Conversion percentages were determined by integration of the most downfield methylene resonance (–C(O)OC***H***$_2$–) of the polymer (^{1}H NMR (benzene-d_6): δ 3.98 (t, J_{HH} = 6.1 Hz, 2H)) relative to residual monomer (^{1}H NMR (benzene-d_6): δ 3.59 (t, J_{HH} = 6.1 Hz, 2H)), as these resonances were most clearly resolved from all other monomer, polymer, catalyst, and residual solvent resonances.

Polymerization reactions at reduced temperature were conducted analogously; however, samples were prepared in toluene-d_8 and allowed to thermally equilibrate at the temperature of interest for a minimum of 20 min prior to reaction initiation. Samples were generally not removed from the instrument for more than 30 s to allow for monomer injection. The 6-caprolactone monomer was measured and injected neat, requiring only very small volumes by comparison to the reaction mixtures. No correction was made for minor deviations from target temperatures as a result of removing samples from the instrument momentarily or for the small volumes of monomer injected at ambient

temperature. Data was collected at 30 s intervals and each collection lasted 20 s. For the purposes of graphical representation, conversion % values have been assigned to the midpoint of the collection window (for example a conversion % quoted at “t = 45 s” was collected between t = 35 s and t = 55 s.

Polymerization Standards:

Though NMR spectral data of **C_1** and **C_2** did not indicate the presence of any notable impurities, trace amounts of highly active precursors could conceivably contribute to the observed polymerization of 6-caprolactone. In order to confirm the activity of **C_1** and **C_2**, as opposed to residual starting materials from their preparation, a series of standard experiments was performed. Using procedures analogous to the one described above (*Monitoring Polymerization Using NMR Spectroscopy*), precursors **L_4**, **A_1**, and **A_2** were found to be inactive in the polymerization of 6-caprolactone. The precursor [Mg^{n}Bu$_2$], however, is known to be catalytically active,[141] although no kinetic studies have yet been reported.

To verify that the observed polymerization was due to the intended catalysts and not residual [Mg^{n}Bu$_2$], preliminary kinetic profiling was conducted. The polymerization of 6-caprolactone is known to obey second-order kinetics (first order in both catalyst and monomer).[18] Polymerization data for **C_2** (Figure 4-3) measured at 0 ºC gave rise to a pseudo first-order kinetic plot (Figure 6-1) which gave an apparent first order rate constant of 2.6 x 10^{-3} s^{-1}. Correcting for the catalyst concentration (assumed to be constant at 2.1 mmol/L based on

sample preparation), an approximate second-order rate constant of 1.2 $mol^{-1}Ls^{-1}$ (0.0026 s^{-1} / 0.0021 mol/L) for the overall process was determined.[†††] Note that while the experimental data agrees well with the first-order kinetic model (R^2 = 0.990 for data obtained within the first 10 minutes) a slight curvature is apparent and may have been caused by an increase in reaction mixture viscosity over the course of the reaction.

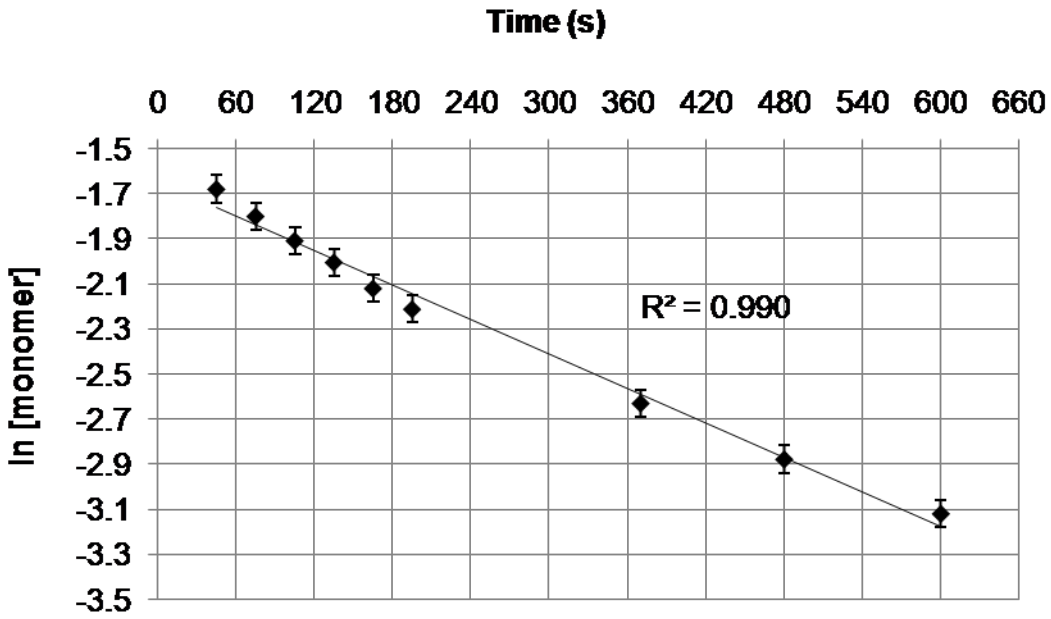

Figure 6-1: Pseudo first-order kinetic plot of the polymerization of 6-caprolactone at 0 ºC using **C_2** (slope = -2.6×10^{-3} s^{-1}).

Following the same procedure, the second-order rate constant associated with [Mg^nBu_2] as a catalyst for 6-caprolactone polymerization was estimated to be 9.7×10^{-3} $mol^{-1}Ls^{-1}$ at 0 ºC (pseudo first-order kinetic plot R^2 = 0.996). As the

[†††] Potential sources of experimental error including integration accuracy, reagent and solvent volumes and masses were considered. Each parameter was manually calculated and the maximum cumulative error was taken as the estimated error of the technique.

rate of polymerization using **C_2** was found to be much greater than that of [Mg^{n}Bu$_2$] alone, it was concluded that even if trace [Mg^{n}Bu$_2$] was present in the isolated complexes, it could not account for the polymerization activity observed.

Preparation of polycaprolactone for GPC analysis:

Under an inert atmosphere, a 50 mL round-bottom flask was charged with 0.0310 g (0.0276 mmol) of catalyst [**L_4**Mg^{n}Bu]$^+$[BPh$_4$]$^-$, to which 10 mL of benzene was added. The solution was stirred rapidly and 1.20 mL (1.24 g, 10.8 mmol, 392 equiv.) of 6-caprolactone was injected resulting in the immediate formation of a thick gel. After 30 min, the reaction mixture was transferred to a 60 mL syringe and added to 100 mL of rapidly stirring methanol under aerobic conditions. This resulted in the immediate precipitation of polymer, which formed a single solid mass that could easily be mechanically separated. The polymer was dried *in vacuo* yielding 0.700 g of material (~57%).

The molecular weight distribution was determined by GPC analysis at a concentration of 1.0 mg/mL in THF (Table 6-1, selected raw data depicted in Figure 6-2). All GPC analysis was conducted using a Viscotek Triple Detector GPC system outfitted with a light-scattering detector. Dr. Andrew McWilliams of Ryerson University is acknowledged for conducting GPC measurements.

Table 6-1: Molecular weight distribution for a polycaprolactone sample produced using **C_2** as a catalyst (determined by GPC analysis).

Trial	M_n (g/mol)	M_w (g/mol)	PDI (Mn/Mw)
1	120 225	193 275	1.60761
2	136 114	206 491	1.51704

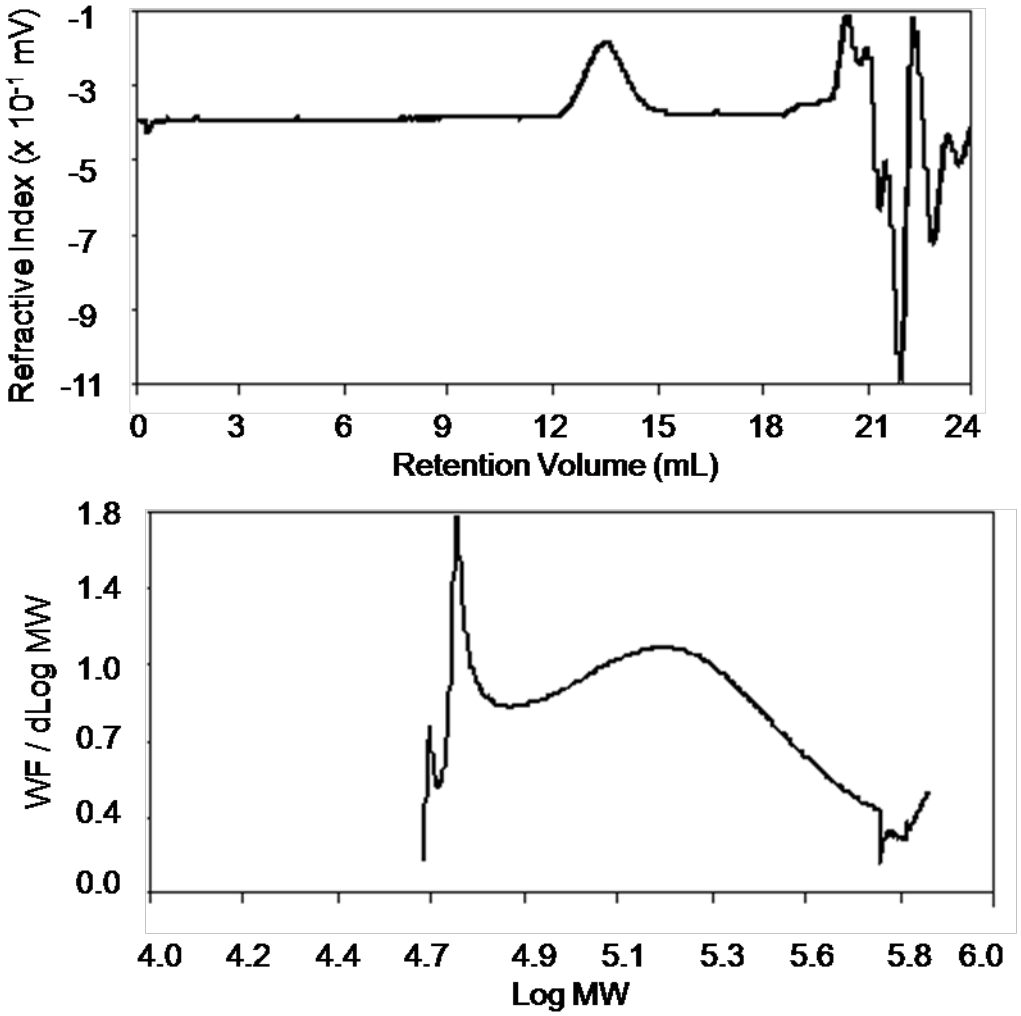

Figure 6-2: GPC trace of polycaprolactone (trial 1) produced using catalyst $\mathbf{C_2}$ (above) and corresponding molecular weight distribution (below).

References

1. Flory, P. J. *Principles of Polymer Chemistry*; Cornell University Press, New York, USA, 1953.

2. Carraher, C. E., Jr. *Polymer Chemistry, 6th Ed.*; Marcel Dekker, Inc., New York, USA, 2003.

3. Arshady, R. *Biodegradable Polymers: Concepts, Criteria, Definitions*. In *Biodegradable Polymers*; Arshady, R; PBM Series, Vol. 2; Kentus Books: London, UK, 2003; 2, pp 1-34.

4. Major Industrial Polymers. *Encyclopædia Britannica [Online]*; Encyclopædia Britannica: Chicago, Il, 2009: http://www.britannica.com/EBchecked/topic/1426103/industrial-polymers/76480/Degradable-polyesters#ref=ref608751 (accessed April 17, 2009).

5. Nyilas, E.; Chiu, T. H. Bioresorbable polyesters and polyester composites. U. S. Patent 4, 481, 353, November 6, 1984.

6. Ajellal, N.; Bouyahyi, M.; Amgoune, A.; Thomas, C. M.; Bondon, A.; Pillin, I.; Grohens, Y.; Carpentier, J.-F. *Macromolecules*, **2009**, *42*, 4, 987-993.

7. Foster, L. J. R. *Appl. Microbiol. Biotechnol.* **2007**, *75*, 1241-1247.

8. Perstorp Caprolactones. http://perstorpcaprolactones.com/ (accessed June 18, 2009).

9. BASF Functional Polymers. http://www.dispersions-pigments.basf.com/portal/basf/ien/dt.jsp?setCursor=1_417477 (accessed June 18, 2009).

10. Shapelock, http://shapelock.com/ (accessed April 17, 2009).

11. Polymorph < Reprap. reprap.org/bin/view/Main/Polymorph (accessed April 17, 2009).

12. Sánchez-Barba, L. F.; Garcés, A.; Fajardo, M.; Alonso-Moreno, C.; Fernández-Baeza, J.; Otero, A.; Antinolo, A.; Tejeda, J.; Lara-Sánchez, A.; López-Solera, M. I. *Organometallics* **2007**, *26*, 6403-6411.

13. Kortaberria, G.; Jimeno, A.; Arruti, P.; de la Caba, K.; Remiro, P.; Eceiza, A.; Mondragon, I. *Macromol. Symp.* **2006**, *239*, 152-158.

14. Krow, G. R. *The Baeyer-Villager Oxidation of Ketones and Aldehydes.* In *Organic Reactions*; Paquette, L. A.; Vol. 43; Wiley: New York, USA, 1993, pp 251-798.

15. Daicel Chemical Industries. http://www.daicel.co.jp/business/index2_e.html (accessed June 18, 2009).

16. Timmins, M.; Liebmann-Vinson, A. *Biodegradable Polymers: Degradation Mechanisms, part 1.* Arshady, R; PBM Series, Vol. 2; Kentus Books: London, UK, 2003; 2, pp 285-328.

17. (a) Wautier, H. Process and catalysts for the preparation of polycaprolactones having high molecular weights. European Patent EP-0626405 (A1), November 30, 1994. (b) Wautier, H.; Detournay, L.; Kaszacs, M. Continuous polymerization of ε-caprolactone using derivative of trialkoxyaluminum as catalyst. European Patent EP-736559 (A1), October 9, 1996.

18. Odian, G., *Principles of Polymerization, 4th Ed.*; John Wiley and Sons, New York, USA, 2004, pp 544-768.

19. Liebmann-Vinson, A.; Timmina, M. *Biodegradable Polymers: Degradation Mechanisms, part 2.* Arshady, R; PBM Series, Vol. 2; Kentus Books: London, UK, 2003; 2, pp 329-372.

20. Yamamoto, M. Procedure for the degradation of biologically degradable polymers. German Patent DE 10063949 (A1), June 27, 2002.

21. (a) Nishida, H.; Tokiwa, Y. *J. Environ. Polym. Degrad.* **1993**, *1*, 227-33. (b) Nishida, H.; Tokiwa, Y. *Chem. Lett.* **1994**, *8*, 1547-1550.

22. Suyama, T.; Tokiwa, Y.; Ouichanpagdee, P.; Kangawa, T.; Kamagata, Y. *Appl. Environ. Microbiol.* **1998**, *64*, 5008-5011.

23. Shimao, M. *Curr. Opin. Biotechnol.* **2001**, *12*, 242-247.

24. Wheaton, C. A.; Hayes, P. G.; Ireland, B. J. *Dalton Trans.* **2009**, 4832-4846.

25. Alonso-Moreno, C.; Garcés, A.; Sánchez-Barba, L. F.; Fajardo, M.; Fernández-Baeza, J.; Otero, A.; Lara-Sánchez, A.; Antinolo, A.; Broomfield, L.; López-Solera, M. I; Rodriguez, A. M. *Organometallics* **2008**, *27*, 1310-1321.

26. Liu, J.; Ling, J.; Li, X.; Shen, Z. *J. Mol. Cat. A: Chem.* **2009**, *300*, 59-64.

27. Biela, T.; Duda, A.; Penczek, S. *Macromol. Symp.* **2002**, *183*, 1-10.

28. (a) Gowda, R. R.; Chakraborty, D. *J. Mol. Cat. A: Chem.* **2009**, *301*, 84-92. (b) Mata-Mata, J. L.; Gutiérrez, J. A.; Paz-sandoval, M. A.; Madrigal, A. R.; Martínez-Richa, A. *J. Polym. Sci.: Part A: Polym. Chem.* **2006**, *44*, 6926-6942. (c) Ning, Y.; Zhang, Y.; Rodriguez-Delgado, A.; Chen, E. Y.-X. *Organometallics* **2008**, *27*, 5632-5640.

29. Sheng, H.-T.; Zhou, H. Gou, H.-D.; Sun, H.-M.; Yao, Y.-M., Wang, J.-F.; Zhang, Y.; Shen, Q. *J. Organomet. Chem.* **2007**, *692*, 1118-1124.

30. Zhang, L.; Nederberg, F.; Pratt, R. C.; Waymouth, R. M.; Hedrick, J. L.; Wade, C. G. *Macromolecules* **2007**, *40*, 4154-4158.

31. Stjerndahl, A.; Rinne-Wistrand, A.; Albertsson, A.-C.; Baecksjoe, C. M.; Lindgren, U. *J. Biomed. Mat. Res. A* **2008**, *87A*, 1086-1091.

32. Duda, A.; Penczek, S.; Kowalski, A.; Libiszowski, J. *Macromol. Symp.* **2000**, *153*, 41-53.

33. Kricheldorf, H. R. *Macromol. Symp.* **2000**, *153*, 55-63.

34. Kricheldorf, H. R.; Stricker, A.; Langanke, D. *Macromol. Chem. Phys.* **2001**, *202*, 2963-2970.

35. Cherdron, H.; Ohse, H.; Korte, F. *Makromol. Chem.* **1962**, *56*, 187-197.

36. Liu, B.; Li, H. Chang-Sik, H.; Kim, I.; Yan, W. *Macromol. Res.* **2008**, *16*, 441-445.

37. Iwasa, N.; Liu, J.; Nomura, K. *Catalysis Commun.* **2008**, *9*, 1148-1152.

38. Lewinski, J.; Horeglad, P.; Dranka, M.; Justyniak, I. *Inorg. Chem.* **2004**, *43*, 5789-5791.

39. Milione, S.; Grisi, F.; Centore, R.; Tuzi, A. *Organometallics* **2006**, *25*, 266-274.

40. Dagorne, S.; Le Bideau, F.; Welter, R.; Bellemin-Laponnaz, S.; Maisse-François, A. *Chem. –Eur. J.* **2007**, *13*, 3202-3217.

41. Haddad, M.; Laghzaoui, M.; Welter, R.; Dagorne, S. *Organometallics* **2009**, DOI: 10.1021/om9003362 (in press).

42. Emig, N.; Nguyen, H.; Krautscheid, H.; Réau, R.; Cazaux, J.-B.; Bertrand, G. *Organometallics* **1998**, *17*, 3599-3608.

43. Chen, C.-T.; Huang, C.-A.; Huang, B.-H. *Macromolecules* **2004**, *37*, 7968-7973.

44. Chen, E. Y.-X.; Marks, T. J. *Chem. Rev.* **2000**, *100*, 1391-1434.

45. Zefirova, A. K.; Shilov, A. E. *Dokl. Akad. Nauk. SSSR* **1961**, *136*, 599-602.

46. Eisch, J. J.; Piotrowski, A. M.; Brownstein, S. K.; Gabe, E. J.; Lee, F. L. *J. Am. Chem. Soc.* **1985**, *107*, 7219-7221.

47. Breslow, D. S.; Newburg, N. R. *J. Am. Chem. Soc.* **1959**, *81*, 81-86.

48. Long, W. *J. Am. Chem. Soc.* **1959**, *81*, 5312-5316.

49. Long, W.; Breslow, D. S. *J. Am. Chem. Soc.* **1960**, *82*, 1953-1957.

50. Deavenport, D. L.; Hodges, J. T., III; Malpass, D. B.; Tran, N. H. Preparation of aluminoxanes using atomized liquid water. US Patent US-5041585 (A), August 20, 1991.

51. Kaminsky, W. *J. Polym. Sci., Part A: Polym. Chem.*, **2004**, *42*, 3911-3921.

52. Sinn, H.; Kaminsky, W.; Vollmer, H. J.; Woldt, R. *Angew. Chem.* **1980**, *92*, 396-402.

53. Zurek, E.; Ziegler, T. *Prog. Polym. Sci.* **2004**, *29*, 107-148.

54. Yang, X.; Stern, C. L.; Marks, T. J. *J. Am. Chem. Soc.* **1991**, *113*, 3623-3625.

55. Yang, X.; Stern, C. L.; Marks, T. J. *J. Am. Chem. Soc.* **1994**, *116*, 10015-10031.

56. Bochmann, M.; Wilson, L. M. *J. Chem. Soc., Chem. Commun.* **1986**, 1610-1611.

57. Bochmann, M.; Wilson, L. M.; Hursthouse, M. B.; Short, R. L. *Organometallics* **1987**, *6*, 2556-2563.

58. Hlatky, G. G.; Upton, D. J.; Turner, H. W. Supported ionic metallocene catalysts for olefin polymerization. International Patent WO 91/09882 September 11,1991.

59. Krossing, I.; Raabe, I. *Angew. Chem., Int. Ed.* **2004**, *43*, 2066-2090.

60. Bochmann, M. *Angew. Chem., Int. Ed.* **1992**, *31*, 1181-1182.

61. (a) Sciarone, T. J. J.; Nijhuis, C. A., Meetsma, A.; Hessen, B. *Organometallics* **2008**, *27*, 2058-2065. (b) Zuccaccia, C.; Stahl, N. G.; Macchioni, A.; Chen, M.-C.; Roberts, J. A.; Marks, T. J. *J. Am. Chem. Soc.* **2004**, *126*, 1448-1464. (c) Köhn, R. D.; Smith, D.; Mahon, M. F.; Prinz, M.; Mihan, S.; Kociok-Köhn, G. *J. Organomet. Chem.* **2003**, *683*, 200-208.

62. Drewitt, M. J.; Niedermann, R. K.; Baird, M. C. *Inorg. Chim. Acta* **2002**, *335*, 43-51.

63. Horton, A. D.; de With, J.; van der Linden, A. J.; van de Weg, H. *Organometallics*, **1996**, *15*, 2672-2674.

64. Korshin, E. E.; Leitus, G.; Shimon, L. J. W.; Konstantinovski, L.; Milstein, D. *Inorg. Chem.* **2008**, *47*, 7177-7189.

65. Hayes, P. G.; Piers, W. E.; Parvez, M. *Chem. –Eur. J.* **2007**, *13*, 2632-2640.

66. O'Keefe, B. J.; Hillmyer, M. A.; Tolman, W. B. *J. Chem. Soc., Dalton Trans.* **2001**, 2215-2224.

67. Han, R.; Parkin, G. *Organometallics* **1991**, *10*, 1010-1020.

68. Han, R.; Parkin, G. *J. Am. Chem. Soc.* **1992**, *114*, 748-757.

69. Chisholm, M. H.; Eilerts, N. W.; Huffmann, S. S.; Pacold, I. M.; Phomphrai, K. *J. Am. Chem. Soc.* **2000**, *122*, 11845-11854.

70. Schofield, A. D.; Barros, M. L.; Cushion, M. G.; Schwarz, A. D.; Mountford, P. *Dalton Trans.* **2009**, 85-96.

71. Wang, Z.-X.; Qi, C.-Y. *Organometallics* **2007**, *26*, 2243-2251.

72. Sánchez-Barba, L. F.; Hughes, D. L.; Humphrey, S. M.; Bochmann, M. *Organometallics* **2006**, *25*, 1012-1020.

73. Sarazin, Y.; Schormann, M.; Bochmann, M. *Organometallics* **2004**, *23*, 3296-3302.

74. Staudinger, H.; Meyer, J. *Helv. Chim. Acta* **1919**, *2*, 635-646.

75. Staudinger, H.; Hauser, E. *Helv. Chim. Acta* **1921**, *4*, 861-886.

76. Nesmeyanov, N. A.; Rebrova, O. A.; Mikul'shina, V. V.; Petrovsky, P. V., Robas, V. I.; Reutov, O. A. *J. Organomet. Chem.* **1976**, *110*, 49-57.

77. Appel, R.; Buchner, W.; Guth, E. *Ann. der Chem.* **1958**, *618*, 53-58.

78. Zimmer, H.; Singh, G. *J. Org. Chem.* **1963**, *28*, 483-486.

79. Appel, R.; Hauss, A. *Angew. Chem.* **1959**, *71*, 626.

80. Abel, E. W.; Mucklejohn, S. A. *Phosphorus and Sulfur* **1981**, *9*, 235-266.

81. Tian, W. Q.; Wang, Y. A. *J. Org. Chem.* **2004**, *69*, 4299-4308.

82. (a) Krannich, L. K.; Kanjolia, R. K.; Watkins, C. L. *Inorg. Chim. Acta* **1985**, *103*, 1-8. (b) Krannich, L. K. *Magn. Res. Chem.* **1987**, *25*, 320-324.

83. Courtenay, S.; Walsh, D.; Hawkeswood, S.; Wei, P.; Das, A. K.; Stephan, D. W. *Inorg. Chem.* **2007**, *46*, 3623-3631.

84. Cavell, R. G.; Kamalesh Babu, R. P.; Aparna, K. J. *J. Organomet. Chem.* **2001**, *617*, 158-169.

85. Welch, G. C.; Piers, W. E.; Parvez, M.; McDonald, R. *Organometallics* **2004**, *23*, 1811-1818.

86. Zhu, D.; Budzelaar, P. H. M. *Organometallics* **2008**, *27*, 2699-2705.

87. Masuda, J. D.; Wei, P.; Stephan, D. W. *Dalton Trans.* **2003**, 3500-3505.

88. Chan, K. T. K.; Spencer, L. P.; Masuda, J. D.; McCahill, J. S. J.; Wei, P.; Stephan, D. W. *Organometallics* **2004**, 381-390.

89. Courtenay, S.; Wei, P.; Stephan, D. W. *Can. J. Chem.* **2003**, *81*, 1471-1476.

90. Alhomaidan, O.; Hollink, E.; Stephan, D. W. *Organometallics* **2007**, *26*, 3041-3048.

91. Alhomaidan, O.; Bai, G.; Stephan, D. W. *Organometallics* **2008**, *27*, 6343-6352.

92. Schmidbaur, H.; Werner, W. *Chem. Ber.* **1967**, *100*, 1016-1022.

93. Wolfsberger, W.; Schmibaur, H. *J. Organomet. Chem.* **1976**, *122*, 5-12.

94. Wolfsberger, W.; Pickel, H. H. *J. Organomet. Chem.* **1973**, *54*, C8-C10.

95. Wolfsberger, W. *Chemiker-Zeitung*, **1981**, *105*, 300-303.

96. Bajpai, K.; Srivastava, R. C. *Synth. React. Inorg. Met.-Org. Chem.* **1982**, *12*, 47-54.

97. Muenzenberg, J.; Noltemeyer, M.; Roesky, H. W. *Chem. Ber.* **1989**, *122*, 1915-1916.

98. Hieber, W.; Winter, E.; Schubert, E. *Chem. Ber.* **1962**, *95*, 3070-3076.

99. Appel, R. Schaff, R. *Z. Naturforsch*, **1961**, *16b*, 405.

100. Beck, W.; Rieber, W.; Kirmaier, H. *Z. Naturforsch.* **1977**, *32b*, 528-532.

101. Schmidbaur, H.; Wolfsberger, W. *Syn. Inorg. Metal-Org. Chem.* **1971**, *1*, 111-116.

102. Bock, H.; Tom Dieck, H. *Z. Naturforsch.* **1966**, *21b*, 739-746.

103. Fukui, M.; Itoh, K.; Ishii, Y. *Bull. Chem. Soc. Jap.* **1975**, *48*, 2044-2046.

104. Seidel, W. *Angew. Chem.* **1965**, *77*, 809-810.

105. Scherer, O. J.; Kuhn, N.; Jungmann, H. *Z. Naturforsch.***1978**, *33b*, 1321-1324.

106. Stephan, D. W.; Guerin, F.; Spence, R. E. v. H.; Koch, L.; Gao, X., Brown, S. J.; Swabey, J. W.; Wang, Q.; Xu, W. Zoricak, P.; Harrison, D. G. *Organometallics* **1999**, *18*, 2046-2048.

107. Stephan, D. W.; Stewart, J. C.; Guerin, F.; Spence, R. E. v. H.; Xu, W.; Harrison, D. G. *Organometallics* **1999**, *18*, 1116-1118.

108. Hill, M. S.; Hitchcock, P. B. *J. Chem. Soc., Dalton Trans.* **2002**, 4694-4702.

109. Zhong-Xia, W.; Chun-Yan, Q. *Organometallics* **2007**, *26*, 2243.

110. Wheaton, C. A.; Hayes, P. G. *Unpublished Results.*

111. Ladd, M. F. C.; Palmer, R. A. *Structure Determination by X-Ray Crystallography, 3rd Ed.*; Plenum Publishing Co., New York, USA, 1994, pp 431-433.

112. Ireland, B. J. Phosphinimine-Containing Heterocyclic Complexes of Group 2 Metals: Potential Catalysts for the Polymerization of Lactide. Undergraduate Thesis, University of Lethbridge, Alberta, 2007.

113. The ether functionality is responsible for directing lithiation to these sites. See: Gschwend, H. W.; Rodriguez, H. R. *Org. React.* **1979**, *26*, 1-360.

114**.** Schwartz, E. B.; Knobler, C. B.; Cram, D. J. *J. Am. Chem. Soc.* **1992**, *114*, 10775-10784.

115. Ahmed, S. A.; Hill, M. S.; Hitchcock, P. B. *Organometallics* **2006**, *25*, 394-402.

116. Wei, P.; Stephan, D. W. *Organometallics* **2003**, *22*, 601-604.

117. Green, S. P., Jones, C., Stasch, A. *Angew. Chem., Int. Ed.* **2008**, *47*, 9079-9083.

118. Hagenbach, A.; Athenstädt, S.; Daróczi, H. E.; Abram, U.; Alberto, R. *Z. Anorg. Allg. Chem.* **2004**, *630*, 2709-2716.

119. Al-Benna, S.; Sarsfield, M. J.; Thornton-Pett, M.; Ormsby, D. L.; Maddox, P. J.; Brès, P.; Bochmann, M. *J. Chem. Soc., Dalton Trans.* **2000**, 4247-4257.

120. Fabicon, R. M.; Pajerki, A. D.; Riche, H. G. *J. Am. Chem. Soc.* **1993**, *115*, 9333-9334.

121. Pajerski, A. D.; Squiller, E. P.; Parvez, M.; Whittle, R. R.; Richey, H. G., Jr. *Organometallics* **2005**, *25*, 809-814.

122. Hannant, M. D.; Schormann, M.; Bochmann, M. *J. Chem. Soc., Dalton Trans.* **2002**, 4071-4073.

123. Hannant, M. D.; Schormann, M.; Hughes, D. L.; Bochmann, M. *Inorg. Chim. Acta.* **2005**, *385*, 1683-1691.

124. AIST: Integrated Spectral Database System of Organic Compounds. http://riodb01.ibase.aist.go.jp/sdbs/cgi-bin/cre_index.cgi?lang=eng (Accessed July 22, 2009).

125. Bondi, A. *J. Phys. Chem.* **1964**, *68*, 441-451.

126. (a) Florjańczyk, Z.; Plichta, A.; Sobczak, M. *Polymer* **2006**, *47*, 1081-1090. (b) Hoskins, J. N.; Grayson, S. M. *PMSE Preprints* **2008**, *98*, 478-479.

127. Zhang, L.; Yu, C.; Shen, Z. *Polym. Bull.* **2003**, *51*, 47-53.

128. Anslyn, E. V.; Dougherty, D. A. *Modern Physical Organic Chemistry*; University Science Books, New York, USA, 2005, pp 370.

129. Wang, R. Y. *Rapid Scan, Stopped-flow Kinetics.* Scott, R. A.; Applications of Physical Methods to Inorganic and Bioinorganic Chemistry; John Wiley and Sons: New York, USA, 2007; 469, pp 469-487.

130. Duff, A. W.; Hitchcock, P. B.; Lappert, M. F.; Taylor, R. G. *J. Organomet. Chem.* **1985**, *293*, 271-283.

131. Ménoret, S.; Fontanille, M. Deffieux, A.; Desbois, P. *Macromol. Chem. Phys.* **2002**, *203*, 1155-1161.

132. Burger, B. J.; Bercaw, J. E. *Experimental Organometallic Chemistry*; American Chemical Society: Washington, D. C., 1987.

133. Haenel, M. W.; Jakubik, D.; Rothenberger, E.; Schroth, G. *Chem. Ber.* **1991**, *124*, 1705-1710.

134. Kranenburg, M.; van der Burgt, Y. E. M.; Kamer, P. C. J.; van Leeuwen, P. W. N. M.; Goubitz, K.; Fraanje, J. *Organometallics* **1995**, *14*, 3081-3089.

135. Spencer, L. P.; Altwer, R.; Wei, P.; Gelmini, L.; Gauld, J.; Stephan, D. W. *Organometallics* **2003**, *22*, 3841-3854.

136. Conroy, K. C. *Personal Communication*, **2007**.

137. Murata, S.; Abe, S.; Tomioka, H. *J. Org. Chem.* **1997**, *62*, 3055-3061.

138. Schrock, R. R. *J. Organomet. Chem.* **1976**, *122*, 209-225.

139. (a) Gottlieb, H. E.; Kotlyar, V.; Nudelman, A. *J. Org. Chem.* **1997**, *62*, 7512-7515. (b) Timokhin, B. V.; Dmitriev, V. I.; Boiko, G. A.; Grechkin, E. F.; Glukhikh, V. I. *Zhurnal Obshchei Khimii* **1977**, *47*, 1267-1270 (c) Grushin, V. V.; *J. Am. Chem. Soc.* **2006**, *128*, 12644-12645. (d) Mercier, H. P. A.; Moran, M. D.; Schrobilgen, G. J.; Christoph, S.; Suontamo, R. J. *J. Am. Chem. Soc.* **2004**, *126*,

5533-5548. (e) Qian, B.; Baek, S. W.; Smith, M. R. III. *Polyhedron* **1999**, *18*, 2405-2414.

140. Sheldrick, G. M. *Acta Cryst.*, **2008**, *A64*, 112-122.

141. Wei, Z.; Liu, L.; Yu, F.; Wang, P.; Qu, C.; Qi, M. *Polym. Bull.*, **2008**, *61*, 407-413.

Appendix 1

Publications Arising From Thesis

The novel ligands $\mathbf{L_2}$ and $\mathbf{L_3}$ have not been published. The ligand $\mathbf{L_4}$ along with the contents of Chapter 3 (species $\mathbf{A_1}$, $\mathbf{A_2}$, $\mathbf{C_1}$, and $\mathbf{C_2}$), preliminary polymerization data for $\mathbf{C_1}$ and $\mathbf{C_2}$, and corresponding experimental details are described in publication 1. The ligand $\mathbf{L_1}$ is described in publication 2.

The author is fully responsible for the contents of publication 1 except for collection and refinement of crystallographic data the preparation of the dicationic ligand derivative $[\mathbf{L_4}H_2]^{2+}[BPh_4]^-_2$ (for which credit is given to Mr. Craig Wheaton of this department). The author contributed to the novel chemistry described in publication 2 in the development, synthesis, and characterization of ligand $\mathbf{L_1}$. Publication 3 does not contain research results by the author except those previously described in publication 2, as it is a review primarily of the works of other scholars. The author played a supporting role in manuscript preparation for publication 3.

1.) Ireland, B. J.; Wheaton, C. A.; Hayes, P. G. Cationic Organomagnesium Complexes as Highly Active Catalysts for the Ring-Opening Polymerization of ε-Caprolactone. *Organometallics* **2009**, submitted.

2.) Wheaton, C. A.; Ireland, B. J.; Hayes, P. G. Activated Zinc Complexes Supported by Neutral, Phosphinimine-Containing Ligands: Synthesis and Efficacy for the Polymerization of Lactide. *Organometallics* **2009**, *28*, 1282-1285.

3.) Wheaton, C. A.; Hayes, P. G.; Ireland, B. J. Complexes of Mg, Ca, and Zn as homogeneous catalysts for lactide polymerization. *Dalton Trans.* **2009**, 4832-4846 (Dalton Perspective Cover Article).

Appendix 2

Crystallographic Details

This section contains crystallographic details for **L_2** and **L_3**, for which the author is responsible, along with selected bond lengths and angles. Credit is given to Mr. Craig A. Wheaton of this department for collection and refinement of structures **L_1**, **L_4**, and **C_2**. Note that the "SQUEEZE" filter (PLATON vers. 60709) was applied to the structure of **L_2** to eliminate disordered solvent (structure refinement values given before and after SQUEEZE for comparison, all other values for **L_2** refer only to the final, structure with solvent removed). The SQUEEZE procedure removed the equivalent electron density of 95 electrons (1.9 equivalents of toluene) per unit cell from a volume of 449.2 $Å^3$ (15.7 % of the unit cell volume) from the dataset.

Table A-1: Crystallographic Data for **L_2**

Crystallographer	Ben Ireland
Formula	$C_{33}H_{28}NOP$
Formula Weight (g/mol)	485.59
Crystal Dimensions (mm)	0.46 x 0.24 x 0.12
Crystal System	Triclinic
Space Group	P(-1) (No. 2)
Unit Cell Parameters	
a (Å)	9.1830(5)
b (Å)	14.4232(7)
c (Å)	22.5008(12)

α (º)	86.958(1)
β (º)	82.190(1)
γ (º)	75.102(1)
V (Å^3)	2852.8(3)
Z	4
ρ_{calcd} (g cm^{-3})	1.130
Data Collection	
Theta range (º)	1.71 - 27.75
Index ranges	–11 < h < 11, –18 < k < 18, –29 < l < 29
Radiation (λ [Å])	0.71073 (Mo kα)
Temperature (ºC)	–100
Reflections	33398
Unique reflections	13124
Data / parameters / restraints	13124 / 746 / 0
Absorption coefficient (mm^{-1})	0.149
Structure Refinement before SQUEEZE	
Method	Direct Methods (SHELXS-97)
Goodness-of-fit (GOF)	2.537
R_1 [$F_o^2 \geq 2\sigma(F_o^2)$]	0.0450
wR_2 [$F_o^2 \geq 2\sigma(F_o^2)$]	0.0827
Structure Refinement after SQUEEZE	
Method	Direct Methods (SHELXS-97) + Squeeze Filter (Platon)
Goodness-of-fit (GOF)	0.947
R_1 [$F_o^2 \geq 2\sigma(F_o^2)$]	0.0372
wR_2 [$F_o^2 \geq 2\sigma(F_o^2)$]	0.1187

Table A-2: Atomic coordinates (x 10^4) and equivalent isotropic displacement parameters ($Å^2$ x 10^3) for **L_2**.

Atom	x	y	z	U(eq)
P(2)	8308(1)	1629(1)	1659(1)	23(1)
P(1)	1693(1)	8371(1)	3340(1)	22(1)
C(60)	7339(3)	1601(1)	2836(1)	26(1)
C(40)	7240(2)	2861(1)	1547(1)	24(1)
C(4)	2763(2)	7143(1)	3457(1)	25(1)
C(11)	2585(2)	6432(1)	3111(1)	22(1)
C(14)	2078(2)	9071(1)	3916(1)	26(1)
C(42)	5373(3)	4107(2)	1085(1)	31(1)
C(26)	2659(3)	8397(1)	2163(1)	26(1)
C(48)	7920(2)	928(1)	1087(1)	26(1)
C(54)	10273(2)	1646(1)	1427(1)	25(1)
C(46)	7393(2)	3603(2)	1896(1)	25(1)
C(2)	4625(3)	5884(2)	3916(1)	32(1)
C(20)	-282(2)	8360(1)	3573(1)	24(1)
C(13)	2867(2)	4967(2)	2715(1)	27(1)
C(45)	8190(2)	4313(1)	2575(1)	26(1)
C(47)	6609(2)	4558(1)	1855(1)	25(1)
C(21)	-1407(3)	9147(2)	3411(1)	32(1)
C(10)	3371(2)	5467(2)	3153(1)	23(1)
C(44)	7157(3)	5028(1)	2297(1)	26(1)
C(55)	11385(2)	858(2)	1592(1)	31(1)
C(27)	4232(3)	8210(2)	1989(1)	29(1)
C(12)	1842(3)	5674(2)	2430(1)	29(1)

C(65)	5765(3)	1793(2)	3012(1)	30(1)
C(25)	-697(3)	7628(2)	3920(1)	30(1)
C(41)	6190(2)	3152(2)	1138(1)	29(1)
C(3)	3815(2)	6841(2)	3866(1)	28(1)
C(59)	10718(3)	2370(2)	1073(1)	30(1)
C(31)	1725(3)	8202(2)	1762(1)	30(1)
C(9)	3136(3)	4024(2)	2525(1)	33(1)
C(43)	5575(2)	4816(2)	1439(1)	28(1)
C(58)	12236(3)	2313(2)	886(1)	34(1)
C(61)	8267(3)	1799(2)	3235(1)	31(1)
C(1)	4425(3)	5187(2)	3561(1)	30(1)
C(35)	6866(3)	5978(2)	2475(1)	33(1)
C(24)	-2222(3)	7684(2)	4111(1)	33(1)
C(64)	5152(3)	2207(2)	3565(1)	37(1)
C(28)	4847(3)	7786(2)	1437(1)	37(1)
C(53)	7185(3)	210(2)	1254(1)	32(1)
C(57)	13323(3)	1520(2)	1054(1)	37(1)
C(15)	2811(2)	9791(2)	3746(1)	31(1)
C(6)	1104(3)	5518(2)	1965(1)	34(1)
C(56)	12911(3)	796(2)	1402(1)	35(1)
C(22)	-2917(3)	9196(2)	3605(1)	36(1)
C(62)	7601(3)	2211(2)	3782(1)	40(1)
C(38)	8914(3)	4481(2)	3041(1)	33(1)
C(36)	7605(3)	6163(2)	2929(1)	39(1)
C(8)	2385(3)	3840(2)	2068(1)	37(1)
C(30)	2404(3)	7788(2)	1214(1)	38(1)

C(37)	8601(3)	5433(2)	3211(1)	38(1)
C(23)	-3326(3)	8464(2)	3954(1)	32(1)
C(7)	1403(3)	4577(2)	1787(1)	38(1)
C(66)	9962(3)	1572(2)	3073(1)	39(1)
C(32)	5244(2)	8468(2)	2390(1)	35(1)
C(19)	1645(3)	8918(2)	4522(1)	37(1)
C(34)	31(3)	8428(2)	1925(1)	38(1)
C(49)	8351(3)	1089(2)	482(1)	38(1)
C(68)	4760(3)	1528(2)	2612(1)	37(1)
C(17)	2705(3)	10169(2)	4773(1)	46(1)
C(52)	6884(3)	-334(2)	815(1)	43(1)
C(51)	7305(3)	-163(2)	215(1)	46(1)
C(16)	3125(3)	10341(2)	4179(1)	45(1)
C(29)	3951(3)	7572(2)	1047(1)	42(1)
C(63)	6045(3)	2431(2)	3962(1)	42(1)
C(33)	4633(4)	7129(2)	440(1)	64(1)
C(50)	8037(3)	547(2)	49(1)	46(1)
C(18)	1970(3)	9460(2)	4951(1)	45(1)
C(67)	5364(3)	2865(2)	4563(1)	63(1)
O(39)	8369(2)	3432(1)	2326(1)	28(1)
O(5)	1633(2)	6568(1)	2677(1)	27(1)
N(1)	2034(2)	8834(1)	2716(1)	26(1)
N(2)	7965(2)	1167(1)	2284(1)	28(1)

Table A-3: Bond Lengths for L_2.

Bond	Length (Å)		Bond	Length (Å)		Bond	Length (Å)
P(2)-N(2)	1.5519(18)		C(60)-N(2)	1.402(3)		C(11)-C(10)	1.398(3)
P(2)-C(48)	1.805(2)		C(60)-C(65)	1.404(3)		C(14)-C(15)	1.387(3)
P(2)-C(54)	1.815(2)		C(60)-C(61)	1.406(3)		C(14)-C(19)	1.391(3)
P(2)-C(40)	1.818(2)		C(40)-C(41)	1.394(3)		C(42)-C(43)	1.392(3)
P(1)-N(1)	1.5507(18)		C(40)-C(46)	1.407(3)		C(42)-C(41)	1.397(3)
P(1)-C(14)	1.808(2)		C(4)-C(11)	1.375(3)		C(26)-C(27)	1.404(3)
P(1)-C(4)	1.816(2)		C(4)-C(3)	1.398(3)		C(26)-N(1)	1.407(3)
P(1)-C(20)	1.821(2)		C(11)-O(5)	1.371(2)		C(26)-C(31)	1.411(3)
C(48)-C(53)	1.384(3)		C(12)-O(5)	1.389(2)		C(19)-C(18)	1.381(3)
C(48)-C(49)	1.390(3)		C(65)-C(64)	1.391(3)		C(49)-C(50)	1.383(3)
C(54)-C(55)	1.389(3)		C(65)-C(68)	1.500(3)		C(17)-C(16)	1.367(4)
C(54)-C(59)	1.392(3)		C(25)-C(24)	1.391(3)		C(17)-C(18)	1.379(3)
C(46)-O(39)	1.377(2)		C(59)-C(58)	1.383(3)		C(52)-C(51)	1.381(4)
C(46)-C(47)	1.384(3)		C(31)-C(30)	1.395(3)		C(51)-C(50)	1.373(3)
C(2)-C(1)	1.379(3)		C(31)-C(34)	1.502(3)		C(29)-C(33)	1.522(3)
C(2)-C(3)	1.396(3)		C(9)-C(8)	1.385(3)		C(63)-C(67)	1.506(3)
C(20)-C(25)	1.381(3)		C(58)-C(57)	1.384(3)		C(47)-C(44)	1.444(3)
C(20)-C(21)	1.394(3)		C(61)-C(62)	1.390(3)		C(21)-C(22)	1.381(3)
C(13)-C(12)	1.392(3)		C(61)-C(66)	1.503(3)		C(10)-C(1)	1.393(3)
C(13)-C(9)	1.397(3)		C(35)-C(36)	1.373(3)		C(44)-C(35)	1.397(3)
C(13)-C(10)	1.442(3)		C(24)-C(23)	1.374(3)		C(55)-C(56)	1.389(3)
C(45)-C(38)	1.377(3)		C(64)-C(63)	1.394(3)		C(27)-C(28)	1.396(3)
C(45)-O(39)	1.378(2)		C(28)-C(29)	1.378(3)		C(27)-C(32)	1.503(3)
C(45)-C(44)	1.395(3)		C(53)-C(52)	1.391(3)		C(12)-C(6)	1.380(3)

C(47)-C(43)	1.393(3)		C(57)-C(56)	1.372(3)		C(8)-C(7)	1.391(3)
C(38)-C(37)	1.392(3)		C(15)-C(16)	1.392(3)		C(30)-C(29)	1.377(3)
C(36)-C(37)	1.393(3)		C(6)-C(7)	1.383(3)		C(22)-C(23)	1.382(3)
C(62)-C(63)	1.389(3)						

Table A-4: Bond Angles for $\mathbf{L_2}$.

Atoms	Angle (º)		Atoms	Angle (º)
N(2)-P(2)-C(48)	109.25(10)		C(11)-C(4)-P(1)	119.13(15)
N(2)-P(2)-C(54)	116.16(10)		C(3)-C(4)-P(1)	125.58(16)
C(48)-P(2)-C(54)	102.88(10)		O(5)-C(11)-C(4)	125.10(17)
N(2)-P(2)-C(40)	116.13(10)		O(5)-C(11)-C(10)	110.88(19)
C(48)-P(2)-C(40)	106.89(9)		C(4)-C(11)-C(10)	124.0(2)
C(54)-P(2)-C(40)	104.37(10)		C(15)-C(14)-C(19)	119.1(2)
N(1)-P(1)-C(14)	109.43(10)		C(15)-C(14)-P(1)	118.92(18)
N(1)-P(1)-C(4)	116.42(10)		C(19)-C(14)-P(1)	122.01(18)
C(14)-P(1)-C(4)	106.46(9)		C(43)-C(42)-C(41)	121.3(2)
N(1)-P(1)-C(20)	115.97(10)		C(27)-C(26)-N(1)	119.43(19)
C(14)-P(1)-C(20)	102.62(10)		C(27)-C(26)-C(31)	119.2(2)
C(4)-P(1)-C(20)	104.69(10)		N(1)-C(26)-C(31)	121.2(2)
N(2)-C(60)-C(65)	119.86(19)		C(53)-C(48)-C(49)	119.3(2)
N(2)-C(60)-C(61)	121.2(2)		C(53)-C(48)-P(2)	119.34(17)
C(65)-C(60)-C(61)	118.9(2)		C(49)-C(48)-P(2)	121.41(17)
C(41)-C(40)-C(46)	114.53(19)		C(55)-C(54)-C(59)	118.8(2)
C(41)-C(40)-P(2)	124.63(16)		C(55)-C(54)-P(2)	117.19(16)
C(46)-C(40)-P(2)	120.80(15)		C(59)-C(54)-P(2)	123.93(16)
C(11)-C(4)-C(3)	115.26(19)		O(39)-C(46)-C(47)	113.00(19)

O(39)-C(46)-C(40)	121.69(19)		C(6)-C(12)-O(5)	123.4(2)
C(47)-C(46)-C(40)	125.3(2)		C(6)-C(12)-C(13)	125.0(2)
C(1)-C(2)-C(3)	121.4(2)		O(5)-C(12)-C(13)	111.57(18)
C(25)-C(20)-C(21)	119.3(2)		C(64)-C(65)-C(60)	119.7(2)
C(25)-C(20)-P(1)	122.74(16)		C(64)-C(65)-C(68)	120.3(2)
C(21)-C(20)-P(1)	117.91(17)		C(60)-C(65)-C(68)	120.0(2)
C(12)-C(13)-C(9)	117.4(2)		C(20)-C(25)-C(24)	120.2(2)
C(12)-C(13)-C(10)	105.07(18)		C(40)-C(41)-C(42)	121.9(2)
C(9)-C(13)-C(10)	137.5(2)		C(2)-C(3)-C(4)	122.0(2)
C(38)-C(45)-O(39)	125.38(19)		C(58)-C(59)-C(54)	120.9(2)
C(38)-C(45)-C(44)	123.6(2)		C(30)-C(31)-C(26)	118.8(2)
O(39)-C(45)-C(44)	111.05(17)		C(30)-C(31)-C(34)	120.6(2)
C(46)-C(47)-C(43)	118.2(2)		C(26)-C(31)-C(34)	120.6(2)
C(46)-C(47)-C(44)	104.43(18)		C(8)-C(9)-C(13)	119.1(2)
C(43)-C(47)-C(44)	137.42(19)		C(42)-C(43)-C(47)	118.84(19)
C(22)-C(21)-C(20)	120.1(2)		C(59)-C(58)-C(57)	119.2(2)
C(1)-C(10)-C(11)	119.6(2)		C(62)-C(61)-C(60)	119.3(2)
C(1)-C(10)-C(13)	133.9(2)		C(62)-C(61)-C(66)	120.1(2)
C(11)-C(10)-C(13)	106.54(18)		C(60)-C(61)-C(66)	120.6(2)
C(45)-C(44)-C(35)	119.4(2)		C(2)-C(1)-C(10)	117.70(19)
C(45)-C(44)-C(47)	106.51(18)		C(36)-C(35)-C(44)	117.8(2)
C(35)-C(44)-C(47)	134.1(2)		C(23)-C(24)-C(25)	120.3(2)
C(56)-C(55)-C(54)	120.4(2)		C(65)-C(64)-C(63)	122.5(2)
C(28)-C(27)-C(26)	119.3(2)		C(29)-C(28)-C(27)	122.0(2)
C(28)-C(27)-C(32)	120.3(2)		C(48)-C(53)-C(52)	119.7(2)
C(26)-C(27)-C(32)	120.4(2)		C(56)-C(57)-C(58)	120.9(2)

C(14)-C(15)-C(16)	120.2(2)		C(51)-C(52)-C(53)	120.6(2)
C(12)-C(6)-C(7)	115.9(2)		C(50)-C(51)-C(52)	119.7(2)
C(57)-C(56)-C(55)	119.8(2)		C(17)-C(16)-C(15)	119.6(2)
C(21)-C(22)-C(23)	120.4(2)		C(30)-C(29)-C(28)	118.2(2)
C(63)-C(62)-C(61)	123.1(2)		C(30)-C(29)-C(33)	120.3(2)
C(45)-C(38)-C(37)	115.8(2)		C(28)-C(29)-C(33)	121.5(3)
C(35)-C(36)-C(37)	121.6(2)		C(62)-C(63)-C(64)	116.6(2)
C(9)-C(8)-C(7)	121.3(2)		C(62)-C(63)-C(67)	121.6(2)
C(29)-C(30)-C(31)	122.4(2)		C(64)-C(63)-C(67)	121.8(3)
C(38)-C(37)-C(36)	121.7(2)		C(51)-C(50)-C(49)	120.1(3)
C(24)-C(23)-C(22)	119.8(2)		C(17)-C(18)-C(19)	119.5(3)
C(6)-C(7)-C(8)	121.3(2)		C(46)-O(39)-C(45)	104.97(15)
C(18)-C(19)-C(14)	120.5(2)		C(11)-O(5)-C(12)	105.89(15)
C(50)-C(49)-C(48)	120.6(2)		C(26)-N(1)-P(1)	129.79(14)
C(16)-C(17)-C(18)	121.1(2)		C(60)-N(2)-P(2)	129.90(14)

Table A-5: Crystallographic Data for $\mathbf{L_3}$

Crystallographer	Ben Ireland (training session with René Boeré)
Formula	$C_{64}H_{60}N_2OP_2$
Formula Weight (g/mol)	935.08
Crystal System	Monoclinic
Space Group	C2/c (No. 15)
Unit Cell Parameters	
a (Å)	23.4354(13)
b (Å)	9.8000(6)
c (Å)	19.8794(11)

β (º)	102.5860(10)
V (Å^3)	4455.9(4)
Z	4
ρ_{calcd} (g cm^{-3})	1.394
Data Collection	
Theta range (º)	1.78 - 28.77
Index ranges	–31 < h < 31, –13 < k < 13, –25 < l < 25
Radiation (λ [Å])	0.71073 (Mo kα)
Temperature (ºC)	–100
Reflections	5463
Unique reflections	4529
Data / parameters / restraints	5463/263/0
Absorption coefficient (mm^{-1})	0.120
Structure Refinement	
Method	Direct Methods (SHELXS-97)
Goodness-of-fit (GOF)	1.037
R_1 [$F_o^2 \geq 2\sigma(F_o^2)$]	0.0408
wR_2 [$F_o^2 \geq -3\sigma(F_o^2)$]	0.1040

Table A-6: Atomic coordinates (x 10^4) and equivalent isotropic displacement parameters (Å^2 x 10^3) for **L_3**.

Atom	x	y	z	U(eq)
P(1)	3797(1)	951(1)	2048(1)	22(1)
C(10)	4246(1)	4836(2)	2555(1)	76(1)
C(12)	3425(1)	5647(2)	3083(1)	74(1)

C(11)	3733(1)	4396(2)	2854(1)	50(1)
C(24)	3158(1)	-2134(2)	727(1)	47(1)
C(25)	2737(1)	-2707(2)	1031(1)	48(1)
C(15)	4434(1)	-1321(2)	4146(1)	44(1)
C(26)	2633(1)	-2182(2)	1638(1)	43(1)
C(9)	3356(1)	-874(2)	4029(1)	42(1)
C(1)	4356(1)	2951(2)	4635(1)	40(1)
C(18)	3121(1)	3614(2)	537(1)	39(1)
C(20)	4149(1)	3588(2)	573(1)	39(1)
C(19)	3596(1)	4083(2)	296(1)	39(1)
C(23)	3474(1)	-1015(2)	1029(1)	37(1)
C(2)	4266(1)	1569(2)	4524(1)	36(1)
C(14)	4190(1)	3841(2)	4091(1)	36(1)
C(17)	3204(1)	2658(2)	1062(1)	35(1)
C(27)	2954(1)	-1068(2)	1948(1)	32(1)
C(21)	4236(1)	2613(2)	1096(1)	32(1)
C(13)	3928(1)	3385(2)	3434(1)	31(1)
C(28)	4697(1)	-1079(1)	2347(1)	30(1)
C(8)	3907(1)	-476(2)	3783(1)	29(1)
C(3)	4016(1)	1051(2)	3873(1)	27(1)
C(22)	3374(1)	-481(1)	1645(1)	26(1)
C(16)	3761(1)	2151(1)	1348(1)	26(1)
C(4)	3847(1)	1966(1)	3317(1)	25(1)
C(6)	4527(1)	247(1)	2262(1)	24(1)
N(1)	3556(1)	1470(1)	2668(1)	26(1)
O(1)	5000	1090(1)	2500	24(1)

Table A-7: Bond Lengths for L_3

Bond	Length (Å)		Bond	Length (Å)		Bond	Length (Å)
P(1)-N(1)	1.550(1)		C(26)-C(27)	1.391(2)		C(14)-C(13)	1.392(2)
P(1)-C(22)	1.8026(14)		C(9)-C(8)	1.530(2)		C(17)-C(16)	1.397(2)
P(1)-C(6)	1.8069(14)		C(1)-C(14)	1.378(2)		C(27)-C(22)	1.387(2)
P(1)-C(16)	1.8104(14)		C(1)-C(2)	1.381(2)		C(21)-C(16)	1.391(2)
C(10)-C(11)	1.514(3)		C(18)-C(19)	1.384(2)		C(13)-C(4)	1.416(2)
C(11)-C(12)	1.542(3)		C(18)-C(17)	1.384(2)		C(28)-C(6)	1.3582(19)
C(11)-C(13)	1.512(2)		C(20)-C(19)	1.380(2)		C(8)-C(3)	1.521(2)
C(24)-C(25)	1.384(3)		C(20)-C(21)	1.394(2)		C(3)-C(4)	1.411(2)
C(24)-C(23)	1.385(2)		C(23)-C(22)	1.397(2)		C(4)-N(1)	1.408(2)
C(25)-(26)	1.382(3)		C(2)-C(3)	1.395(2)		C(6)-O(1)	1.3809(15)
C(15)-C(8)	1.530(2)		C(28)-C(28)’	1.418(3)			

Table A-8: Bond Angles for L_3

Atoms	Angle (º)		Atoms	Angle (º)
N(1)-P(1)-C(22)	110.37(6)		C(14)-C(13)-C(11)	120.20(14)
N(1)-P(1)-C(6)	115.37(6)		C(4)-C(13)-C(11)	120.75(13)
C(22)-P(1)-C(6)	102.02(6)		C(6)-C(28)-C(28)’	107.00(8)
N(1)-P(1)-C(16)	115.76(6)		C(3)-C(8)-C(9)	110.14(12)
C(22)-P(1)-C(16)	103.60(6)		C(3)-C(8)-C(15)	112.35(13)
C(6)-P(1)-C(16)	108.22(6)		C(9)-C(8)-C(15)	111.27(13)
C(13)-C(11)-C(10)	110.61(18)		C(2)-C(3)-C(4)	119.01(13)
C(13)-C(11)-C(12)	112.33(17)		C(2)-C(3)-C(8)	119.52(13)
C(10)-C(11)-C(12)	110.61(18)		C(4)-C(3)-C(8)	121.43(12)

C(25)-C(24)-C(23)	119.73(16)		C(27)-C(22)-C(23)	119.77(13)
C(26)-C(25)-C(24)	120.59(15)		C(27)-C(22)-P(1)	120.26(11)
C(25)-C(26)-C(27)	119.90(15)		C(23)-C(22)-P(1)	119.97(11)
C(14)-C(1)-C(2)	119.20(14)		C(21)-C(16)-C(17)	119.20(13)
C(19)-C(18)-C(17)	119.60(15)		C(21)-C(16)-P(1)	125.55(11)
C(19)-C(20)-C(21)	120.68(14)		C(17)-C(16)-P(1)	115.23(11)
C(20)-C(19)-C(18)	120.12(15)		N(1)-C(4)-C(3)	119.70(12)
C(24)-C(23)-C(22)	120.09(15)		N(1)-C(4)-C(13)	120.68(13)
C(1)-C(2)-C(3)	121.61(15)		C(3)-C(4)-C(13)	119.41(13)
C(1)-C(14)-C(13)	121.69(15)		C(28)-C(6)-O(1)	109.77(12)
C(18)-C(17)-C(16)	120.84(14)		C(28)-C(6)-P(1)	129.15(10)
C(22)-C(27)-C(26)	119.92(15)		O(1)-C(6)-P(1)	119.98(9)
C(16)-C(21)-C(20)	119.55(14)		C(4)-N(1)-P(1)	130.94(10)
C(14)-C(13)-C(4)	119.05(14)		C(6)-O(1)-C(6)	106.45(14)